Diastereoselectivity in Bimetallic Complexes Containing Chiral Tridentate Ligands

A Dissertation Submitted to the
Indian Institute of Technology Guwahati as
Partial Fulfillment for the Degree of Doctor of Philosophy
in Chemistry

by

Himanshu Sekhar Jena
Roll No. 07612219

Department of Chemistry
Indian Institute of Technology Guwahati
Guwahati – 781 039

May 2012

Dedicated to My Family and Friends…

DEPARTMENT OF CHEMISTRY
INDIAN INSTITUTE OF TECHNOLOGY GUWAHATI
GUWAHATI-781039

DECLARATION

I hereby declare that this thesis entitled "**Diastereoselectivity in Bimetallic Complexes Containing Chiral Tridentate Ligands**" is the outcome of research work carried out by me under the supervision of Dr. V. Manivannan, at the Department of Chemistry, Indian Institute of Technology Guwahati, Assam, India.

In keeping with the general practice of reporting scientific observations, due acknowledgement has been made whenever work described here has been based on the findings of other investigators.

IIT Guwahati
May, 2012

Himanshu Sekhar Jena
(Roll. No. 07612219)

DEPARTMENT OF CHEMISTRY
INDIAN INSTITUTE OF TECHNOLOGY GUWAHATI
GUWAHATI-781039

Certificate

This is to certify that Mr. Himanshu Sekhar Jena has been working under my supervision since January, 2008 as a regular registered Ph. D. student. I am forwarding his thesis entitled "**Diastereoselectivity in Bimetallic Complexes Containing Chiral Tridentate Ligands**" being submitted for the Ph. D. Degree (Chemistry) of this Institute.

I certify that he has fulfilled all the requirements according to the rules of this institute regarding the investigations embodied in his thesis and this work has not been submitted elsewhere for a degree.

IIT Guwahati
May, 2012

Dr. V. Manivannan
(Thesis Supervisor)

Acknowledgements

This thesis might not have seen through its completion unless I had the support and encouragement of numerous people around me. Today, when I bring it to an end, I would like to express few words of appreciation to the people who actually made this thesis a reality and an unforgettable experience for me.

I am extremely grateful to my supervisor Dr. V. Manivannan for his constant guidance and encouragement throughout the doctoral degree course. As my mentor his insight, observations and suggestions helped me to establish the overall direction of research and contributed immensely to the success of present work.

I would like to acknowledge my sincere gratitude to all my doctoral committee members for their insightful advices and valuable suggestions. I am grateful to the entire faculty and staff in the Department of Chemistry, Indian Institute of Technology Guwahati for providing a wonderful work atmosphere throughout this period. I am also grateful to Dr. Sambit Mallick, Department of Humanities and Social Sciences, Indian Institute of Technology Guwahati for his advices and valuable suggestions.

I am grateful to Prof. J. Subramanian for his cordial help for fitting the low temperature VSM data.

I would like to extend my pleasure to C.I.F. IIT Guwahati for providing various facilities and Mr. Babulal Das for collecting the X-ray data of the crystals discussed in this thesis.

This thesis wouldn't have seen the light of this day without the care, encouragement and emotional support of. Dr. Monalisa. I would like to furnish my sincere gratitude for her motivation which made me to reach this point.

My heartiest gratefulness goes towards my lab mates and my batch mates for their relentless effort and cooperation during this time span as well as Laxmidhar, Subash, Biswaranjan, Nihar, Santosh, Bigyan, Saroj, Santosh, Ratnakar, Somasekhar, Devendra, Subhashis, Dipankar and Ziyauddin for their timely help, support and also for the wonderful time we shared together.

The financial support from Indian Institute of Technology Guwahati is duly acknowledged.

Finally, I would like to thank my family members for their understanding, encouragement, patience, unending support and blessings in my every endeavor without which my Ph.D. could not be completed. They are the main soul and inspiration for each and every step that I achieve in my life.

Himanshu Sekhar Jena

Preface

During the last few decades; a significant amount of information related to the characterization of chiral Schiff bases and their complexes with several metals has appeared. Only the ligands such as salicylaldimines and α–hydroxy naphthaldimines were selectively employed because they can promote chelation and provide extra stability to the metal centers. Most previous studies have used enantiopure ligands, and so the materials formed are necessarily homochiral. A more complex and less explored situation arises when racemic ligands are used. Reactions with racemic ligands result in either ligand self-recognition whereby ligands of the same handedness associate to form homochiral complexes (*RR* or *SS*) or ligand self-discrimination whereby ligands of opposite handedness associate to form a heterochiral complex (*RS*). During the formation of coordination polymers ligand self-assembly can occur with ligand self-recognition to give homochiral polymers. In such cases, the crystal most commonly contains a racemic mixture, containing equal amounts of the *RRR*⋯ and *SSS*⋯ polymers. The solid state structures then necessarily differ significantly from that of the homochiral polymer (*RRR*⋯ or *SSS*⋯ only) prepared from the enantiopure ligand. So the self-assembly is significantly different when using racemic versus enantiopure ligands and there is great potential for discovering new and interesting solid-state architectures and molecular materials.

In this thesis 2-pyridyl derived chiral amines have been synthesized, which on reaction with 2-hydroxybenzaldehyde and with 2-hydroxy-1-naphthaldehyde gives respective chiral tridentate imines. The isolated imines undergo reduction with $NaBH_4$ to give corresponding amines. The resultant chiral tridentate imines and amines are further used for the synthesis of Ni(II), Cu(II) and Zn(II) complexes. Pseudo-halides such as azide, cyanate, thiocyanate and dicyanamide ions are used for the synthesis of bimetallic dimers having M_2X_2 [X = O, N, Cl] core. The results described here constitute a rare example for the diastereoselectivity of chiral tridentate imines and amines around dimetallic core. The effects of bridging ligands, coligands and ligand geometry on diastereoselective self-assembly are noted. The role of solvent and non-covalent

interaction on self-assembly of racemic imines and amines are also described. It is also important to note that, all the complexes are racemic in nature as racemic mixture of chiral tridentate ligands are employed.

Chapter 1 summarizes the literature on the self-assembly of chiral imines, amines, amides along with some macrocyclic as well as box ligands and defines the objective of the thesis work. This Chapter highlights the role of ligand geometry, anions, bridging ligands, pH and non-covalent interactions on the self-assembly process. The importance of self-assembly in biology and applications of chiral tridentate ligands are also reviewed in this Chapter.

Chapter 2 describes about three centrosymmetric nickel(II) mono-chelates of a racemic tridentate Schiff base ligand containing N_3^-, NCS^-, $(NC)_2N^-$(dca) and OAc^- as co-ligands. Co-ligands such as N_3^- and NCS^- acts as terminal ligands resulting a heterochiral dimerization of ligands around dinickel core, whereas dca ion acts as μ–1,5– bridging mode assembling homochiral dimers ({$Ni_2(\mu$–$O_P)_2(\mu$–OAc)}) to a non-centrosymmetric 1D homochiral chain. The low temperature magnetic moment data suggests negligible intramolecular exchange coupling in the dinickel core due to the orthogonality of *d*-orbitals of Ni^{2+} ion.

Chapter 3 describes the effect of bridging ligands on the diastereoselectivity of chiral tridentate imines around dinickel and dicopper core. The bridging ligands such as Cl^- and NO_3^- results heterochiral combination of ligands whereas OAc^- and SO_4^{2-} results homochiral combination of ligands around dimetallic core. Two homochiral chains are cross-linked by H-bonding interactions between sulfate ion and solvated water molecules resulting a 1D water chain. The dca ion bridges two alternating *RR* and *SS* homochiral dimers through H-bonding interactions between bridging methanol, solvent methanol and dca ion, forming a zig-zag centrosymmetric 1D heterochiral chain.

Chapter 4 describes about three centrosymmetric isostructural complexes containing racemic mixture of a tridentate Schiff base ligand and end–on–end dca ion. All the three compounds are centrosymmetric in nature as the center of symmetry lies inside the dimeric unit $[M_2(N(CN)_2)_2]$ and crystallizes selectively only as methanol solvate. In lattice, solvent methanol plays an important role in stabilizing the phenoxo-O of ligand by strong H-bonding interaction. Ligand and

zinc complex shows solid state photo-luminescence that can be attributed to intraligand transitions.

Chapter 5 describes about four centrosymmetric copper complexes containing racemic mixture of a tridentate Schiff base ligand and dca ion. The formation of these compounds clearly depends on the nature of Cu(II) salt. The dca ion plays major role in assembling the racemic Schiff base, by either of its μ–1,5 or μ–1 bridging mode. It separates Cu(II) and Cu(I) having all Cu(I) are on the strip whereas $Cu^{II}_2O_2$ are on the back bone forming 1D zipper structure. Enantioselective and diastereoselective H-bonding interaction are noted. The dca ion bridged the Cu_2O_2 cores forming a molecular rectangle which leads to 2D copper grid structure.

Chapter 6 describes about six Zn(II) complexes containing Zn_2O_2 core using a racemic mixture of tridentate imine and their reduced amine ligands. The tridentate imine and amine ligands respectively span *meridional* and *facial* positions leaving the vacant coordination site for coligand. The *meridionally* coordinating imine allow center of symmetry to lie inside the Zn_2O_2 core assembling heterochiral dimerization of imines, whereas *facially* coordinating amine due to lack of center of symmetry results in homochiral dimerization around Zn_2O_2 core. The isolated Zn(II) bis-chelates have *cis*,*cis*,*trans*-$(O_P)_2(N_A)_2(N_Y)_2$ stereochemistry and *cis*-$(O_P)_2$ disposition further coordinate to tetrahedral zinc center. DMF molecules assemble *RR* and *SS* bis-chelates through N–H···O interactions. The *RR* bis-chelates have a Δ configuration whereas the *SS* bis-chelates have Λ configuration. Since the overall crystal lattice has an equal proportions of *RR* and *SS* bis-chelates, Δ and Λ isomers are also in equal amounts.

In overall the self-assembly observed in this thesis will boost the understanding of self-sorting process of chiral tridentate imine and amine ligands around the dimetallic core.

Any remaining errors are, of course, solely my own responsibility. I welcome your critique.

Himanshu Sekhar Jena
IIT Guwahati

Abbreviations

a	Unit cell dimension a
b	Unit cell dimension b
c	Unit cell dimension c
D	Density of the crystal
α	Interfacial angle α in a unit cell
β	Interfacial angle β in a unit cell
γ	Interfacial angle γ in a unit cell
Z	Unit cell formula units
λ	Wave length
ν	Wave number
μ	Absorption coefficient
ε	Molar extinction coefficient
τ	Geometric parameter applicable for five-co-ordinate structures as an index of the degree of trigonality between trigonal bipyramidal and rectangular pyramidal
$\mu_{s.o.}$	Spin-only magnetic moment
μ_{eff}	Effective magnetic moment
χ	Magnetic susceptibility
χ_M	Molar susceptibility
H	Applied magnetic field
g	Lande splitting factor
A	Hyperfine splitting constant
Θ	Temperature
$N\alpha$	Temperature–independent paramagnetism
J	Intramolecular exchange coupling

Contents

Chapter 1

Introduction, Materials and Methods

Abstract

The aim of this Chapter is to provide an overall view on the self-assembly of racemic ligands around the metal center. This Chapter highlights the role of ligand geometry, anions, bridging ligands, pH and non-covalent interactions on the self-assembly process. The importance of self-assembly in biology and applications of chiral tridentate ligands are also included in this Chapter. The materials used in this study, their commercial sources, specifications of the instruments used for the characterization of the compounds, procedures of crystallographic data collection and refinement etc., are also briefed in the end.

1. Introduction

1.1 Schiff bases

The reversible condensation between amino and carbonyl groups to form imine bonds is one of the most fundamental and ubiquitous reactions in chemistry. It is hardly surprising therefore that, Hugo Schiff (Fig. 1), the German chemist [1], who discovered the reaction in 1864, has since been immortalised in the common name for compounds – they are now known routinely as ‘‘Schiff’s bases’’ – containing imine bonds.

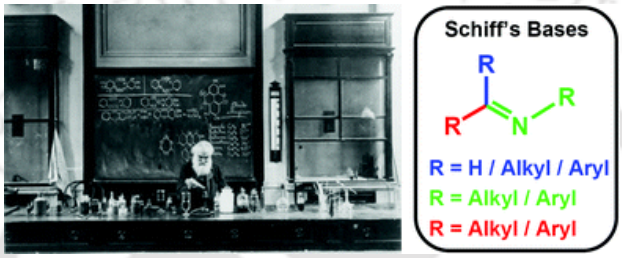

Fig. 1. Photograph of “Hugo Schiff” working in his lab taken in 1864 and his bases (adopted without permission from: Chem. Soc. Rev. 36 (2007) 1705–1723).

The definition [2, 3] of a Schiff’s base – also known as an azomethine or anil, as well as an imine – which is designated constitutionally as $RR^1C{=}NR^2$, requires that R is an alkyl or aryl group, R^1 is a hydrogen atom, or an alkyl or aryl group, and R^2 is either an alkyl or aryl group which contains [4] an alkyl- or aryl- substituted carbon atom at the point of attachment to the nitrogen atom. There are handful of other functional groups that deviate slightly from this definition, examples hydrazones ($R^2 = NR_2$) and oximes ($R^2 = OH$).

Imine bond formation is a simple condensation reaction which involves loss of H_2O within a single molecule or between two molecules containing amino and carbonyl groups, such that a C=N bond is formed either intra- or inter- molecularly. Addition of H_2O to an imine leads to hydrolysis and drives the condensation in the opposite direction, leading to the recovery of the starting material(s). The reaction which is acid-catalyzed is executed typically by refluxing the starting material(s) under azeotropic conditions. In addition to hydrolysis, imines commonly participate in another two types of equilibrium-controlled reactions such as *exchange* (Fig. 2(b)) and *metathesis* (Fig. 2(c)) reactions. Many external factors, including solvent, concentration, pH, temperature, steric and electronic properties, can influence the equilibrium. As such, there are many parameters

that can be altered in order to drive the reaction forward – or indeed backwards. For a dynamic reaction, like imine bond formation, to proceed in the direction of products, i.e., imines, the change in the free energy during the reaction must be favourable, i.e., ΔG^0 in eqn (1) must be less than zero.

$$\Delta G^0 = \Delta H^0 - T\Delta S^0 \qquad (1)$$

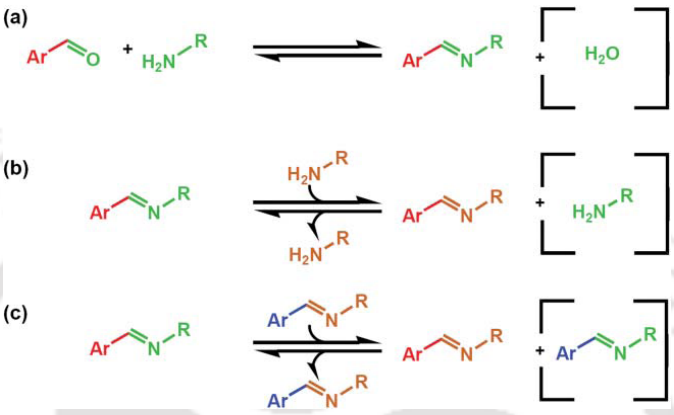

Fig. 2. The three fates involving imine reactants: (a) imine condensation, (b) exchange and (c) metathesis.

Schiff bases deserve a relevant role for several reasons [5]:

(*a*) They can be obtained by simple self-condensation of suitable formyl- or keto- and primary amine-precursors. Multiple self-condensation processes give rise to complex planar or 3D compounds in one step.

(*b*) They generally can contain additional donor sets (O, S, P, etc.) and this makes them good candidates for metal ion complexation and for mimicking biological systems.

(*c*) Alternatively they can be obtained by template syntheses; this procedure directly gives the designed complexes. Moreover, these complexes can undergo transmetallation reactions when reacted with a different metal salt; this synthetic procedure allows the formation of accessible complexes. Template and transmetallation reactions quite often give rise to the designed complexes in high yield and in a satisfactory purity grade.

(*d*) They can be functionalized by inserting appropriate groups in the aliphatic and/or aromatic chains of the formyl- or keto- and amine- precursors.

(*e*) They can give rise to reductive decomplexation reactions when treated with appropriate reductants with the consequent formation of the corresponding polyamine

derivatives less sensitive to hydrolysis and more flexible. These reduced compounds contain >NH groups which may be further functionalized by appropriate synthetic procedures.

(*f*) The use of particular Schiff bases can exhibit unusual complexation; for instance helicates derivatives have been obtained with imine derivatives containing appropriate chains and/or suitable donor sets.

(*g*) They can be linked to an appropriate support (e.g. silica) giving rise to modified catalysts or modified surfaces, bearing well defined molecular assemblies.

(*h*) It is well known that other systems are excellent ligands for specific metal ions (i.e. crown ether, macrocyclic thioether, polyaza derivatives, etc.). Thus the fusion of different coordinating entities (i.e. a Schiff base and crown-ether moiety) into a unique ligand can give rise to very interesting systems capable of multiple selective and/or different metal ions recognition processes.

1.2 Chirality

Chirality is central to coordination chemistry and unites fields as diverse as transition-metal catalysis, metallo-supramolecular chemistry and bioinorganic chemistry. One research theme which plays a pivotal role in this field is the exploration of methods for the stereoselective synthesis of coordination compounds [6–10]. During the last few years; a significant amount of information related to the characterization of chiral Schiff bases and their complexes with several metals has appeared. Only the ligands such as salicylaldimines and *α*–hydroxynaphthaldimines were selectively employed because they can promote chelation and provide extra stability to the metal centers. Again the development of a wide variety of chiral transition metal complexes that mediate enantioselective reactions has been the subject of many investigations in recent years. Chiral salen complexes have emerged as very effective catalysts for epoxidation of alkenes [11–15]. Besides steric effects, electronic properties of the metal center seem to have an important influence on the enantioselectivities in asymmetric reactions.

It is also possible for a molecule to be chiral without having actual point chirality. Common examples include 1,1'-bi-2-naphthol (BINOL) and 1,3-dichloro-allene, which have *axial chirality* [16], (*E*)-cyclooctene, which has *planar chirality* [17], and certain

calixarenes and fullerenes, which have *inherent chirality* [18, 19]. Basically chirality arises from three major factors such as; (*a*) due to presence of *asymmetric-C atom* (tetrahedral *C*-atom attached to four different substituents) (*b*) due to *restricted C-C bond rotation* (ex. BINOL and its derivative) (*c*) due to *chiral propeller-like arrangement* {*facial* or *meridional* arrangement of ligands around metal center resulting a stereogenic metal center, ex. tris(bipyridine)ruthenium(II) complex} [20–22].

A racemic mixture or racemate is one that has equal amounts of left- and right-handed enantiomers of a chiral molecule. The first known racemic mixture was "racemic acid", which Louis Pasteur found to be a mixture of the two enantiomeric isomers of tartaric acid. A racemic mixture is denoted by the prefix (±)- or dl- (for sugars the prefix dl- may be used), indicating an equal (1:1) mixture of dextro and levo isomers [23–25]. Also the prefix *rac*- (or *racem*-) or the symbols *RS* and *SR* (all in *italic* letters) are used [26]. A racemate is optically inactive, meaning that there is no net rotation of plane-polarized light. Although the two enantiomers rotate plane-polarized light in opposite directions, the rotations cancel because they are present in equal amounts. A racemate sometimes has different properties from either of the pure enantiomers, different melting points are most common, but different solubilities and boiling points are also possible. Racemic materials can crystallize as illustrated in Fig. 3.

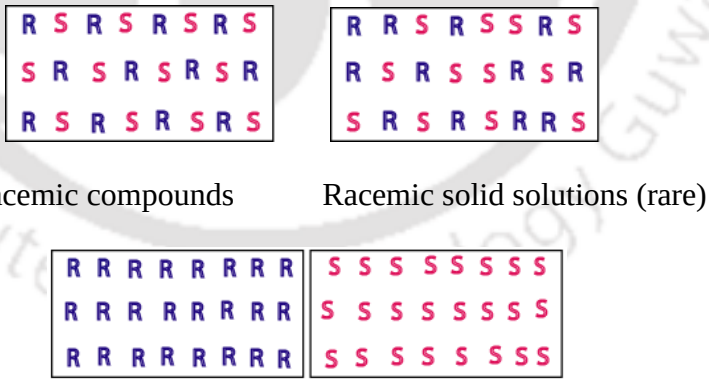

Racemic compounds Racemic solid solutions (rare)

Conglomerates (~ 5-10%)

Fig. 3. Ways of crystallization of racemic crystal.

Most racemates crystallize as racemic compounds in which the two component enantiomers are regularly arrayed within the crystal lattice in equal numbers [27, 28]. Thus, analysis of any single crystal always reveals a 1:1 ratio of the two component

enantiomers. Much rarer is a racemic solid solution in which the two component enantiomers are randomly arrayed within the crystal lattice.

Racemate crystallization is the vast majority of crystallizations of solutions containing enantiomers (about 90%). In the crystal lattice there are pairs of enantiomers, interrelated by symmetry planes, inversion centers etc.

Pseudoracemate or racemic solid solutions are a very rare type of crystallization restricted to a couple of cases only. The lattice contains the enantiomers randomly distributed.

Conglomerate crystallization involves the crystallization of one enantiomer in a single crystal for symmetry reasons, which leads to the conglomerate situation. It is assumed that about 10% may be a little less, of all the crystallizations of enantiomers give conglomerates, although the crystals usually are too small for manual separation.

It is also relevant to mention that *quasi-racemate* contains a mixture of two similar but distinct compounds, one of which is left-handed and the other right-handed. Although chemically different, they are sterically similar (isosteric) and are still able to form a racemic crystalline phase. One of the first such racemates studied, by Pasteur in 1853, forms from a 1:2 mixture of the bis ammonium salt of (+)-tartaric acid and the bis ammonium salt of (-)-malic acid in water.

1.3 Schiff bases having chiral center(s)

In the following sections self-assembly of racemic mixture of Schiff bases having one or two chiral centers around the metal center, reported in the literature are reviewed. In addition, self-assembly of some chiral amine(s), amide(s), macrocyclic as well as box ligands are included for discussions.

1.3.1 Self-assembly of racemic Schiff base(s)

Chiral ligands have been widely used in chemical [29–32] and biological process [33–40] to control metal-centered and helical chirality [41–52], in self-assembled metal complexes and to direct self-sorting [53, 54]. Enantiomeric self-recognition and self-discrimination are part of the chiral recognition [55–59]. Most previous studies have used enantiopure ligands, and so the materials formed are necessarily homochiral. A more

complex and less explored situation arises when racemic ligands are used. Reactions with racemic ligands result in either ligand self-recognition whereby ligands of the same handedness associate to form a racemic mixture of homochiral complexes (*RR* or *SS*) or ligand self-discrimination whereby ligands of opposite handedness associate to form a heterochiral complex (*RS*) [60–75]. During the formation of coordination polymers ligand self-assembly can occur with ligand self-recognition to give homochiral polymers. In such case, the crystal most commonly contains a racemic mixture, containing equal amounts of the *RRR*··· and *SSS*··· polymers. The solid state structures then necessarily differ significantly from that of the homochiral polymer (*RRR*··· or *SSS*··· only) prepared from the enantiopure ligand [76–78]. In supramolecular systems, enantiomeric self-recognition has been achieved either by the consequence of hydrogen bonds, or on bonding to a metal center. The self-assembly is significantly different when using racemic versus enantiopure ligands, and there is great potential for discovering new and interesting solid-state architectures and molecular materials when the racemic ligands are used. In the field of magnetic materials, the combination of ferromagnetism and chirality can result in magneto-chiral dichroism (MChD) [79, 80] and chiral magneto-structural effects, [81–85] which can be applied to magneto-optical multifunctional materials. Recently, dielectric relaxation and second harmonic generation (SHG) were, respectively, observed in molecule based chiral single chain magnets (SCMs) [86, 87]. Single molecule magnets (SMMs) [88–90] and SCMs [91] are single domain magnets below their critical temperatures and the former show quantum tunneling of magnetization (QTM). Although SCMs with chiral spin centers are expected to show enhanced synergistic effects of chirality and magnetism, the number of chiral SCMs is still limited. Self-assembly of the metal ion with racemic Schiff bases and suitable bridging units (pseudohalides or *N*–donor bases) is an efficient approach to prepare mono-, di- and polynuclear coordination complexes exhibiting interesting properties such as ion-exchange, adsorption, catalytic, molecular recognition, photoluminescence and magnetic features [92–102].

Metal-assisted self-assembly of independent ligands to form helices [103–109], grids [110], knots [111], cylinders [112, 113], platonic shapes [114, 115], and circular helicates [116] quantitatively with labile metals represent impressive feats of molecular design and

assembly [117–120]. Many forms of supramolecular complexes are intrinsically chiral, even if the individual ligands are achiral. Achiral ligands can yield a racemic mixture of complexes such as a mixture of left- and right- handed helices under equilibrium conditions. Appropriately designed, enantiopure, polynucleating ligands can stereospecifically form a single, homochiral isomer through "chiral directed self-assembly", in which the chirality of all metal centers is identical and is dictated by ligand chirality. Stack and coworkers have reported ligand recognition in dimeric copper(I) complexes of tetradentate ligands (*rac*-**1**^{6H}, *rac*-**1**^{6Br}) that have a *trans*–1,2–cyclohexane diamine frame [121]. In solution, *rac*-**1**^{6H} assembles to two diastereomeric pair and is heterochiral in nature whereas *rac*-**1**^{6Br} exclusively forms one enantiomeric pair and is homochiral in nature (Fig. 4). The most interesting aspect of this system is the ligand self-recognition in the assembly process. It can be concluded that all conformationally restricted ligands that project their chirality would exhibit ligand self-recognition and assemble in a homochiral fashion. The enhanced ligand selectivity exhibited by *rac*-**1**^{6Br} relative to *rac*-**1**^{6H} probably does not arise from favorable nonbonded interactions of the bromine atoms within the complex formed, but rather through destabilization of unformed heterochiral complexes.

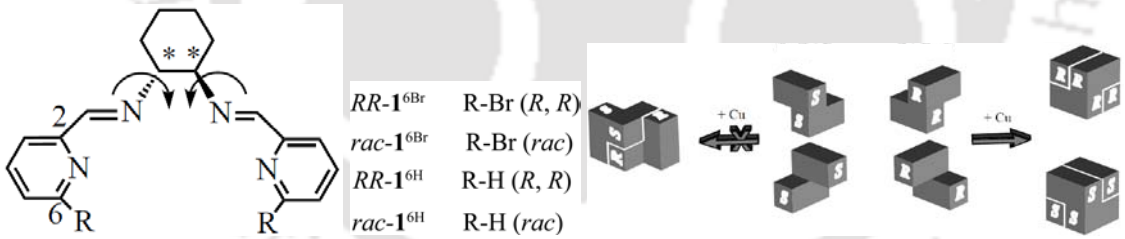

Fig. 4. Self-assembly of a racemic mixture (*rac*-**1**$^{6H\ (Br)}$) of rigid fragments to either a discrete heterochiral (Z-shaped) or homochiral (cube-shaped) species.

Racemic Schiff bases due to restricted rotation about C–C bond: 1, 1'–Binaphthyl units that are functionalized at the 2 – and 2' – positions are often chiral due to restricted rotation about the transannular bond. Though their importance in asymmetric synthesis cannot be overstated, chiral ligands based on binaphthyl frameworks have also found wide application in coordination and metallo-supramolecular chemistry. Salicaldimine derivatives have been particularly well-studied (X = OH) and have found applications in asymmetric catalysis and biomimetic chemistry [122, 123]. The self-assembly of

binaphthyl derived Schiff bases (**2**, **3**) (Scheme 1) in presence of $CuSO_4 \cdot 5H_2O$ has been reported by Kuroda *et al*. [124]. Using enantiopure Schiff base **3**, homochiral copper(II) complexes containing hydrolysed product are isolated where as heterochiral (meso) complexes are isolated using the racemic Schiff base **3** (Fig. 5). The relative position of amine moiety in **3** was the striking features in both homochiral and heterochiral dimers (Fig. 6). For the heterochiral dimer, *anti*-arrangement of the amine groups; allows for the formation of only two hydrogen bonds where as a *syn*-arrangement of the amine groups for the homochiral dimer have four hydrogen bonds. In both complexes, significant H–bonding interaction between these amine groups and the sulfate oxygen plays important role in the self-assembly process.

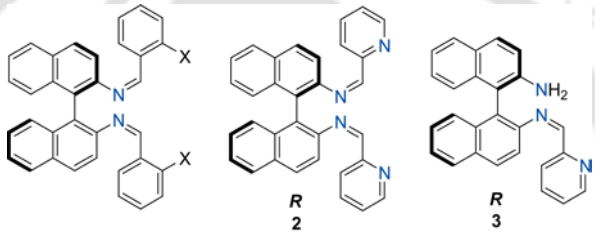

Scheme 1

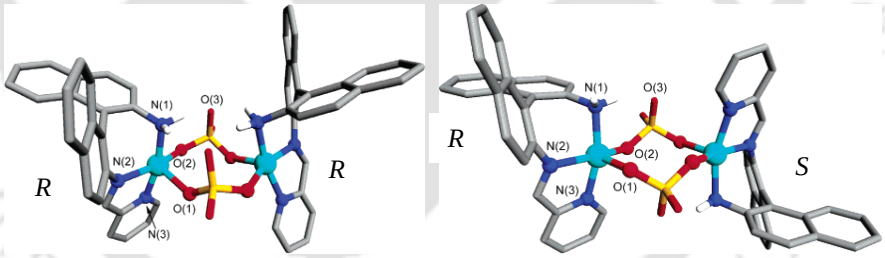

Fig. 5. Crystal structure of homochiral and heterochiral dimer of copper(II) complexes of **3**.

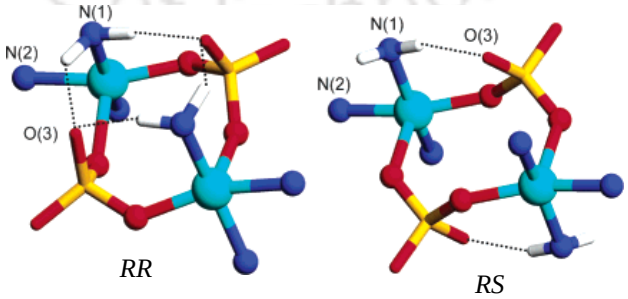

Fig. 6. Close up view of homochiral and heterochiral dimer in copper(II) complexes of **3** exhibiting different H–bonding interactions.

Interactions of chiral amine with chiral copper salen adducts: Salen ligands are one of the very versatile classes of organic ligand for homogeneous asymmetric catalysis. Much of this versatility originates from its simple synthesis and the structural rigidity of the ligand and can thus easily stabilize metal ions in an asymmetric environment. Early pioneering work on these ligands for asymmetric catalysis was performed by Jacobsen and Katsuki [125–132]. Chromium and cobalt complexes of the salen ligand (*N*, *N′*–bis(3,5–ditert–butylsalicylidene)–1,2–diaminocyclohexane (**4**)) (Scheme 2) were also found to catalyze the highly enantioselective ring-opening reactions of epoxides [133]. DFT calculation showing the differentiation and discrimination between enantiomers of a chiral amine (*R*- and *S*-methylbenzylamine (MBA)) by copper(II) complexes of ligand **4** has been reported [134].

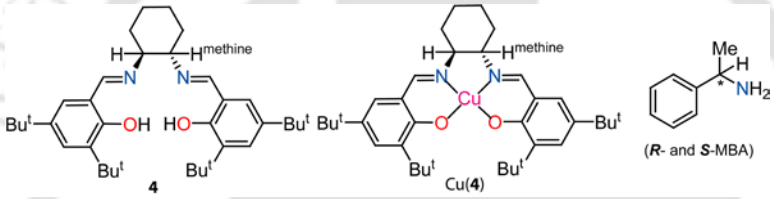

Scheme 2

The chiral amines (*R*- and *S*- MBA) and chiral copper complexes (*R*, *R*)- and (*S*, *S*)-[Cu(**4**)] can form four different penta-coordinate diastereomeric adducts; namely, (*R*, *R*)-[Cu(**4**)] + *R*-MBA, (*R*, *R*)-[Cu(**4**)] + *S*-MBA, (*S*, *S*)-[Cu(**4**)] + *R*-MBA, and (*S*, *S*)-[Cu(**4**)] + *S*-MBA (abbreviated to *RR*-*R*, *RR*-*S*, *SS*-*R*, and *SS*-*S*). From DFT calculation, the slight difference in steric crowding caused by the α-proton of *S*-MBA appears to be sufficient to tip the balance of selectivity in favor of the heterochiral adduct (Fig. 7C). In between (*R*, *R*)-[Cu(**4**)] + *R*-MBA (Fig. 7A) and (*S*, *S*)-[Cu(**4**)] + *S*-MBA (Fig. 7B) (for the homochiral adduct), structure A is more stable than B due to the absence of unfavorable amount of steric crowding.

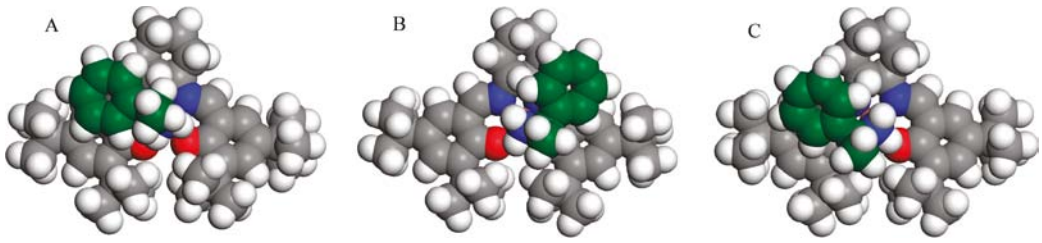

Fig. 7. QMMM-optimized structures for *R*- and *S*-MBA with [Cu(**4**)].

1.3.2 Self-assembly of racemic amine/amide ligands

Self-assembly *via* intermolecular non-covalent interactions is one of the powerful tools for designing and synthesizing polar crystals as well as enantioselective chiral host frameworks. The spatial disposition of the functional groups participating in the intermolecular non-covalent interactions is expected to control the alignment of the host and guest molecules as well as spontaneous resolution of chiral guest compounds. Synthesis of inclusion compounds having polar host frameworks that can confine and align guest molecules in a polar order is one of the successful strategies [135–138]. In this regard, it may well be noted that the synthesis of host frameworks with chiral cavities is a noteworthy challenge as these solids also have potential applications in the separation of enantiomers and in asymmetric catalysis [51, 53, 139–142]. The enantioselective isolation of the right-handed (*P*) and the left-handed (*M*) gauche form of 1, 2–dichloroethane in the host lattices formed by the chiral square-pyramidal Cu(II) complexes has been reported (Fig. 8) [143, 144].

There are three rotamers possible for 1, 2–dichloroethane. These are the *trans* or *anti*, the *cis* or *eclipsed* and the *gauche* forms. The eclipsed form is energetically most unfavorable. Between the *trans* and the *gauche* forms the former is more stable (by ~1 kcal mol^{-1}) [23]. The gauche form is chiral and also polar. One of the enantiomers has the right-handed (*P*) form and the other one has the left-handed (*M*) form. The molecule is in gauche form in each structure (Fig. 9). The molecule is trapped in the *P*–form in [Cu(*R*-**5**)$_2$(H_2O)]·$C_2H_4Cl_2$ and *M*–form in [Cu(*S*-**5**)$_2$(H_2O)]·$C_2H_4Cl_2$. Thus the chiral host complexes [Cu(*R*-**5**)$_2$(H_2O)]·$C_2H_4Cl_2$ and [Cu(*S*-**5**)$_2$(H_2O)]·$C_2H_4Cl_2$ produce the appropriate frameworks in the crystal lattice for exclusive accommodation of the *P*– and *M*– forms of 1, 2–dichloroethane respectively. The same case arises when 1, 2–dibromoethane was used in place of 1, 2–dichloroethane.

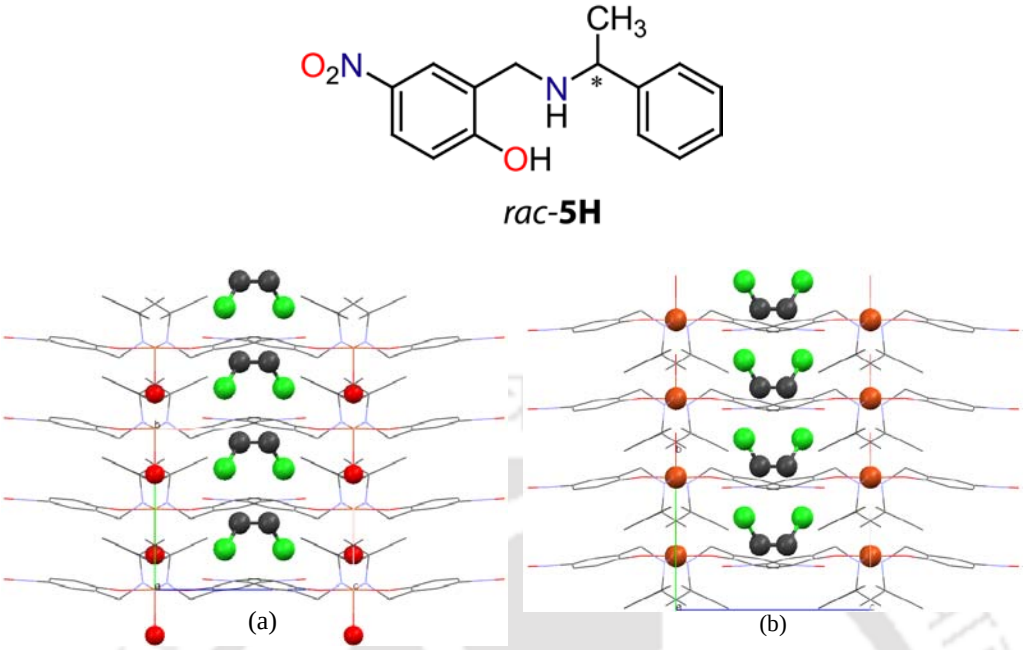

Fig. 8. The polar alignments of (a) [Cu(*R*-**5**)$_2$(H$_2$O)]·(*P*)-C$_2$H$_4$Cl$_2$ and (b) [Cu(*S*-**5**)$_2$(H$_2$O)] ·(*M*)-C$_2$H$_4$Cl$_2$ viewed along the *a*-axis.

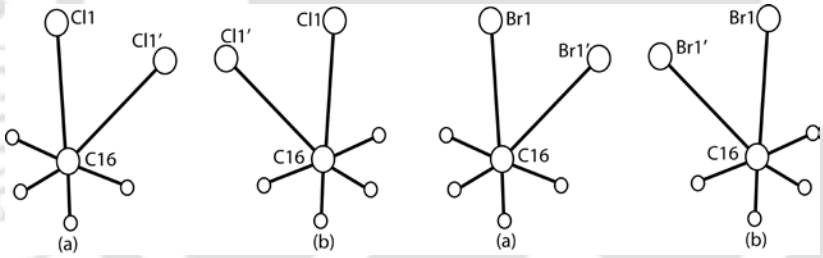

Fig. 9. (a) The right-handed (*P*) and (b) the left-handed (*M*) forms of 1, 2–dichloroethane /1, 2–dibromoethane in [Cu(*R*-**5**)$_2$(H$_2$O)]·C$_2$H$_4$Cl$_2$(Br$_2$) and [Cu(*S*-**5**)$_2$(H$_2$O)]·C$_2$H$_4$Cl$_2$(Br$_2$), respectively.

Racemic ABC-type ligand having chiral propeller-like arrangement: In general mononuclear case, two linear ABC-type ligands can coordinate to a metal center in either a *facial* (**A**) or *meridional* (**B**) fashion (Scheme 3). The facial mode has 11 possible stereoisomers, whereas the *meridional* mode has two, the minus (*M*) and plus (*P*) helical forms [145–148] (alternately Λ and Δ, respectively). Thus, stereochemical control is more easily achieved for *meridional* complexes. For a chiral non-racemic ligand, the *M* and *P* forms are diastereomeric, and it is possible to obtain a single chiral isomer upon coordination.

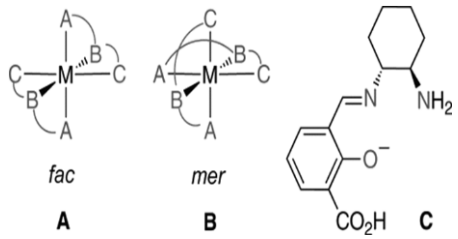

Scheme 3

Chiral, propeller-shaped complexes were shown to be effective chiral solvating agents for sulfoxides by forming diastereomeric complexes which can be easily distinguished in ^{1}H NMR spectra [149, 150]. The conformation of the ligand in the metal complexes has been studied which suggest that incorporation of a single chiral center in one of the three arms of the tripod could bias the conformation [151]. The achiral ligands tris(2–pyridylmethyl)amine (TPA) should adopt rapidly interconverting enantiomeric conformations in complexes with metal ions exhibiting trigonal bipyramidal coordination geometry. Incorporation of a chiral center in one of the three arms of the ligand would create conformational diastereomers, so that one conformation should predominate in solution [152] (Fig. 10). This was supported by exciton-coupled circular dichroism (ECCD) and molecular modeling studies. Tripodal ligands without chiral center can be able to show ECCD by complexation with chiral amines which could be further developed to produce ‘‘sensors’’ of chirality capable of determining enantiomeric excess of guest molecules [153].

ECCD can be used as a sensitive probe of changes in molecular conformation or intermolecular association. In particular, copper(II) and zinc(II) complexes showed ECCD spectra consistent with solid-state propeller-like structures. The conformationally mobile free ligand (**6**) gives a relatively weak CD spectrum, while zinc(II) and copper(II) complexes afford the characteristic ECCD spectra (Fig. 11). Fluorescence and exciton coupled circular dichroism signals of sensor α–MeBQPA (**6**) has been studied [154]. A strong CD signals was observed upon complexation with trigonal bipyramidal metal ions (Zn^{II}, Cu^{II}), whereas a weak CD signals was observed with octahedral metal ions (Cd^{II}, Fe^{II}).

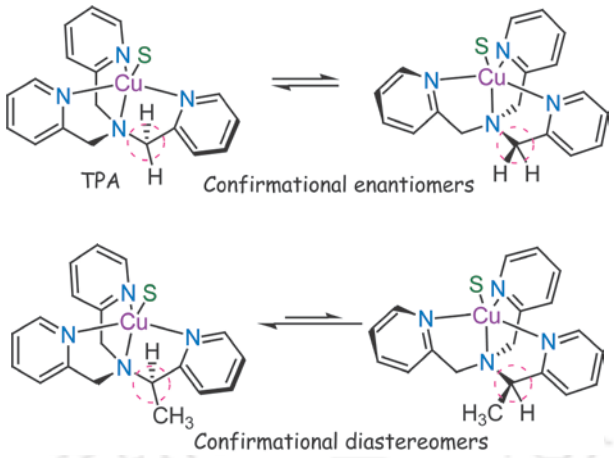

Fig. 10. The propeller shaped, C_3–symmetric conformational enantiomers of **TPA** that interconvert rapidly. S-solvent or coligands.

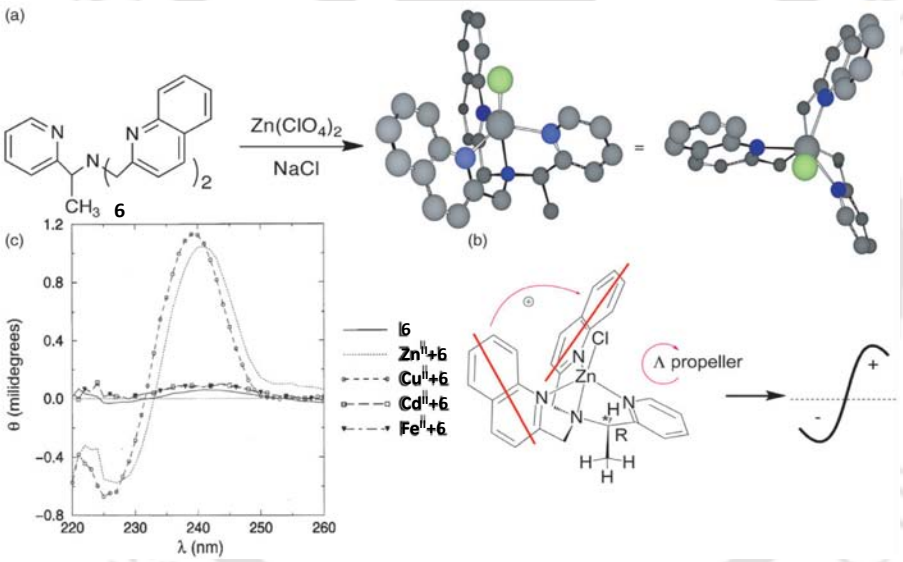

Fig. 11. CD spectra of perchlorate complexes of **6**, where Zn^{2+} and Cu^{2+} show strong amplitude compared to free ligand (**6**) and weak amplitude for octahedral Cd^{2+} and Fe^{2+} complexes.

Racemic tetradentate carboxamide ligand having asymmetric–C atom: The self-assembly reaction of copper(II) complexes containing chiral tetradentate carboxamide ligand (**7H**) has been studied by Mascharak group [155]. It has been reported that although a racemic mixture of **7H** is employed, the isolated dimeric complex $[Cu_2(\mathbf{7})_2](ClO_4)_2$ comprises only homochiral dimers $[Cu_2(\mathit{R}\text{-}\mathbf{7})_2](ClO_4)_2$ and $[Cu_2(\mathit{S}\text{-}\mathbf{7})_2](ClO_4)_2$ in the crystalline state. The absence of heterochiral species $[Cu_2(\mathit{S}\text{-}2)(\mathit{R}\text{-}$

7)](ClO$_4$)$_2$ confirmed the chiral recognition process. During the conversion of monomeric complex [Cu(**7**)(Cl)(H$_2$O)] (isolated as a racemic mixture) to the dimeric species *via* reaction with Ag$^+$, one can only obtain the homochiral dimers [Cu$_2$(*R*-**7**)$_2$](ClO$_4$)$_2$ and [Cu$_2$(*S*-**7**)$_2$](ClO$_4$)$_2$ as the final product; that is the recognition process remains active during the monomer-dimer conversion (Fig. 12).

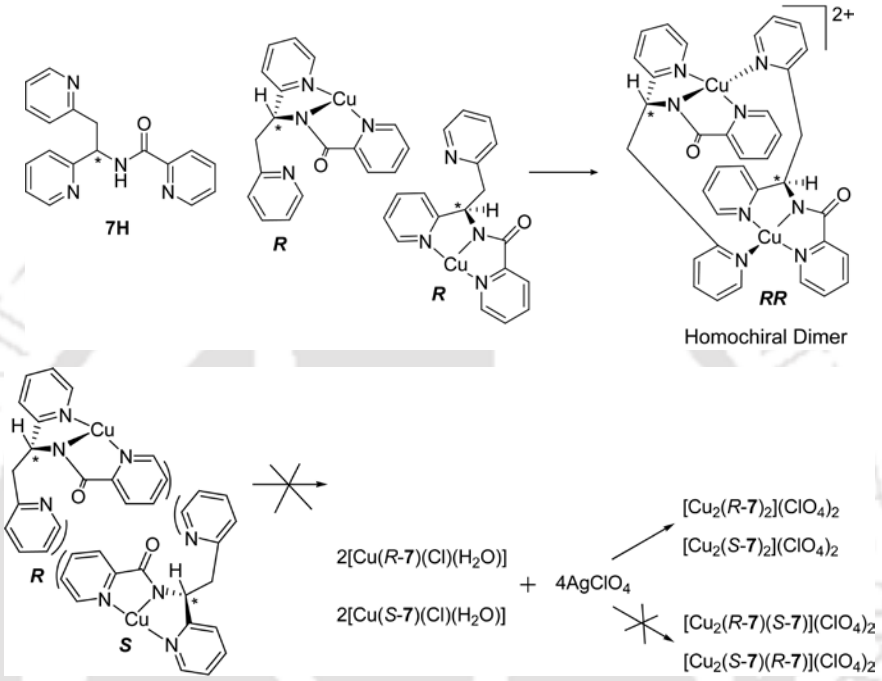

Fig. 12. Schematic representation of the dimerization of two [Cu(*R*-**7**)]$^+$ units (top) as well as [Cu(*S*-**7**)]$^+$ and [Cu(*R*-**7**)]$^+$ units (bottom left) and AgClO$_4$ mediated self-assembly (bottom right).

Binaphthyl derivative such as binaphthyl–bis–(amidopyridyl) derived ligands have a natural helicity due to the restricted rotation about the C–C bond of the binaphthyl moiety and so the complexes formed are helical in nature [156]. The amido pyridyl groups impart additional helicity and flexibility to the ligands and allows them to adopt a range of conformations, which may be modified by the formation of an intramolecular hydrogen bond between an N-H and C=O group [157–167]. The self-assembly of mercury(II) halides with the racemic form of binaphthyl–bis–(amidopyridyl) ligands [*rac*-**8** (2–Py) and *rac*-**9** (3–Py)] was reported by Puddephatt and his group [76–78, 168] (Scheme 4).

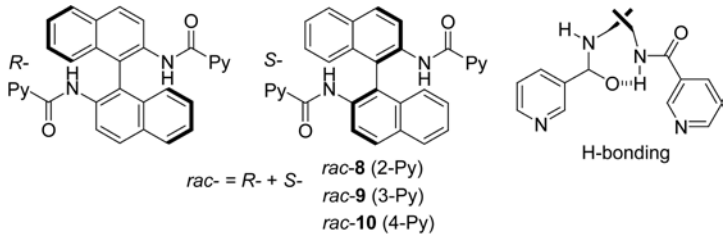

Scheme 4

In binaphthyl–bis–(amidopyridyl) derived ligand system, amide hydrogen bonding was important in organizing the polymers and macrocycles into ordered networks in the solid state. In the majority of complexes, the intermolecular hydrogen bonding occurred between ligands of opposite chirality (···*R*···*S*···), but in some complex, the hydrogen bonding was between ligands of like chirality (···*R*···*R*···, ···*R*···*S*···). The molecules of *rac*-**8** associate to form a racemic mixture of homochiral supramolecular polymers [···*R*···*R*···, ···*S*···*S*···] through hydrogen bonding between NH and pyridyl groups [N(1)···N(3A) = 3.008(2) Å]. In *rac*-**9**, the molecules were associate to form heterochiral polymers [···*R*···*S*···*R*···] through hydrogen bonding between NH and pyridyl groups [N(3)···N(4A) = 2.991(4) Å] (Fig. 13). The association of polymer chains through hydrogen bonding creates small pockets in the sheet structure where solvent molecules are encapsulated (Fig. 14).

The coordinating strength of anions such as $CF_3CO_2^-$, $CF_3SO_3^-$ and NO_3^{2-} and ligand structure on the self-assembly of silver complexes of *rac*-**9** and *rac*-**10** (4-py) has been reported [169]. In silver complexes of *rac*-**9** and *rac*-**10**, incorporation of amide moiety into the ligand backbone gives the potential for higher order self-assembly through H–bonding as well as through Ag···Ag interaction or through weak Ag···anion interaction. In case of $CF_3SO_3^-$ and NO_3^{2-}, the silver complexes self-assemble as heterochiral complex (Fig. 15). But in case of $CF_3CO_2^-$ anions, each polymer chain was homochiral with all binaphthyl groups having the same chirality having ···*RRR*···or ···*SSS*··· sequence and the pairs of homochiral chains are further associated through secondary bonding interactions to form a double stranded polymer with one ···*RRR*··· strand and one ···*SSS*··· strand, as shown in Fig. 16. This difference seems to be purely ligand dependent, with 4–pyridyl ligand (*rac*-**10**) gives the homochiral polymer whereas the 3–pyridyl ligand (*rac*-**9**) gives the heterochiral polymers.

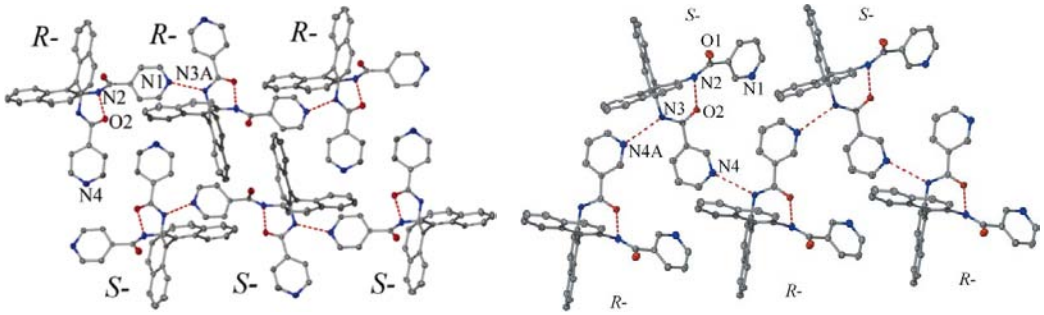

Fig. 13. The zig-zag polymeric structure formed by intermolecular N–H···N interactions in *rac*-**8** and *rac*-**9**.

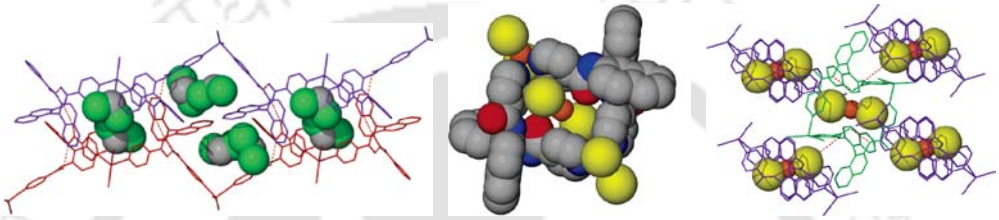

Fig. 14. Packing diagram containing solvent and guest molecules inside the channels of *rac*-**8** and *rac*-**9**.

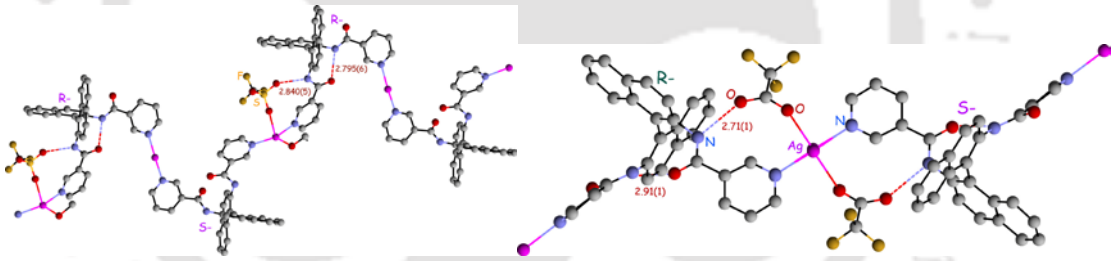

Fig. 15. Heterochiral polymeric chain in *rac*-**9** *via* N–H···O interactions in case of $CF_3SO_3^-$ anions

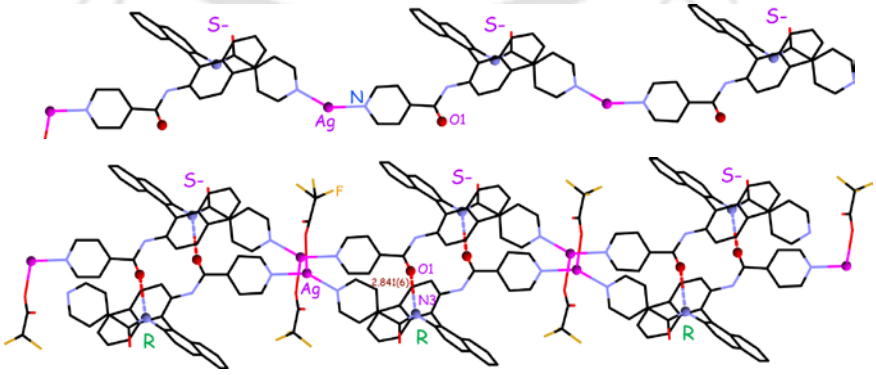

Fig. 16. Homochiral ···*SSS*··· chain (top) and double-stranded polymeric chain (bottom) in *rac*-**10**.

1.3.3 Self-assembly of macrocyclic ligand

The control of helicity at the supramolecular level is a fascinating challenge for chemists, and the construction of artificial helical compounds has attracted much attention recently, not only because of their aesthetically appealing topologies but also their potential applications in asymmetric catalysis and nonlinear optical materials [170–175]. The macrocyclic ligand, 5,5,7,12,12,14–hexamethyl–1,4,8,11–tetraazacyclotetradec–ane (**11**), was prepared 40 years ago by Curtis (Scheme 5) [176–178]. Its nickel(II) complexes exist as two diastereomers of *meso* and *rac* (racemic) forms (Fig. 17) [179–182]. In the *meso* form, the two asymmetric carbon atoms adopt opposite (*R* and *S*) configurations, while they adopt the same (*RR* or *SS*) configuration in the *rac* form. The two diastereomers can be separated by crystallization. The two isomers can interconvert with each other in solution as the energy difference between the two isomers is very small, so precise control the experimental conditions to form a defined isomer still remains difficult.

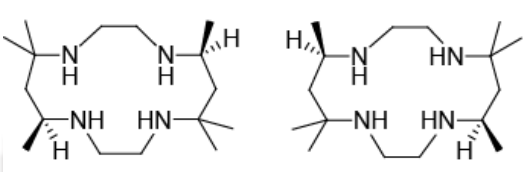

Scheme 5. Structure of *SS*-**11** and *RR*-**11**.

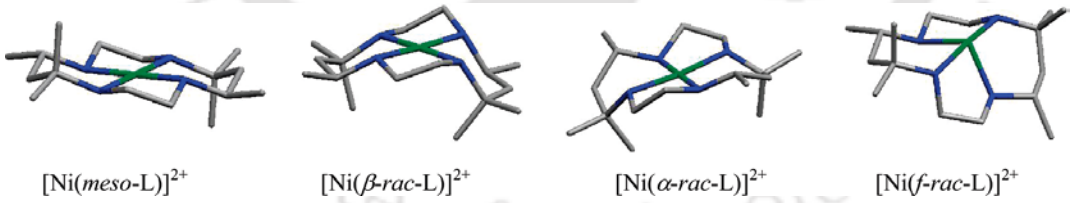

Fig. 17. Coordination geometries of *meso*-**11** and *rac*-**11** in nickel(II) complexes.

Dicyanamide (dca) directed helicity in nickel(II) complexes of macrocyclic ligand **5** has been reported [183]. The reactions of [Ni(*α*-*SS*-**11**)]$(ClO_4)_2$/[Ni(*α*-*RR*-**11**)]$(ClO_4)_2$ with dca gave two enantiomers of (a) [Ni(*α*-*SS*-**11**)]$(dca)_2$ and (b) [Ni(*α*-*RR*-**11**)]$(dca)_2$ whereas the reaction of racemic [Ni(*α*-*rac*-**11**)]$(ClO_4)_2$ with dca produced a trimer of (c) [Ni(*α*-*rac*-**11**)(dca)]$_3$·(dca)·$(ClO_4)_2$·MeCN in acetonitrile/water or acetonitrile/DMF mixture (Fig. 18). The [Ni(*α*-*SS*-**11**)]$(dca)_2$/[Ni(*α*-*RR*-**11**)]$(dca)_2$ monomers are linked

through intermolecular hydrogen bonds to form a two-dimensional sheet whereas {[Ni(*α*-*rac*-**11**)(dca)]$_3$}$_3$ forms a triangular structure in which the macrocyclic ligand **11** adopts unsymmetrical *RR*/*RR*/*SS* or *RR*/*SS*/*SS* configurations.

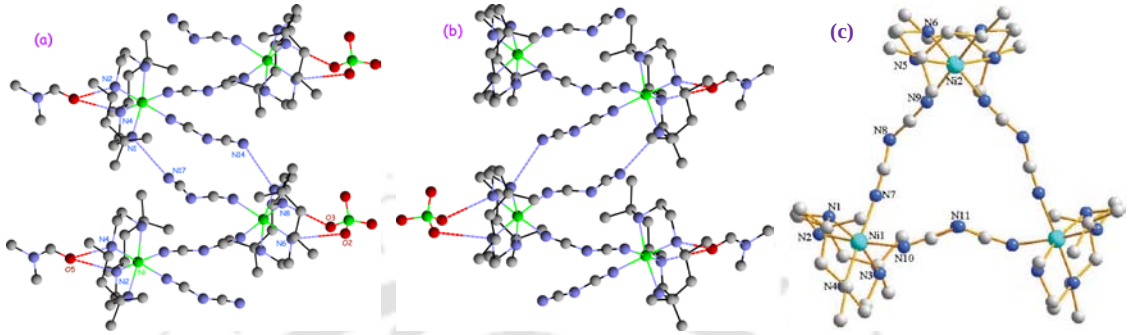

Fig. 18. The intermolecular hydrogen bonding interactions in [Ni(*SS*-**11**)](dca)$_2$ (a) and [Ni(*RR*-**11**)](dca)$_2$ (b) and the trinuclear complex {[Ni(*rac*-**11**)(dca)]$_3$}$_3$ (c).

The effect of pH on the helicity in nickel(II) complexes of macrocyclic ligand **11** has been studied [184]. Under acidic condition, the reactions of [Ni(*α*-*rac*-**11**](ClO$_4$)$_2$ with l/d-leucine gave the left-handed helical chains of {[Ni(*α*-*SS*-**1**)(*l*-HLeu)](ClO$_4$)$_2$}$_n$ (Λ) and right-handed helical chains of {[Ni(*α*-*RR*-**11**)(*d*-HLeu)](ClO$_4$)$_2$}$_n$ (Δ), respectively, in which two carboxylate oxygen atoms of the neutral l/d-leucine are coordinated to nickel(II) in *cis*-position, and the protonated nitrogen atom of l/d-leucine is not coordinated (Fig. 19). However, in basic condition, deprotonation of the nitrogen proton of l/d-leucine in Λ/Δ makes one carboxylate oxygen atom and one nitrogen atom in *cis*-position, changes the coordination model (Fig. 20). The changed coordination model of l-leu in Δ caused the helicity change from left-handed in Λ to right-handed in {[Ni(*α*-*SS*-**11**)(*l*-Leu)](ClO$_4$)}$_n$ (Δ). In contrast, the helicity was also changed from right-handed in Δ to left-handed in {[Ni(*α*-*RR*-**11**)(*d*-Leu)](ClO$_4$)}$_n$ (Λ). The effect of racemic penicillamine on nickel(II) complexes of macrocyclic ligand **5** for the construction of homochiral metal organic framework (HMOF) has been studied (Fig. 21) [185]. [Ni(*α*-*SS*-**11**)]$^{2+}$/[Ni(*α*-*RR*-**11**)]$^{2+}$ recognizes the l/d enantiomer from the racemic penicillamine to form [Ni(*α*-*SS*-**11**)(*l*-pen)]$^+$/[Ni(*α*-*RR*-**11**)(*d*-pen)]$^+$ respectively.

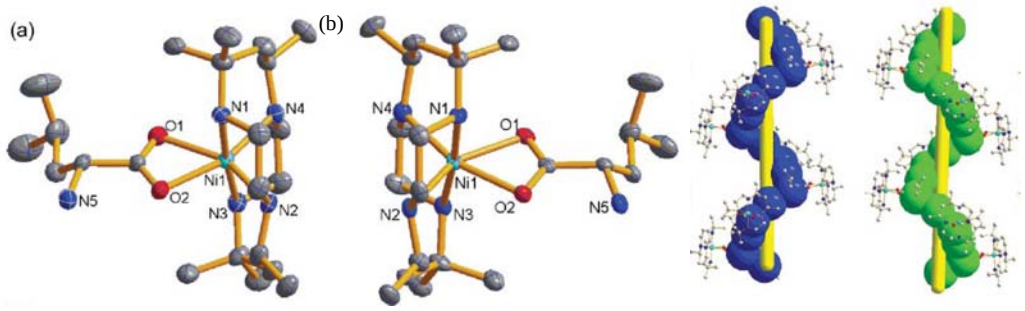

Fig. 19. A pair of enantiomers of (a) [Ni(*α*-*RR*-**11**)(*l*-HLeu)]$^{2+}$ (Δ**)** and (b) [Ni(*α*-*SS*-**11**)(*d*-HLeu)]$^{2+}$ (Λ) and their corresponding H–bonded right handed (blue) and left handed (green) helical chains.

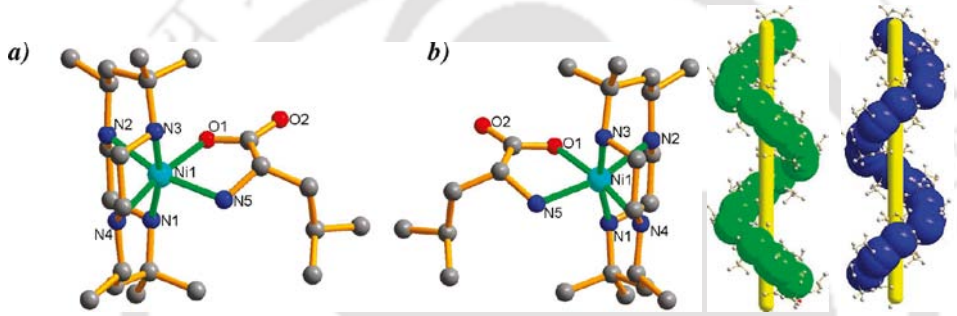

Fig. 20. Structures of (a) [Ni(*α*-*SS*-**11**)(*l*-Leu)]$^{+}$ (Δ) and (b) [Ni(*α*-*RR*-**11**)(*d*-Leu)]$^{+}$ (Λ) and their corresponding H–bonded right handed (blue) and left handed (green) helical chains.

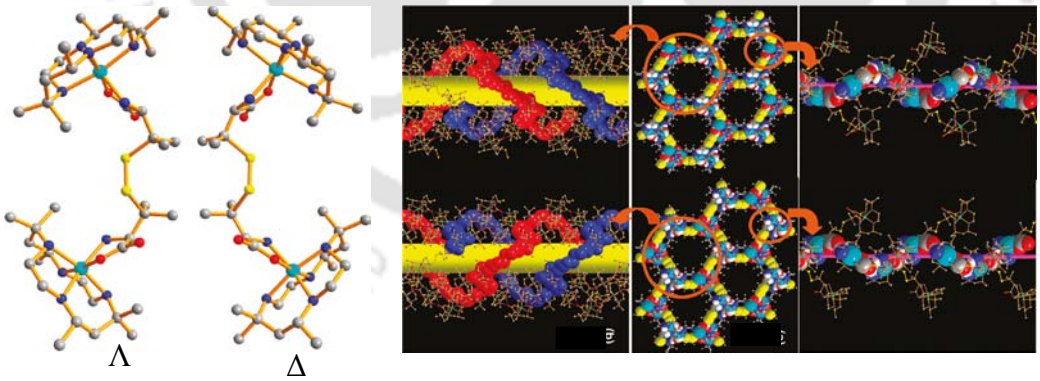

Fig. 21. Pair of enantiomers of {[Ni(*α*-*SS*-**11**)]$_2$(*l*-pends)}$^{2+}$ and {[Ni(*α*-*RR*-**11**)]$_2$(*d*-pends)}$^{2+}$ in Λ and Δ (left) respectively and their honeycomb-like 3D homochiral frameworks with 1D tubular pores (right).

In situ oxidation of (–SH) group of penicillamine results {[Ni(*α*-*SS*-**11**)]$_2$(*l*-pends)}$^{2+}$/{[Ni(*α*-*RR*-**11**)]$_2$(*d*-pends)}$^{2+}$ dimer. During the reaction of racemic [Ni(*α*-*rac*-

11)](ClO$_4$)$_2$ with racemic penicillamine under the same conditions, a conglomerate of Λ and Δ was generated in which each crystal is chiral. In addition, the chirality of the 1D tubular pores in 3D homochiral frameworks are controlled by the chirality of the precursors. The 1D hydrophobic chiral pores in Λ and Δ make it facile to recognize and separate racemic alcohols such as 2-butanol.

1.3.4 Self-assembly of box ligand(s)

Multi-component self-assembly of supramolecules relates to the design of functional materials such as catalysts, sensors, and molecular machines [186–194]. Two approaches are often employed to direct multi-component self-assembly: self-recognition or self-discrimination. These are typically reduced to practice by constructing pairs of complementary hydrogen-bonding motifs or pairs of ligands possessing complementary steric or electronic motifs to bias their assembly [195]. Metal-directed multi-component self-assembly for the formation of chiral, heteroleptic complexes in the design of new hetero bimetallic asymmetric catalyst systems are an active area of research. The reversible metal-directed multi-component self-assembly of chiral bisoxazolines has been reported which proceeds with a high level of chiral self-discrimination (Fig. 22) [196]. A neutral, homochiral complex Zn(*R*, *R*′-**12**) were isolated from the enantiopure box ligand (*R*, *R*′-**12**). However, when a racemic mixture of box ligands [i.e., 1 equiv. each of (*S*, *S*′)-**12** and (*R*, *R*′)-**12**] are combined with Zn(OAc)$_2$, three complexes can form: the homochiral complexes Zn(*S*, *S*′-**12**) and Zn(*R*, *R*′-**12**) (i.e., chiral self-recognition) and/or the heterochiral complex Zn(*R*, *S*-**12**) (i.e., chiral self-discrimination). The heterochiral complex Zn(*S*, *R*-**12**) exhibits near-perfect tetrahedral coordination while the homochiral complex (*S*, *S*′)-**12**, for which there are two closely related conformers in the unit cell, distorts from tetrahedral coordination to minimize steric interactions between the phenyl substituent of the two box ligands (Fig. 23).

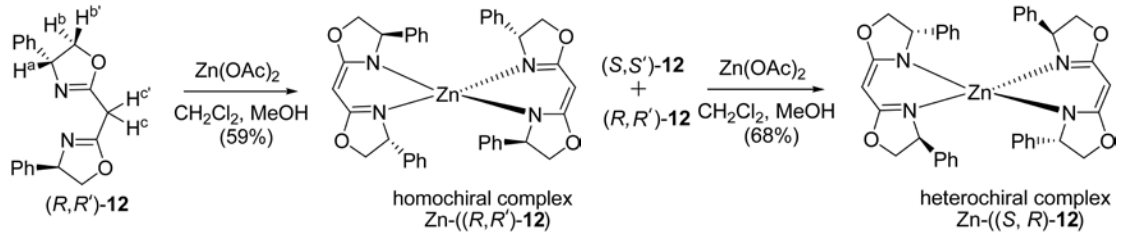

Fig. 22. Schematic representation for the synthesis of homo or heterochiral dimer in zinc(II) complexes of box ligand **12**.

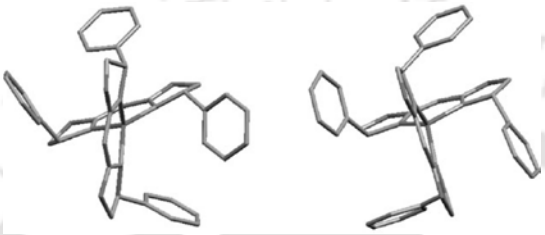

Fig. 23. The crystal structures of Zn(*S*, *S*-**12**) (left) and Zn(*S*, *R*-**12**) (right).

1.3.5 Self-assembly in Biology

Schiff bases have been proved for DNA replication process by substituting the static phosphodiester bonds found in the DNA backbone with a dynamic imine bond [197]. In this process, one end of a set of short oligonucleotides was modified with an aldehyde, while the other end of a different set of oligonucleotides was modified with a primary amine to allow for imine bond formation between pairs of oligonucleotides to take place (Fig. 24).

Competitive metathesis between two *N*–terminal imines of different lengths competes for the ligation to a *C*–terminal imine to form either an octomer or dodecamer [198]. To increase the size-selectivity of the formation of larger oligomers, a dumbbell-shaped guest was used as an additional driving force to template imine ligation of oligomers of certain sizes selectively (Fig. 25).

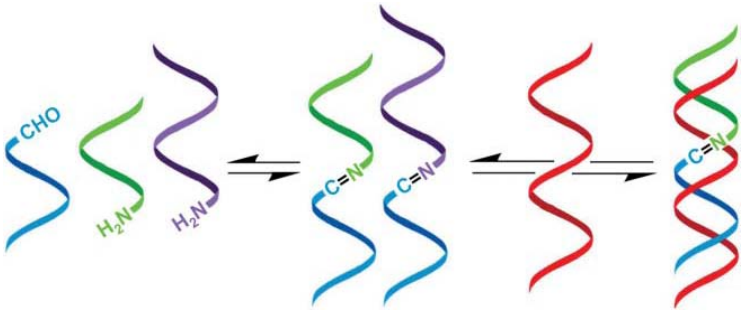

Fig. 24. Schematic representation of DNA replication.

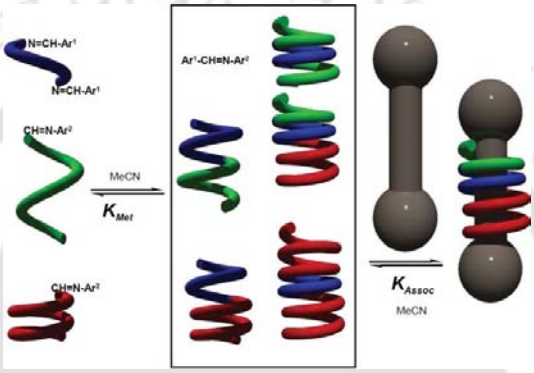

Fig. 25. Cartoon representation of the imine metathesis.

Binary hydrogen bond pairing such as A···T and G···C in a DNA double helix, plays an important role in the generation of supramolecular self-assembly and processing genetic information [93, 199]. Development of a new binary hydrogen bonding motifs may bring about not only a well-defined supramolecular architecture but also a processing method for molecular information in supramolecular chemistry [200]. The binary hydrogen bonding motifs of organic molecules incorporating two kinds or more of functional groups have been explored in the liquid and solid states [201]. Such molecules are designed to undergo self-assembly in a homolytic mode; however, control of selectivity between the homolytic and heterolytic modes is still a challenging problem due to structural interference between molecular functionalities and low energetic differences between the hydrogen bonding modes [202, 203]. On the other hand, homochiral recognition of a chiral molecule is a binary recognition process like a handshake, which is discrimination of the same and the opposite configuration. Homochiral recognition is usually mediated by stereoselective hydrogen bonding to result in two types of homochiral self assembly, *R*···*R* and *S*···*S*. A meso-compound incorporating both

enantiomeric interaction moieties has the potential to follow two types of chirality-directed self-assembly [204]: homochiral (*R*-*S*···*S*-*R*···*R*-*S*···) and heterochiral (*R*-*S*···*R*-*S*) self-assembly.

Enantiomeric self-recognition of nucleosides is particularly interesting, since the genetic material is homochiral [205, 206]. The cations dependent enantiomeric self-recognition of G-quadruplexes has been reported [207]. Cations of similar size, but of different charge, promote formation of stereoisomeric assemblies from the same racemic nucleoside. Specifically, (D, L)–5'–silyl–2',3'–*O*–isopropylidene guanosine (G **1**) forms homochiral aggregates in the presence of Ba^{2+} picrate but gives heterochiral diastereomers when K^+ is the guest (Fig. 26). Since $Ba^{2+}$and K^+ are similar in size, the cation's charge density is the major factor controlling enantiomeric self-association of (D, L)–G **1**.

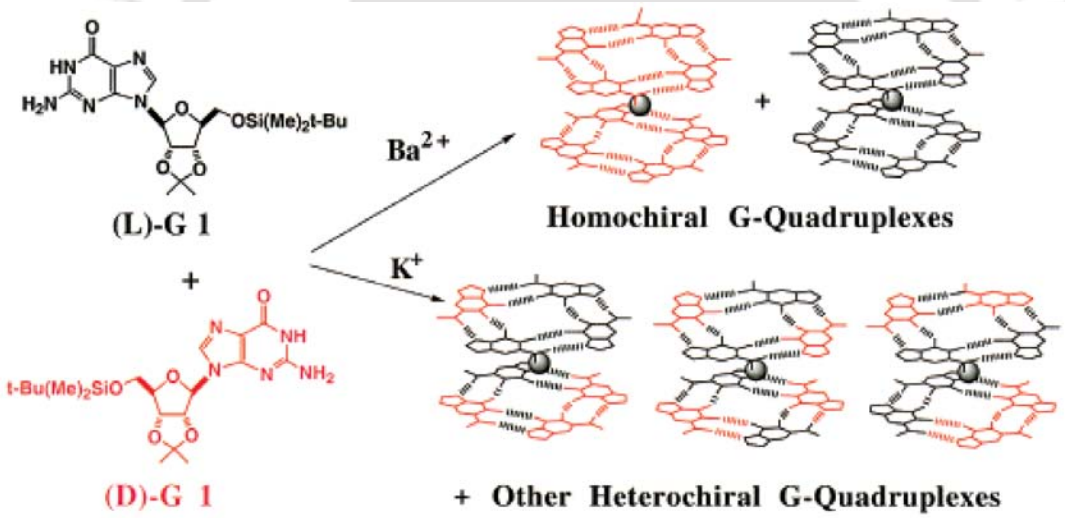

Fig. 26. Schematic representation showing cations dependent enantiomeric self-recognition of (D, L)–G **1**.

1.4 Application of chiral Schiff base complexes

Considerable interest exists in the coordination chemistry of transition metals with Schiff bases due to their wide range of applications and structural aspects of the resulting complexes [208–212]. Metal complexes of chiral Schiff bases have been used as catalysts in various reactions such as oxidation of olefins [213–215], polymerization of olefins [216–218], enantioselective epoxidation of olefins [147, 219, 220], enantioselective trimethylsilylcyanation of carbonyl compounds [221, 222], enantioselective ring opening of meso aziridines [223], asymmetric hetero-Diels-Alder reactions [224], and enantioselective cyclopropanation of olefins [225–227].

A large number of Schiff base complexes shows wide range of magnetic materials, including metamagnets [228], room-temperature magnets [229], spin-crossover materials [230], single-molecule magnets (SMMs) [231], single chain magnets (SCMs) [232], and photomagnets [233]. To enhance the intrachain interactions, short ligands, such as cyano, hydroxyl, azido, oxalate/oxamate, oximato and carboxylate, have most commonly been employed as bridging ligands because they can efficiently transmit magnetic coupling between adjacent spin centers [234]. In particularly chiral Schiff base complexes are important for the magneto-chiral dichroism (MChD), chiral magneto-structural effects, dielectric relaxation; second harmonic generation (SHG), chiral single chain magnets (SCMs) and chiral single molecule magnets (SMMs) [235–238].

Due to the flexibility of their stereochemistry, the luminescent d^{10} and Ln series metal complexes of Schiff base system exhibits various interesting structural features and potential applications in light emitting diodes (LEDs), biomedical analyses, fluorescence imaging and cancer phototherapy [239]. In photosynthesis manganese core containing Schiff bases, present in PSII plays a crucial role in the oxygen-evolving process [240]. Molecular organic cages obtained from Schiff bases has been shown to be effective and atom-economical and are attracted wide interest in host-guest systems, porous materials, catenanes, nano confined chemical reactions and inclusion of various guests [151, 241–245]. The stability of chiral Schiff bases plays very important role in chiral sensors, enantioselective adsorbents, catalysts, nano fibers, gel fiber formation and chiral recognition [199, 246, 247].

Along with the above mentioned application of Schiff bases, they also have pronounced biological activities against microbes, viruses, cancer cells, cell viability, DNA binding and photo cleavage [248–258].

1.5 Definition of the Problem

"**Diastereoselectivity in Bimetallic Complexes Containing Chiral Tridentate Ligands**"

Most previous reports have used enantiopure ligands and hence the compounds formed from them are necessarily homochiral. Reactions with racemic ligands result in either ligand self-recognition (homochiral complex) or ligand self-discrimination (heterochiral complex). When coordination polymers are formed, ligand self-assembly can occur with ligand self-recognition to give homochiral polymers and the crystal will most commonly contain a racemic mixture. The solid state structures will then necessarily differ significantly from that of the homochiral polymer prepared from the enantiopure ligand. The self-assembly can therefore be significantly important when using racemic ligands. As inferred from the literature survey, the self-assembly of racemic tridentate Schiff bases around **dimetallic (M_2X_2) core** (X = O, N, Cl) was not explored. So "*a study has been undertaken, to understand the self-assembly of racemic tridentate Schiff base ligands around the dimetallic center, by using different metal centers, bridging ligands as well as some amine ligands?*" and the results are delineated in the subsequent Chapters of this thesis.

1.6 Materials and Methods

1.6.1 Materials

$Cu(NO_3)_2 \cdot 3H_2O$, $Cu(ClO_4)_2 \cdot 6H_2O$, $CuCl_2 \cdot 2H_2O$, $CuSO_4 \cdot 5H_2O$, $Ni(NO_3)_2 \cdot 6H_2O$, $Ni(OAc)_2 \cdot 4H_2O$, $NiCl_2 \cdot 4H_2O$, $Zn(NO_3)_2 \cdot 6H_2O$, 2–hydroxy benzaldehyde, NaN_3, anahydrous $MgSO_4$, anahydrous Na_2SO_4, Zn dust, KOH, CH_3COONa, NaOH and $NaBH_4$ were purchased from Merck India. 2–acetyl pyridine, 2–benzoyl pyridine, 2–hydroxy–1–naphthaldehyde, NaNCO, NaSCN, KSCN, NH_4SCN, KNCO, $NaN(CN)_2$, $CDCl_3$, DMSO–d^6 and KBr were from M/S Aldrich, USA. All the chemicals and solvents were of reagent grade and were used as received without further purifications.

1.6.2 Instrumentation and Methods

Elemental analysis was performed by Elemental analyses were performed using a Carlo Erba 1108 elemental analyzer or Perkin-Elmer Series II CHNS/O Analyzer 2400. UV–Vis spectrum was recorded in Perkin-Elmer Lambda 25 spectrometer. Waters Q–TOF premier mass spectrometer. FT–IR spectrum in the range 4000–250 cm^{-1} was recorded using Perkin-Elmer spectrum one. Cary Eclipse EL05033882 was used for fluorescence spectra. ^1H and ^{13}C–NMR spectrum was recorded on a Varian Mercury plus 400 MHz NMR Spectrometer. A Lakshore VSM setup for room temperature magnetic data, were used for performing the relevant measurements.

1.6.3 EPR Measurements

The X–band EPR spectrum (9.056 GHz frequency and 0.998 mW power) was recorded on a JEOL JES FA–200 X–band EPR spectrometer having a maximum field of 1.30 T with a spin sensitivity of 5×10^9 spins / 10^{-4} T (at 100 kHz modulation) and homogeneity 1×10^{-5}. The measurement of g-tensors was achieved using the MnO lines marker which acts as a spin standard. The modulation frequency was 100 MHz, with a width of 0.35 mT kept constant for all the samples. The spectrometer fitted with a quartz dewar for measurements at liquid nitrogen temperature. The spectra were recorded for the polycrystalline sample or its solution at room as well 77 K using suitable glass forming solvents within 0–800 mT.

1.6.4 X-ray Crystallography

X-ray crystallographic data were collected using Bruker SMART APEX–CCD diffractometer with Mo Kα radiation (λ = 0.71073Å). The intensity data were corrected for Lorentz and polarization effects and empirical absorption corrections was applied using SAINT program [259, 260]. All the structures were solved by direct methods using SHELXS–97 [261]. Non-hydrogen atoms located from the difference Fourier maps were refined anisotropically by full-matrix least-squares on F^2, using SHELXL–97 [261]. The hydrogen atoms were included in the calculated positions and refined isotropically using a riding model and in some cases it has been added.

1.6.5 Thermal Measurements

Thermogravimetry were studied by a computer controlled METTLER TOLEDO STAR^e system of module TGA/SDTA851^e under static nitrogen atmosphere using platinum pan at a heating rate of 10 °C min^{-1} in the temperature range 25–700 °C. The instrument was calibrated using RTypSDTA sensor. Onset temperature obtained from DTG curve is used to evaluate the onset decomposition temperature of the samples.

Chapter 2

Molecular Structures of Nickel(II) Monochelates of a Racemic Tridentate Ligand and Co-ligand Induced Structural Variations†

Abstract

Using a racemic mixture of the chiral tridentate ligand, 2–((1–(2–pyridyl)ethylimino)methyl)phenolate ion (**L1**) and N_3^-, NCS^-, $(NC)_2N^-$, OAc^- as co-ligands, complexes having the formula [Ni(**L1**)(N_3)] (**1**), [Ni(**L1**)(NCS)]$_2$ (**2**), [Ni_2(**L1**)$_2$(OAc)(N(CN)$_2$)]$_n$ (**3**) were prepared and structurally characterized. In **1**, Ni(II) has a square planar geometry and phenolate oxygen is involved in dipolar $O_P^{\delta-}\cdots N^{\delta+}$ interaction with electrophilic central nitrogen atom of coordinated azide ion. Complex **2** is dimeric in nature and nickel(II) is *penta*-coordinated. Compounds **1** and **2** exist as centrosymmetric dimers made up of a pair of *R* and *S* enantiomers of **L1**. In **3**, an acetate and phenoxo bridged dinickel complex is present which is further linked to a zig-zag coordination polymer by end–on–end dicyanamide ion. In a given chain of **3**, both **L1** have same enantiomeric form and either *RR* or *SS* dimers are repeated along the chain. The magnetic properties are described.

† This work has been published in:

H. S. Jena, J. Subramanian, V. Manivannan, Inorg. Chim. Acta 365 (2011) 177–182.

Molecular Structures of Nickel(II) Monochelates of a Racemic Tridentate Ligand and Co-ligand Induced Structural Variations

In this Chapter, synthesis and structural characterization of three racemic Ni(II) complexes derived from the chiral tridentate Schiff base ligand, 2–((1–(2–pyridyl)ethylimino)methyl)phenolate ion (**L1**) and Ni(II) salts in presence of co-ligands such as N_3^-, SCN^-, $N(CN)_2^-$ and OAc^- are described. The structural characterization of these three complexes reveal the presence of rare occurrences of (a) involvement of the electrophilic central nitrogen atom of the coordinated azide in a $O_P^{\delta-}\cdots N^{\delta+}$ type dipolar interaction with the phenolate oxygen (b) existence of a distorted square-pyramidal coordination geometry around the Ni(II) ion and (c) a co-ligand dependent hetero- or homochiral dimerization of the monochelates around the dimetallic core.

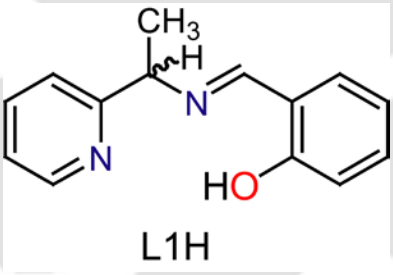

L1H

2.1 Experimental

2.1.1 Syntheses

(*R*, *S*) 1–(2–pyridyl)ethylamine is prepared using the same reported procedure [262].

*2.1.1.1 (R, S) 2-(1-(pyridin-2-yl)ethylimino)methyl)phenol (**L1H**)*

A mixture of 1–(2–pyridyl)ethylamine (4.5 g, 0.036 mol) and 2–hydroxy benzaldehyde (4.5 g, 0.036 mol) in 50 mL methanol was heated at reflux for 3 h. The solvent was removed in vacuum and the remaining yellow oil was triturated with a 1:1 methanol-water (10 mL) mixture. The resultant yellow oil was dried in desiccators over P_4O_{10} and was pure enough as inferred from the ^{1}H NMR spectrum, to be used without further purification. Yield: 7.0 g (86%). ESI-MS: *m/z* calcd. for $C_{14}H_{14}N_2O^+$ 226.11. Found

(M^++H) 227.11. IR (KBr, cm^{-1}): 3445, 2975, 2930, 1630, 1589, 1460, 1277, 1207, 1150, 1130, 976, 755. 400 MHz ^{1}H NMR (δ (*J*, Hz), $CDCl_3$): 13.52 (OH, s), 8.55 (1H, d, 5.6), 8.51 (1H, s), 7.68 (1H, t, 7.8), 7.45 (1H, d, 7.6), 7.32 (1H, d, 8.4), 7.29 (1H, t, 6.0), 7.18 (1H, t, 6.2), 6.99 (1H, d, 8.4), 6.89 (1H, t, 7.4), 4.71 (1H, q, 6.8), 1.96 (3H, d, 6.8). 100 MHz ^{13}C NMR (δ, $CDCl_3$): 164.1, 161.7, 160.5, 148.4, 136.3, 131.9, 131.2, 121.8, 120.0, 118.3, 118.2, 116.4, 69.3, 22.7.

*2.1.1.2 [Ni(**L**)(N_3)] (**1**)*

To a methanol (10 mL) solution of $NiCl_2 \cdot 6H_2O$ (1.05 g, 4.0 mmol) was added **L1H** (1 g, 4.0 mmol) dissolved in methanol (30 mL). To this mixture Et_3N (0.404 g, 4.0 mmol) was added and the resulting mixture was heated at reflux for 2 h. Solid sodium azide (0.3 g, 4.0 mmol) was added and reflux was continued for another 1 h. Red crystals of **1** deposited and were collected by suction filtration, washed with cold methanol and dried over $CaCl_2$. Yield: 1.0 g (78 %). *Anal*. Calc. for $C_{14}H_{13}N_5ONi$: C, 51.58; H, 4.02; N, 21.48%. Found: C, 51.49; H, 4.00; N, 21.35%. Selected IR (KBr, cm^{-1}) bands: 3430, 2980, 2932, 2035 (azide), 1614, 1568, 1449, 1357, 1096, 1033, 774, 760. UV–Vis [λ_{max}, nm (ε, $M^{-1}cm^{-1}$), CH_3OH solution]: 850(19); 745(12); 575(11); 390(2610); 282(6450).

*2.1.1.3 [Ni(**L**)(NCS)]$_2$ (**2**)*

To a methanol (10 mL) solution of $NiCl_2 \cdot 6H_2O$ (1.05 g, 4.0 mmol) was added **L1H** (1 g, 4.0 mmol) dissolved in methanol (30 mL). To this mixture Et_3N (0.404 g, 4.0 mmol) was added and the resulting mixture was heated at reflux for 2 h. Solid potassium thiocyanate (0.430 g, 4.0 mmol) was added and reflux was continued for 1 h. The solvent was removed and the residue was dissolved in CH_3CN (30 mL) and the resulting solution was left undisturbed at room temperature. The green crystals deposited after a week were collected by suction filtration, washed with ice-cold methanol and dried over $CaCl_2$. Yield: 1.12 g (75 %). *Anal*. Calc. for $C_{15}H_{13}N_3OSNi$: C, 52.67; H, 3.83; N, 12.29%. Found: C, 52.50; H, 3.82; N, 12.20%. Selected IR (KBr, cm^{-1}) bands: 3430, 2924, 2088 (thiocyanate), 1633, 1600, 1540, 1446, 1402, 1301, 1025, 903, 750, 737. UV–Vis [λ_{max}, nm (ε, $M^{-1}cm^{-1}$), CH_3OH solution]: 630(470); 458(455); 375(10240); 270(35880).

*2.1.1.4 $[Ni_2(\mathbf{L})_2(OAc)((NC)_2N)]\cdot(CH_3CN)\cdot(H_2O)$ (**3**)*

To a methanol (10 mL) solution of $Ni(OAc)_2\cdot 4H_2O$ (0.990 g, 4.0 mmol) was added **L1H** (1 g, 4.0 mmol) dissolved in methanol (30 mL). To this mixture Et_3N (0.404 g, 4.0 mmol) was added and the resulting mixture was stirred for 2 h. Solid sodium dicyanamide (0.356 g, 4.0 mmol) was added and the solution heated at reflux for 1 h. The solvent was removed and the green residue was washed with ice-cold methanol. Yield: 1.04 g (69%). Single crystals of **3** suitable for X-ray diffraction study were obtained by layering the CH_3CN solution of the crude green solid over dichloromethane. *Anal*. Calc. for $C_{34}H_{34}N_8O_5Ni_2$: C, 54.30; H, 4.56; N, 14.90%. Found: C, 54.17; H, 4.48; N, 14.87%. Selected IR (KBr, cm^{-1}) bands: 3430, 2277, 2170 (dicyanamide), 1643, 1594, 1410, 1327, 1050, 898, 764, 756. UV–Vis [λ_{max}, nm (ε, $M^{-1}cm^{-1}$), CH_3OH solution]: 842(43); 746(31); 573(25); 373(11630); 281(16050).

2.2 Molecular structures

The molecular structures of **1**–**3** were determined using single-crystal X-ray diffraction techniques. The crystal data and refinement parameters are listed in Table 1. Selected bond parameters observed in **1** and **2** are listed in Table 2. Selected bond parameters observed in **3** is listed in Table 3.

Compound **1** crystallized in space group *C*2/*c*. The Ni(II) atom is bound by the *meridionally* coordinating tridentate ligand **L1** and by a monodentate azide ligand. The bivalent nickel has a distorted square-planar geometry. **L1** is bound to the Ni(II) atom by a five-membered and a six-membered chelate ring. The asymmetric carbon atom deviate from the otherwise nearly planar five-membered chelate ring, which is evident from the dihedral angle of 6.97º between the two planes C5C6N2 and C5N1Ni1N2. The six-membered chelate ring is slightly puckered and has an envelope form with the Ni1 being displaced out-of-plane, as is inferred from the dihedral angle of 8.83º between the planes formed by N2Ni1O1 and O1C14C9C8N2. The Ni–N_P bond length is longer than Ni–N_I bond (N_P = pyridyl–N; N_I = imine–N) and these two are shorter than the Ni–N_A (N_A = azide–N). The azide ligand is coordinated in the usual end-on bent fashion with the bending being uniquely towards the phenolic oxygen atom and is also out-of-plane from the donor atoms of **L1** (the torsional angle between O1–Ni–N3 and Ni–N3–N4 is 15.28º).

Significantly, the O1 atom of the phenol group is involved in a dipolar interaction (O1···N4 = 2.612(3) Å) with the central nitrogen atom of the coordinated azide group. It is pertinent to note that as per the valence structure of the N_3^- ion, the central nitrogen atom is electrophilic in nature [263] and hence the dipolar $O_P^{\delta-}\cdots N^{\delta+}$ interaction with the phenolate oxygen (O_P = phenolate–O) atom is explained. Probably this interaction partially compensates for the lack of O_P bridged heterochiral dimerization as are observed in **2** and **3** (*vide infra*). Such a dipolar interaction can also be traced to a few other cases but they have longer non-bonded contacts (2.836(8) – 3.333(4) Å) [264–266]. In another case an intermolecular dipolar interaction between the central and terminal nitrogen atoms of the azide ion has also been observed [267].

Table 1. Crystallographic data and refinement parameters for complexes **1–3**.

	1	**2**	**3**
Formula	$C_{14}H_{13}N_5NiO$	$C_{15}H_{13}N_3NiOS$	$C_{34}H_{34}N_8Ni_2O_5$
CCDC number	761006	761007	761008
Formula weight	326.00	342.05	752.08
T (K)	296(2)	296(2)	296(2)
Wavelength (Å)	0.71073	0.71073	0.71073
Crystal system	Monoclinic	Monoclinic	Monoclinic
Space group	*C*2/c	$P2_1/n$	$P2_1/c$
a (Å)	19.9346(8)	7.5309(4)	11.3420(8)
b (Å)	7.3389(2)	18.0493(9)	19.6294(15)
c (Å)	19.5348(7)	11.6295(6)	15.6958(11)
β (°)	106.684(3)	108.467(3)	101.618(5)
V (Å^3)	2737.59(17)	1499.37(13)	3422.9(4)
Z	8	4	4
D_{calcd} (g m^{-3})	1.582	1.515	1.459
μ (mm^{-1})	1.423	1.434	1.155
F(0 0 0)	1344	704	1552
Reflection collected	3135	3414	5355
Unique reflections	2038	1703	3244
Goodness-of-fit (GOF)[a] on F^2	1.013	1.013	1.019
R_1[b], wR_2[c] ($I \geq 2\sigma(I)$)	0.0284, 0.0739	0.0508, 0.0763	0.0504, 0.0985
R_1[b], wR_2[c] (all data)	0.0395, 0.0779	0.1363, 0.0925	0.1050, 0.1173

[a]GOF = $\sum[w(F_0^2 - F_c^2)^2] / M - N]^{1/2}$ (M =number of reflections, N = number of parameters refined).
[b]$R_1 = \sum \| F_0 | - | Fc \| / \sum | F_0$, [c]$wR_2 = [\sum[w(F_0^2 - F_c^2)^2] / \sum[w(F_0^2)^2]]^{1/2}$

During the synthesis of **L1H**, a racemic mixture of the 1–(2–pyridyl)ethylamine has been used. Accordingly the crystal lattice is made up of an equal mixture of *R* and *S* enantiomers of **L1** bound to the Ni(II) ion. A packing diagram reveals that the complex exists in the form of centrosymmetric dimers (heterochiral dimers) made up of *R* and *S* enantiomers and a perspective view of the dimer $[Ni(\mathbf{L1})(N_3)]_2$ is displayed in Fig. 1. As a result the crystal lattice is racemic in nature. The dimer is held together by the weak interaction, Ni1···N3 (3.130(2) Å) leading to formation of a rectangular Ni_2N_2 unit and the non-bonded Ni···Ni distance within this rectangle is 3.960(1) Å.

Complex **2** crystallized in the $P2_1/n$ space group and the Ni(II) atom is bound by the *meridionally* coordinating tridentate ligand **L1** and by the nitrogen end of the ambidentate thiocyanate ion. Overall the bivalent nickel has a distorted square-pyramidal geometry. Both the five- and six- membered chelate rings are puckered. Ongoing from **1** to **2**, as a result of the effective increase in coordination number, lengthening of all the Ni–N and Ni–O bonds are observable. In **2**, the $Ni–N_P$ bond length is longer than $Ni–N_I$ bond and the Ni–O bond is shorter than the Ni–N bonds. Packing diagram reveals that the crystal lattice is racemic and the centrosymmetric dimeric unit $[Ni(\mathbf{L1})(NCS)]_2$ has *R* and *S* mixture of **L1**. A perspective view of the heterochiral dimer is displayed in Fig. 2.

Table 2. Selected bond distances (Å) and angles (º) in **1** and **2**.

	1	**2**
Ni1–N1	1.8928(17)	2.007(3)
Ni1–N2	1.8545(13)	1.930(3)
Ni1–N3	1.9078(15)	1.942(3)
Ni1–O1	1.8195(13)	1.921(2)
Ni1–O1A		2.407(2)
O1–Ni1–N1	178.39(6)	174.27(12)
O1–Ni1–N2	94.85(6)	92.09(11)
O1–Ni1–N3	88.64(7)	91.69(11)
N1–Ni1–N3	91.71(7)	93.80(14)
N1–Ni1–N2	84.97(7)	82.20(14)
N2–Ni1–N3	173.03(6)	167.23(13)
N1–Ni1–O1A		93.74(11)
N2–Ni1–O1A		98.87(10)
N3–Ni1–O1A		93.47(11)
O1–Ni1–O1A		87.56(9)

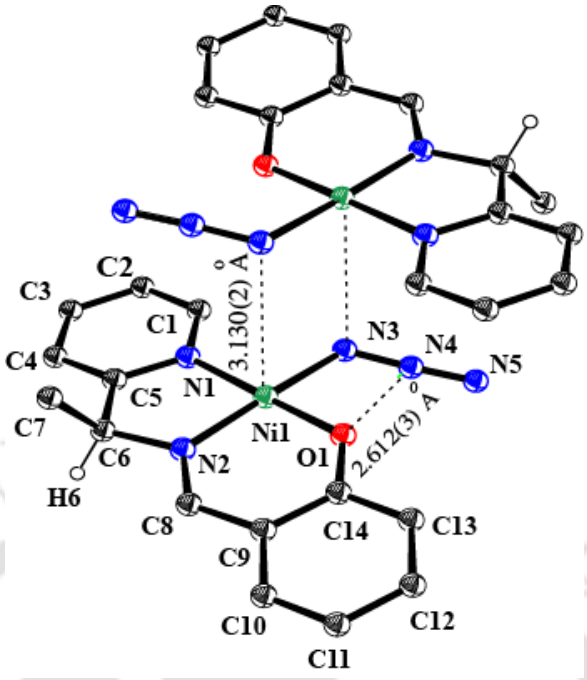

Fig. 1. A shaded-ball and stick model for **1** (H–atoms except H6 are omitted for clarity).

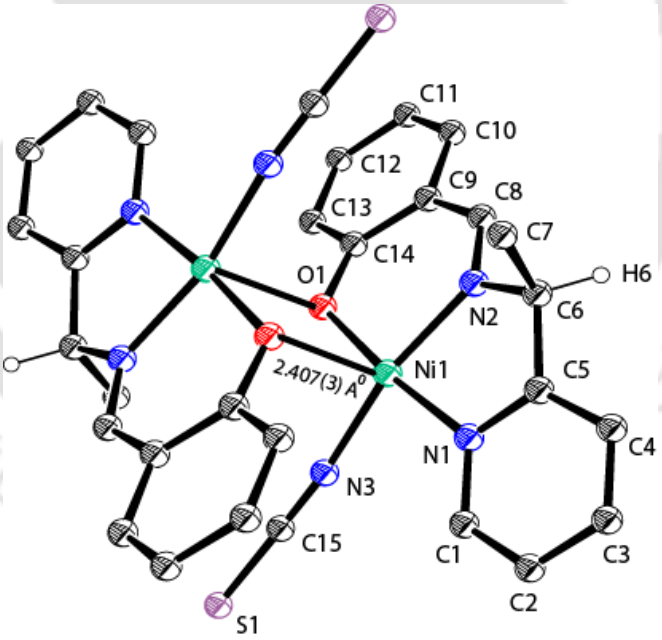

Fig. 2. ORTEP diagram (30%) and atom labeling scheme in **2** (H–atoms except H6 are omitted for clarity).

The dimer is held by a strong Ni1···O1 (2.407(3) Å) interaction. Therefore a rectangular Ni_2O_2 unit is formed with a non-bonded Ni···Ni distance of 3.143(1) Å. It is relevant to say that the rectangular Ni_2N_2 (in **1**) and Ni_2O_2 cores (in **2**) has the center of symmetry

inside the rectangular unit and hence lead to the formation of a heterochiral dimers. A square-pyramidal complex ion $[Ni(NCS)_5]^{3-}$ has been reported recently [268] having a calculated τ value [269] of 0.003 – 0.093 and the same in **2** is 0.117, which is suggestive of a distorted square-pyramidal geometry around the nickel atom.

Complex **3** crystallizing in the $P2_1/c$ space group, contains a *hexa*-coordinated dinickel complex having the $\{Ni_2(\mu\text{–}O_P)_2(\mu\text{–}OAc)\}$ core, in which the two Ni(II) atoms are bridged by an acetate ion and by two phenoxo groups. Each of the Ni(II) atoms in the dinickel core is further bound by the tridentate mono anionic ligand **L1** and by the terminal nitrogen of the dicyanamide ligand. Both the nickel centers have distorted pseudo-octahedral geometry and the dicyanamide ion link make them into a zig-zag 1D coordination polymer (*vide infra*). The perspective views of two distinct $[Ni_2(\mathbf{L1})_2(OAc)((NC)_2N)]$ units present in the lattice is displayed in Fig. 3. **L1** is bound to the Ni(II) atom by a five-membered and a six-membered chelate ring and both the chelate rings are puckered.

Ongoing from **1** to **3**, as the result of the effective increase in coordination number, a systematic lengthening of all the Ni–N and Ni–O_P bonds is observable. As in **2**, the Ni–N_P bond length in **3** is also longer than Ni–N_I bond. The two nickel atoms are unsymmetrically bridged by the phenolate oxygen atom: the Ni1–O1 distance is shorter by 0.189(3) Å than the Ni2–O1 distance; the Ni1–O2 distance is longer by 0.212(3) Å than the Ni2–O2 distance. The acetate ion is slightly asymmetrically bridging forming Ni–O distances of 2.013(3) and 2.029(3) Å. The $[NiO_P]_2$ core has a butterfly shape with an angle of 141.02º and the non-bonded Ni···Ni distance is 3.110(1) Å. The Ni–N_A distance of 1.9078(15) Å in **1** is smaller than the reported range (2.017(5)–2.249(8) Å) for terminally coordinating Ni–N_A bonds [270–273]. This is due to difference in the coordination numbers and same trend is also observed in the values of Ni–N_I, Ni–N_P and Ni–O_P bond distances. The Ni–N_T (thiocyanate–N) distance of 1.942(3) Å is also smaller than the reported range 1.978(5)–2.158 (4) Å [274]. All the Ni–N and Ni–O distances observed in **3** lies in the range of values found in similar reported compounds [275–277].

The packing diagram of **3** reveals several interesting features. Although, overall crystal lattice is achiral and an equal amount of *R* and *S* forms of **L1** are present, *R* and *S*

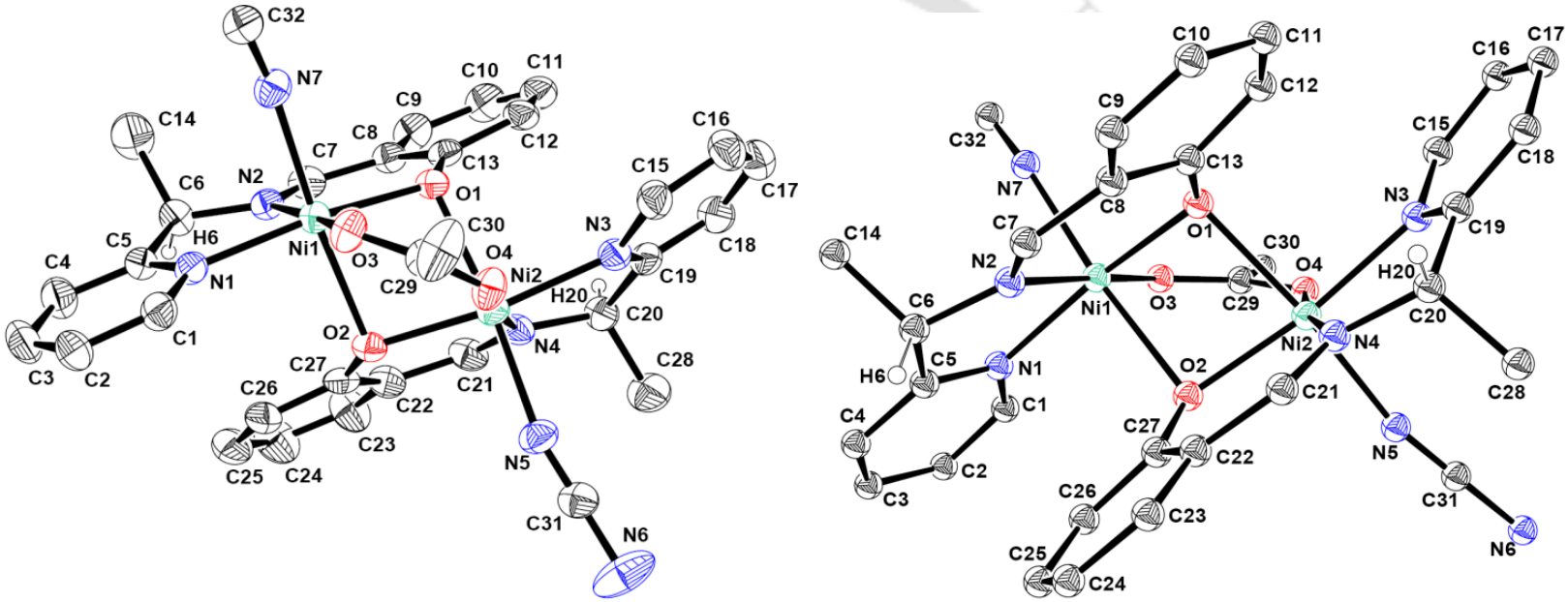

Fig. 3. ORTEP diagram (30%) and atom labeling scheme of *RR*– and *SS*–[Ni_2(**L1**)$_2$(OAc)((NC)$_2$N)] units in **3** (All H–atoms except H6 are omitted for clarity).

moieties are clearly segregated. In a given dimeric unit both the **L1** groups have the same enantiomeric forms (in contrast to the presence of *R* and *S* mixture within a dimer that is observed in **1** and **2**) that are either *RR* or *SS* forms. Since the $\{Ni_2(\mu\text{–}O_P)_2(\mu\text{–}OAc)\}$ core cannot have a center of symmetry within the core, homochiral dimer has formed.

The zig-zag polymeric chain formed in **3** contains exclusively either *RR* or *SS* homochiral dimers and a schematic representation is shown in Fig. 4. Therefore there are two types of homochiral chains *viz.*, *RR* and *SS* chains and these two chains are packed alternatively such that *RR* chains are surrounded by the *SS* chains and *vice versa*. The homochiral dimeric 1D chains are symmetrically related to their opposites by center of symmetry. The shortest intra-chain distance between the two nickel atoms of the adjacent dimers is 7.771 Å and that of the inter chain is 8.009 Å. A single layer in the packing diagram on viewing down the *a*-axis is depicted in Fig. 5. The solvate water is involved in hydrogen-bonding with the O4 of acetate ion and the non-bonded O4···O5 contact is 2.930(7) Å.

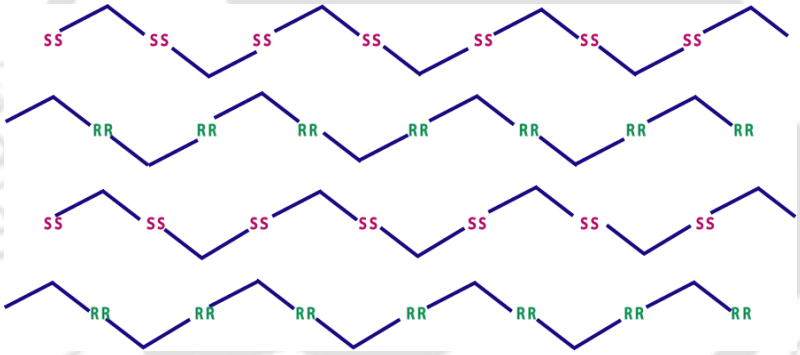

Fig. 4. Schematic representation showing 1D chains of *RR* and *SS* forms in **3**.

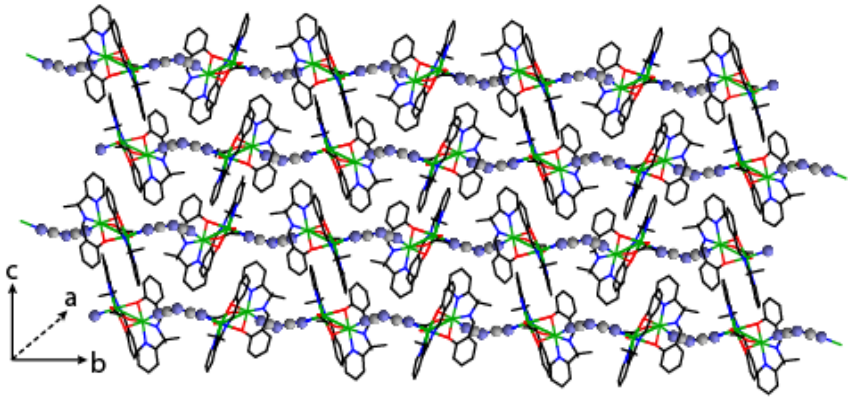

Fig. 5. Packing diagram showing the zig-zag chains of $[Ni_2(\mathbf{L1})_2(OAc)((NC)_2N)]_n$ in **3**.

Table 3. Selected bond distances (Å) and angles (º) in **3**.

		3	
Ni1–N1	2.066(4)	Ni(2)–N(3)	2.084(4)
Ni1–N2	1.987(4)	Ni(2)–N(4)	1.990(4)
Ni1–N7	2.106(5)	Ni(2)–N(5)	2.106(5)
Ni1–O1	2.015(3)	Ni(2)–O(1)	2.204(3)
Ni1–O2	2.234(3)	Ni(2)–O(2)	2.022(3)
Ni1–O3	2.029(3)	Ni(2)–O(4)	2.013(3)
N1–Ni1–N7	91.42(16)	N3–Ni2–O1	91.10(13)
N1–Ni1–O2	92.88(14)	N4–Ni2–N5	90.63(17)
N2–Ni1–N1	80.90(17)	N4–Ni2–N3	80.37(17)
N2–Ni1–N7	90.84(16)	N4–Ni2–O1	90.50(13)
N2–Ni1–O1	92.77(15)	N4–Ni2–O2	92.52(15)
N2–Ni1–O2	93.11(14)	N4–Ni2–O4	169.74(16)
N2–Ni1–O3	171.27(16)	N5–Ni2–O1	172.71(15)
O1–Ni1–N1	169.84(14)	O2–Ni2–N3	168.22(14)
O1–Ni1–N7	96.64(15)	O2–Ni2–N5	94.59(15)
O1–Ni1–O2	79.47(12)	O2–Ni2–O1	80.04(12)
O1–Ni1–O3	95.55(13)	O4–Ni2–O2	97.16(13)
O3–Ni1–N1	91.21(15)	O4–Ni2–N3	90.61(15)
O3–Ni1–N7	85.61(15)	O4–Ni2–N5	85.26(16)
O3–Ni1–O2	90.98(13)	O4–Ni2–O1	90.50(13)
N7–Ni1–O2	174.57(14)	Ni2–O2–Ni1	93.79(12)
Ni1–O1–Ni2	94.88(13)		

2.3 Magnetism

Compound **1** is diamagnetic in nature as expected for a square-planar bivalent nickel complex and the presence of a weak dimeric unit (*vide supra*) has little effect on the magnetism. The variable temperature (18 – 300 K, at 200 G) magnetic susceptibility data of **2** and **3** were collected and the experimental molar susceptibility data were fitted for the Curie-Weiss law. The best fit of the curves were obtained with $\theta = 0.0036$ and $g = 2.048$ for **2**; $\theta = 0.1248$ and $g = 2.157$ for **3**. The experimental and calculated curves are

presented in Fig. 6. The intramolecular exchange integral *J* was obtained by fitting the χ_M data using the expression [183] shown below:

$$H = -2J\,\mathbf{S_1}\cdot\mathbf{S_2}$$

$$\chi_M = \frac{Ng^2\beta^2}{3kT}\{\frac{30\exp(6J/kT)+6\exp(2J/kT)}{5\exp(6J/kT)+3\exp(2J/kT)+1}\} + N\alpha$$

Where in the terms have their usual meanings and Nα is the temperature–independent paramagnetism. The very small values of *J* (–0.008244 cm^{-1} for **2** and –0.008774 cm^{-1} for **3**) indicate negligible intramolecular exchange coupling in both the complexes. This suggests that the *d*-orbitals of one Ni^{2+} ion are nearly-orthogonal with those of the second one. The magnetic moment values are also temperature independent in the observed range of temperatures supporting the above view.

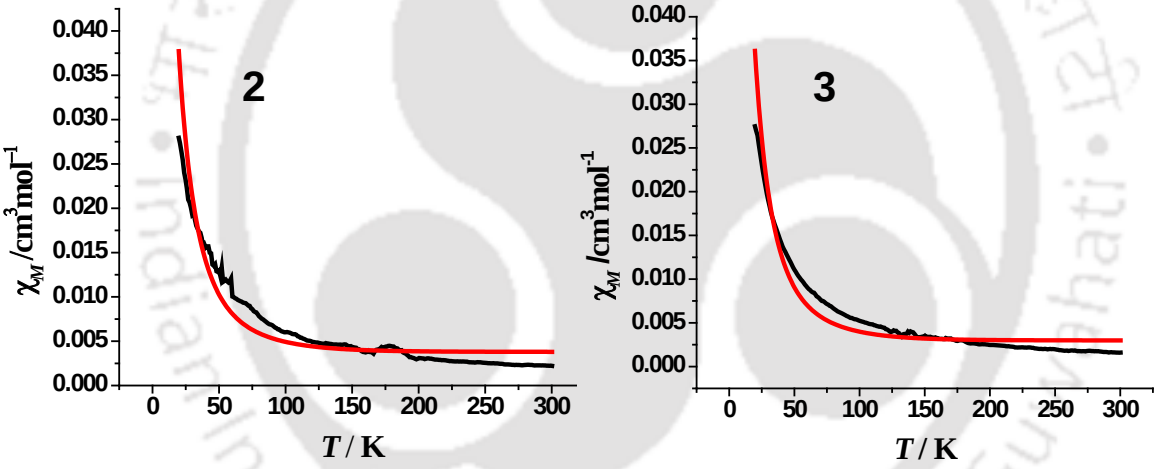

Fig. 6. Plots of χ_M *vs.T* The black and red lines are respectively the experimental and the calculated best-fit curves.

2.4 Conclusion

Three nickel(II) mono-chelates of a racemic mixture of the tridentate Schiff base ligand using the co-ligands N_3^-, NCS^-, $(NC)_2N^-$ and OAc^- were isolated. Determination of the molecular structures of **1** and **2** reveal the presence of centrosymmetric dimers based on a pair of *R* and *S* enantiomers of **L1**. In **1**, the phenolate oxygen is involved in a dipolar interaction of the type $O_P^{\delta-}\cdots N^{\delta+}$ with the electrophilic central nitrogen atom of the coordinated azide ion. In **3**, an acetate and phenoxo bridged dinickel core is encapsulated

by the same enantiomeric form of **L1**. This core is further linked by the dicyanamide ions to a one-dimensional coordination polymer. In a given chain either *RR* or *SS* dimers are repeated all along the chain. The *RR* and *SS* chains are packed alternatively such that *RR* chains are surrounded by the *SS* chains and *vice versa*. The rectangular Ni_2N_2 (in **1**) and Ni_2O_2 cores (in **2**) has the center of symmetry inside the rectangular unit hence, leading to the formation of a heterochiral dimer. However, $\{Ni_2(\mu\text{–}O_P)_2(\mu\text{–}OAc)\}$ core in **3** do not have the center of symmetry within itself, hence a homochiral dimer has formed. A negligible intramolecular exchange coupling present in **2** and **3** is suggestive of the *d*-orbitals of the two Ni^{2+} ions being nearly-orthogonal to each other.

Chapter 3

Diastereoselectivity in Dinuclear Complexes of Chiral Tridentate Ligands†

Abstract

Using a racemic mixture of two chiral tridentate ligands 2–((1–(2–pyridyl)ethylimino)methyl)phenolate ion (**L1**) and 2–((phenyl(2–pyridyl)methyl-imino)methyl)phenolate ion (**L2**) and Cu(II) or Ni(II) salts, complexes having formulae [Cu(**L2**)(μ–1,1–NO_3)]$_2$ (**1**), [Cu(**L2**)(μ–Cl)]$_2$ (**2**), [Cu_2(**L2**)$_2$(μ–1,2–SO_4)] (**3**), [Cu_2(**L1**)$_2$(μ–1,2–SO_4)] (**4**) and [Ni_2(**L2**)$_2$(OAc)(N(CN)$_2$)(MeOH)] (**5**) were synthesized and characterized. Determination of molecular structures of all five complexes confirmed the presence of a dimetallic core constructed by monochelates of the ligands. Compound **1** and **2** have NO_3^- and Cl^- bridge between two copper centers and **3**–**5** have phenoxo as well as SO_4^{2-} (**3**, **4**) and OAc^- (**5**) bridges. Compounds **1**, **2** have center of inversion in the dicopper core and are heterochiral. Whereas, in **3**–**5** center of inversion do not lie in the dimetallic core and are homochiral. Compound **1** has a rare feature of μ–1,1–NO_3^- bridge between two copper centers.

† This work has been published in:

H. S. Jena, V. Manivannan, Inorg. Chim. Acta 2012 (doi:10.1016/j.ica.2012.04.017).

Diastereoselectivity in Dinuclear Complexes of Chiral Tridentate Ligands

In this Chapter, synthesis and structural characterization of five racemic Cu(II) and Ni(II) complexes derived from the tridentate racemic Schiff base ligands, 2–((1–(2–pyridyl)ethylimino)methyl)phenolate ion (**L1**) and 2–((phenyl(2–pyridyl)methyl-imino)methyl)phenolate ion (**L2**) and Cu(II) or Ni(II) salts are described. The structural characterization of these compounds reveal that the end capped monochelated metal complex formed from racemic mixture of chiral tridentate ligands, in the presence of suitable bridging ligands can dimerize to form a dimetallic core in three ways having *RS* or *RR* or *SS* combinations of the ligands. Compounds **1**, **2** have center of inversion in the dicopper core and are heterochiral. Whereas, in **3**–**5** center of inversion do not lie in the dimetallic core and are homochiral. The bridging ligands dependent chiral preference (Scheme 1) based on its ability/inability to accommodate the center of symmetry at the dimetallic core are described.

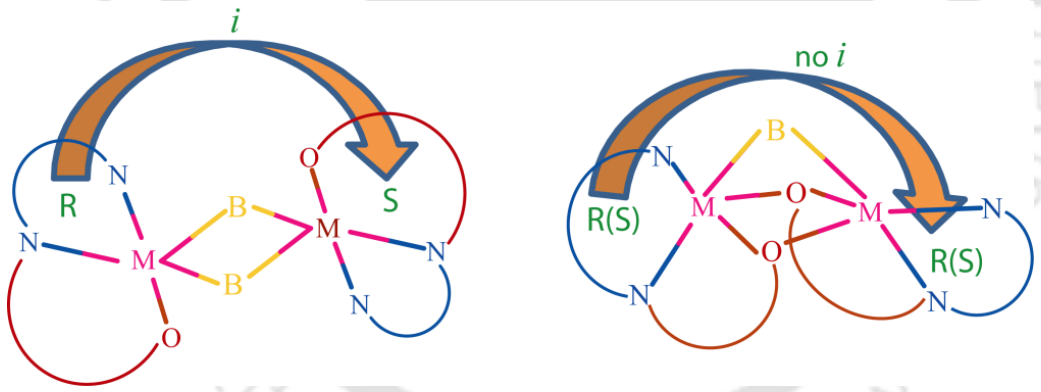

Scheme 1. Chirality selective dimetallic core (B = bridging ligand)**.**

3.1 Experimental

3.1.1 Syntheses

Synthesis of **L1H** is already described in Chapter 1.

3.1.1.1 Phenyl(2–pyridyl)ketoxime

To a mixture of phenyl(2–pyridyl)ketone (10.0 g, 55 mmol) and $NH_2OH{\cdot}HCl$ (6.0 g, 86 mmol) in methanol (50 mL), an aqueous solution (50 mL) of NaOH (11.0 g, 275 mmol) was added and stirred at 100 °C for 24 h. The reaction mixture was cooled first

to room temperature and then kept in refrigerator (at 0–4 °C). After standing for overnight, the pale pink crystals deposited was filtered, washed with water and dried in desiccators. Yield: 9.51 g (87%). IR (KBr, cm^{-1}): 3152(b), 3009(s), 2852(s), 1627(w), 1591(s), 1560(w), 1475(s), 1435(s), 1411(w), 1325(s), 1241(w), 1179(s), 1156(s), 1052(w), 995(s), 947(s), 913(w), 790(s), 778(s), 748(s), 699(s), 623(s). 400 MHz ^{1}H NMR (δ (*J*, Hz), $CDCl_3$): 9.42 (OH, s), 8.62 (1H, d, 8.0), 7.69 (1H, t, 7.6), 7.58 (1H, d, 7.6), 7.50–7.41 (3H, m), 7.26 (1H, t, 5.2). 100 MHz ^{13}C NMR (δ, $CDCl_3$): 158.8, 154.7, 149.5, 136.7, 129.6, 129.2, 128.7, 128.5, 128.2, 123.1.

3.1.1.2 (R, S) Phenyl(2–pyridyl)methaneamine

To an ice-cold mixture of phenyl(2–pyridyl)ketoxime (5.0 g, 25.2 mmol), acetic acid (50 mL) and ethanol (100 mL), zinc dust (50 g) was added in 2 g increments over a period of 2 h and then the heterogeneous mixture was stirred at ambient temperature for 24 h. The mixture was filtered to remove undissolved zinc and washed with sufficient quantity of ethanol. The combined filtrate and washings was concentrated in vacuo, several 10 mL portions of H_2O were added to it and evaporated to remove acetic acid. The pH of the mixture was adjusted to ~12 using aqueous KOH solution and then extracted with 3 × 50 mL of diethyl ether. The combined ether portions were dried over Na_2SO_4 and the solvent was removed in vacuo. Yield: 4.5 g (96.8%). IR (KBr, cm^{-1}): 3445(b), 3307(b), 3255(s), 3180(s), 3101(w), 1630(s), 1604(s), 1549(w), 1519(s), 1477(s), 1466(s), 1441(s), 1363(s), 1282(s), 1252(s), 1211(w), 1161(w), 1097(s), 1038(s), 766(s), 658(w), 640(w), 543(s). 400 MHz ^{1}H NMR (δ (*J*, Hz), $CDCl_3$): 8.53 (1H, d, 4.8), 7.56 (1H, t, 7.6), 7.39 (1H, d, 8), 7.30 (1H, t, 7.6), 7.24 (1H, t, 6.4), 7.19 (1H, d, 6.4), 7.10 (1H, t, 6.2), 5.21 (1H, s), 2.75 (NH_2, s). 100 MHz ^{13}C NMR (δ, $CDCl_3$): 158.6, 154.2, 149.6, 136.7, 131.0, 129.2, 128.7, 128.5, 123.1, 56.2.

*3.1.1.3 (R, S) 2–((Phenyl(2–pyridyl)methylimino)methyl)phenol (**L2H**)*

A mixture of phenyl(2–pyridyl)methaneamine (4.5 g, 26.3 mmol) and 2–hydroxybenzaldehyde (3.2 g, 26.3 mmol) in methanol (100 mL) was stirred for 3 h. Yellow precipitate of **L2H** deposited were collected by suction filtration, washed with cold methanol and dried over $CaCl_2$. Yield: 7.2 g (95%). ESI-MS: *m/z* calcd. for $C_{19}H_{16}N_2O^+$ 288.13. Found (M^++H) 289.10. IR (KBr, cm^{-1}): 3081(s), 3009(s), 2897(s), 1622(s), 1586(s), 1464(s), 1430(s), 1383(w), 1313(s), 1279(s), 1215(w),

1200(s), 1151(s), 1053(s), 1028(s), 988(s), 938(w), 914(s), 859(s), 780(w), 757(s), 695(s), 621(s), 611(s), 539(s), 480(w), 463(s). 400 MHz ^{1}H NMR (δ (*J*, Hz), $CDCl_3$): 13.50 (OH, s), 8.55 (1H, s), 8.54 (1H, d, 6.8), 7.65 (1H, t, 4.6), 7.42 (1H, d, 8.0), 7.40 (1H, d, 8.4), 7.36 (1H, t, 8.4), 7.32 (1H, t, 7.6), 7.30 (1H, t, 8.4), 7.28 (1H, d, 7.6), 7.15 (1H, t, 6.0), 6.99 (1H, d, 8.0), 6.89 (1H, t, 7.6), 5.75 (1H, s). 100 MHz ^{13}C NMR (δ, $CDCl_3$): 166.1, 161.7, 161.1, 149.4, 141.5, 137.2, 132.9, 132.0, 128.9, 127.8, 127.5, 122.6, 122.0, 119.0, 117.2, 116.4, 78.9.

*3.1.1.4 [Cu_2(**L2**)$_2$(μ–1,1–NO_3)$_2$] (**1**)*

To **L2H** (0.29 g, 1.0 mmol) dissolved in methanol (30 mL), solid $Cu(NO_3)_2 \cdot 3H_2O$ (0.24 g, 1.0 mmol) was added and the resulting green solution was stirred at room temperature for 1 h. The solvent was removed and the green residue was washed with ice-cold methanol. Yield: 0.55 g (66%). Single crystals of **1** suitable for X-ray diffraction study were obtained slow evaporation of methanol solution. *Anal.* Calc. for $C_{38}H_{30}Cu_2N_6O_8$: C, 55.27; H, 3.66; N, 10.18%. Found: C, 54.97; H, 3.58; N, 9.87%. IR (KBr, cm^{-1}): 3458(b), 3308(s), 3238(b), 1610(s), 1599(s), 1570(s), 1487(s), 1446(w), 1398(b), 1384(b), 1315(w), 1258(s), 1151(s), 1098(s), 1071(w), 1009(s), 999(w), 824(s), 771(s), 701(s), 666(s), 621(w), 542(s). UV–Vis [λ_{max}, nm (ε, $M^{-1}cm^{-1}$), CH_3OH solution]: 635(173); 405(268); 382(5442); 289(6861). EPR (CH_3OH solution, 298 K): g = 2.233, A = 72 G. μ_{eff}/ Cu (298 K), 1.91 B. M.

*3.1.1.5 [Cu_2(**L2**)$_2$(μ–Cl)$_2$]·2CH_3OH (**2**)*

To **L2H** (0.29 g, 1.0 mmol) dissolved in methanol (30 mL), solid $CuCl_2 \cdot 2H_2O$ (0.17 g, 1.0 mmol) was added and stirred at room temperature for 1 h. The green solution was kept in room temperature and after a week green crystals of **2** suitable for X-ray diffraction study were obtained and washed with cold methanol. Yield: 0.53 g (63%). *Anal.* Calc. for $C_{40}H_{38}Cl_2Cu_2N_4O_4$: C, 57.42; H, 4.58; N, 6.70%. Found: C, 56.87; H, 4.28; N, 6.54%. IR (KBr, cm^{-1}): 3363(b), 3115(w), 3021(w), 2909(w), 1625(s), 1600(w), 1569(w), 1537(s), 1469(s), 1446(s), 1438(w), 1395(s), 1348(w), 1323(s), 1283(s), 1211(w), 1152(s), 1129(w), 1078(w), 1045(s), 1030(s), 979(w), 935(w), 913(w), 878(w), 852(w), 765(s), 755(s), 707(s), 625(s), 552(s), 454(w). UV–Vis [λ_{max}, nm (ε, $M^{-1}cm^{-1}$), CH_3OH solution]: 635(144); 382(2735); 288(4331). EPR (CH_3OH solution, 298 K): g = 2.101, A = 70 G, μ_{eff}/ Cu (298 K), 1.94 B. M.

*3.1.1.6 [Cu_2(**L2**)$_2$(μ–1,2–SO_4)]·7H_2O (**3**)*

To **L2H** (0.29 g, 1.0 mmol) dissolved in methanol (30 mL), solid $CuSO_4$·5H_2O (0.25 g, 1.0 mmol) was added and stirred at room temperature for 1 h. The green solution was kept in room temperature and after a week green crystals of **3** suitable for X-ray diffraction study were isolated and washed with cold methanol. Yield: 0.652 g (71%). *Anal.* Calc. for $C_{38}H_{30}Cu_2N_4O_{13}S$: C, 50.16; H, 3.32; N, 6.16%. Found: C, 49.97; H, 3.01; N, 5.94%. IR (KBr, cm^{-1}): 3426(b), 3054(w), 3038(w), 2925(s), 1618(s), 1570(w), 1548(s), 1483(w), 1457(s), 1441(w), 1420(s), 1392(w), 1336(s), 1301(s), 1286(w), 1243(s), 1192(w), 1147(s), 1165(w), 1147(w), 1100(w), 1022(b), 963(s), 875(s), 818(s), 759(s), 736(w), 704(s), 686(w), 632(w), 589(b), 568(s), 516(w), 484(s). UV–Vis [λ_{max}, nm (ε, $M^{-1}cm^{-1}$), CH_3OH solution]: 638(165); 381(1793); 287(2449). EPR (CH_3OH solution, 298 K): g = 2.117, A = 71 G. μ_{eff}/ Cu (298 K), 1.84 B. M.

*3.1.1.7 [Cu_2(**L1**)$_2$(μ–1,2–SO_4)]·2H_2O·CH_3OH (**4**)*

To a methanolic solution (30 mL) of **L1H** (0.23 g, 1 mmol), solid $CuSO_4$·5H_2O (0.250 g, 1.0 mmol) was added and stirred for 4 hour. From the green solution dark green crystals of **4** were formed on standing for few days. Yield: 0.450 g (60%). *Anal.* Calc. for $C_{29}H_{30}Cu_2N_4O_9S$: C, 47.21; H, 4.10; N, 7.59%. Found: C, 47.04; H, 3.89; N, 7.44%. IR (KBr, cm̄ ^{1}): 3420(b), 3277(s), 3138(w), 3068(w), 2970(w), 1626(w), 1605(s), 1567(s), 1480(s), 1442(s), 1292(s), 1401(w), 1379(w), 1362(w), 1292(s), 1247(s), 1117(b), 1039(b), 979(s), 905(w), 791(s), 764(s), 743(w), 701(w), 649(w), 618(s), 477(w). UV–Vis [λ_{max}, nm (ε, $M^{-1}cm^{-1}$), CH_3OH solution]: 636(208); 377(4323); 284(3028). EPR (CH_3OH solution, 298 K): g = 2.114, A = 76 G, μ_{eff}/ Cu (298 K), 1.86 B. M.

*3.1.1.8 [Ni_2(**L2**)$_2$(OAc)(DCA)(CH_3OH)]·CH_3OH (**5**)*

To Ni(OAc)$_2$·4H_2O (0.990 g, 4.0 mmol) dissolved in methanol (60 mL), **L2H** (1.14 g, 4.0 mmol) and sodium dicyanamide (0.352 g, 4.0 mmol) were added and the solution was stirred at room temperature for 24 h. The solvent was removed and the green residue was washed with ice-cold methanol. Yield: 1.04 g (69%). Single crystals of **5** suitable for X-ray diffraction study were obtained by slow diffusion of methanolic solution of the crude **5** into dichloromethane. *Anal.* Calc. for $C_{44}H_{40}N_7O_6Ni_2$: C, 60.04; H, 4.58; N, 11.14%. Found: C, 59.87; H, 4.48; N, 10.87%.

IR (KBr, cm^{-1}): 3431(b), 3408(b), 3050(b), 3007(w), 2891(b), 2297(s), 2243(s), 2185(s) (dicyanamide), 1641(s), 1598(s), 1568(w), 1543(w), 1493(w), 1467(s), 1443(s), 1394(s), 1349(s), 1288,(s), 1244(w), 1196(s), 1147(s), 1120(w), 1081(w), 1047(w), 933(w), 898(w), 849(s), 784(s), 756(s), 703(s), 623(s), 553(w). UV–Vis [λ_{max}, nm (ε, $M^{-1}cm^{-1}$), CH_3OH solution]: 841(36); 746(23); 576(16); 377(2510); 286(2299). μ_{eff}/ Ni (298 K), 2.84 B. M.

3.2 Results and discussion

The nature of metal ion and its preferred coordination stereochemistry, electronic and steric requirements of multidentate ligands as well as coordination mode of bridging ligand are crucial factors in synthesis of coordination complexes. During the formation of a dinuclear core self-assembly of monochelated chiral tridentate ligand could occur and the role of bridging ligands on binucleation is scanty [278, 279]. To make an illuminating investigation on this effect, it is necessary to synthesize a variety of compounds with variety of bridging ligand by keeping the other parameters to a near constant. From this perspective, we have synthesized a set of five complexes **1**–**5**, having a dimetallic core using two racemic tridentate end-capped Schiff bases (**L1H** and **L2H**, (Scheme 2)) and different copper salts and a nickel salt. Determination of their molecular structures (*vide infra*) reveal a bridging dependent preference of *RS* combination of two **L2** ligands coordinated to dicopper core of **1**, **2** and *RR*(*SS*) combination of **L1** and **L2** (Scheme 3) in **3**–**5**. Such chiral combinations can be rationalized to the ability or inability of the bridging ligands in allowing a center of symmetry at dimetallic core.

The IR spectra of **1**–**5**, show a strong peak in the range 1610–1640 cm^{-1} assignable to azomethine group. In addition the characteristic peaks for NO_3^- in **1** at 1384 cm^{-1}, SO_4^{2-} in **3**, **4** at 1441 cm^{-1}, OAc^- in **5** at 1467 cm^{-1} and $\nu_{(Cu–Cl)}$ in **2** at 454 cm^{-1} are noteworthy. In methanol the electronic spectra of compounds **1**–**4** display a *d*–*d* transition at around 635 nm whereas **5** exhibits the same at 841 and 576 nm as a broad band as well as at 746 nm as a sharp band (Fig. 1). The allowed transitions in **1**–**5** were observed at around 380 and 287 nm. The room-temperature magnetic moment values of polycrystalline samples are consistent with the presence of one unpaired electron in **1**–**4** and two unpaired electrons per nickel atom in **5**. In methanol medium,

the EPR spectra of **1**–**4** at 298 K are isotropic in nature with the hyperfine splitting (Fig. 2).

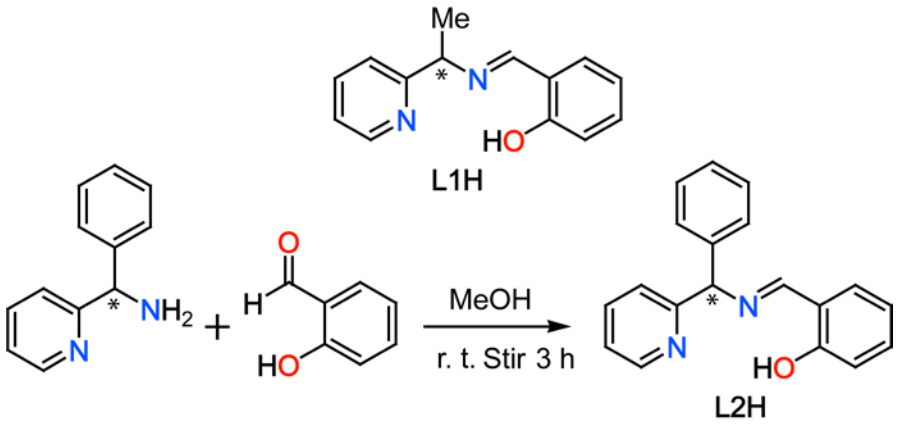

Scheme 2. Structure of **L1H** and synthesis of **L2H**.

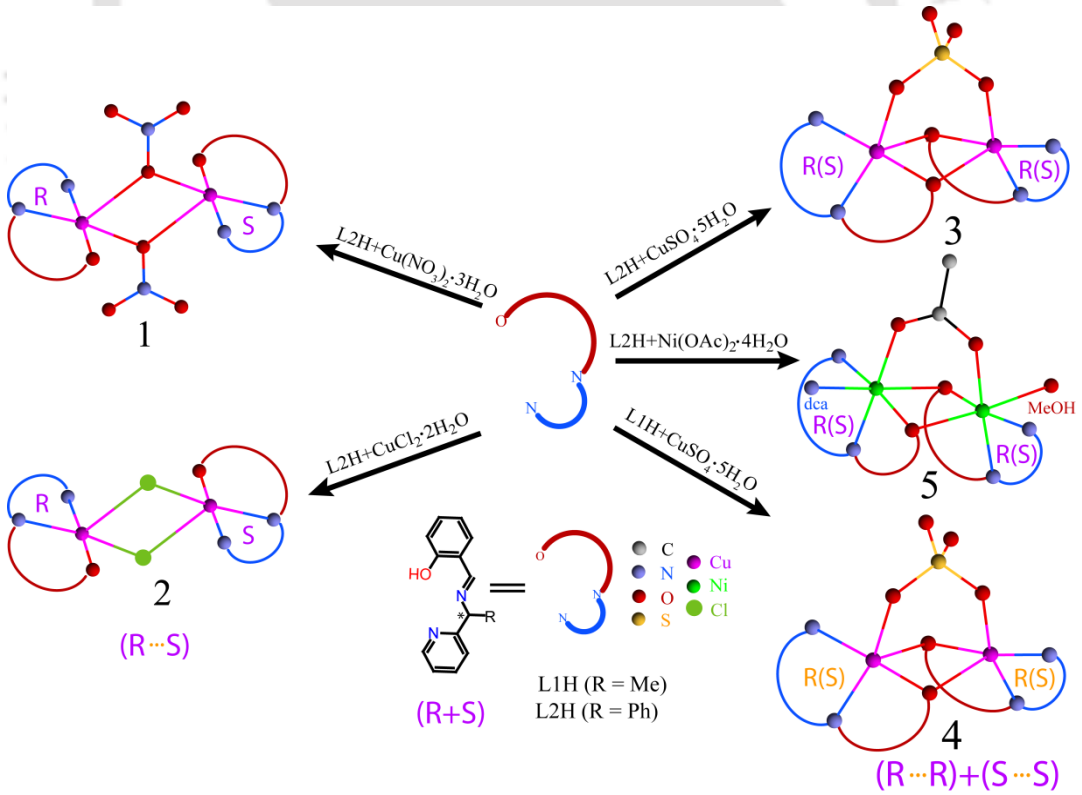

Scheme 3. Schematic representation of bridging ligand dependent chirality selectivity in dimetallic core.

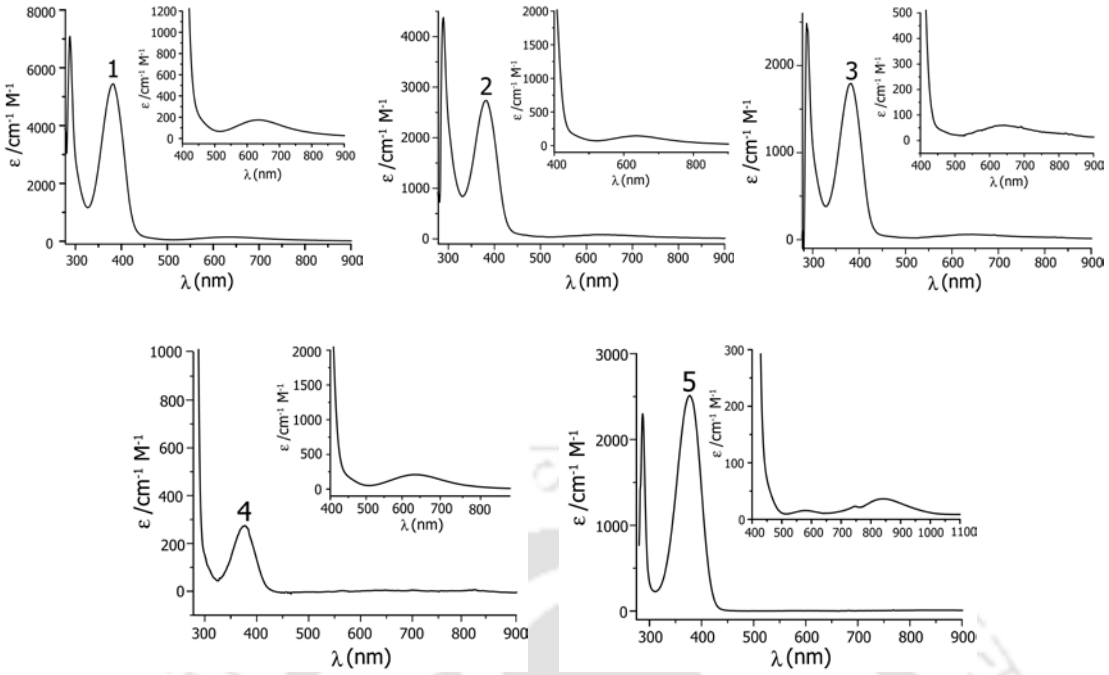

Fig. 1. UV–Visible spectra of **1**–**5** in methanol at room temperature (insert shows the *d*–*d* transitions).

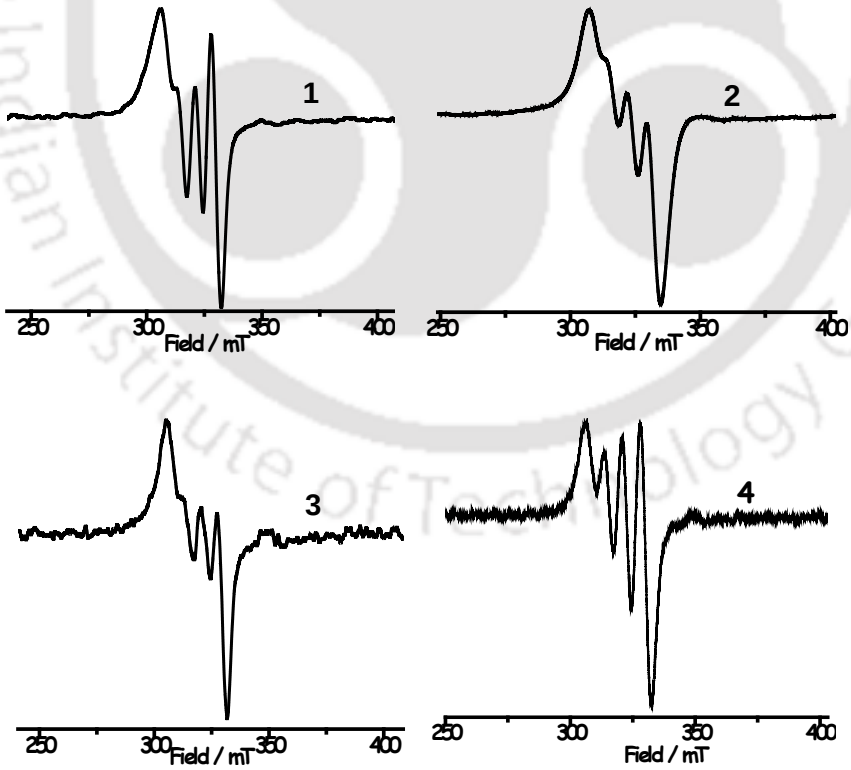

Fig. 2. EPR spectra of **1**–**4** in methanol at room temperature.

The thermogravimetric analyses of **3**–**4** were carried out after keeping the freshly prepared samples in desiccators, overnight (Fig. 3). In **3**, a weight loss of 14.0% (Calcd. 13.8%) was observed in the temperature range 37 – 196 °C that corresponds to the loss of all seven water molecules. Sample of **4** shows a weight loss of 9.0% (Calcd. 9.2%) for loss of one methanol and two water molecules in the temperature range 78 – 113 °C.

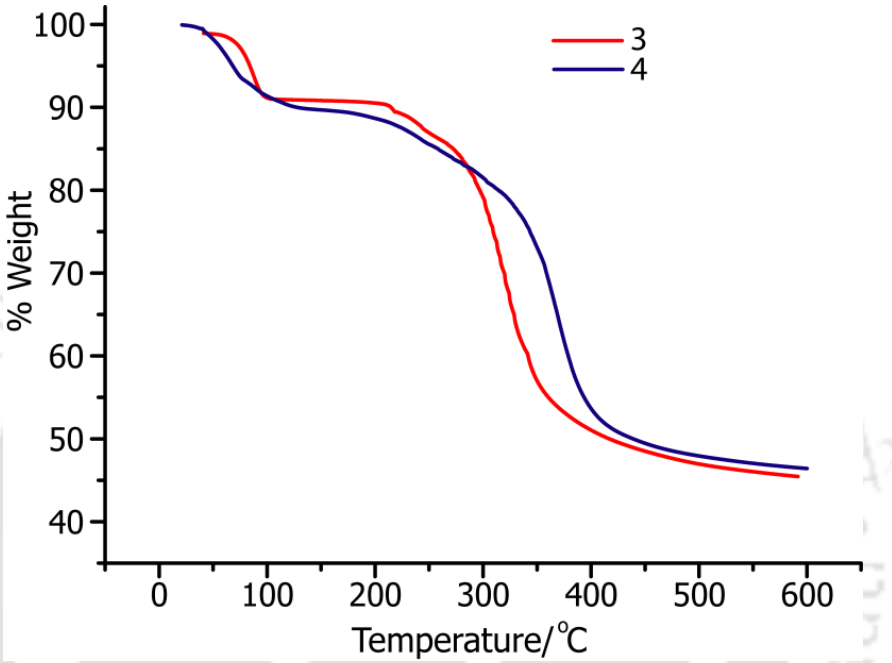

Fig. 3. TG profile of **3** and **4**.

3.3 Molecular Structures

The molecular structures of **1**–**5** were determined and the crystallographic and refinement parameters are listed in Table 1. Both **L1** and **L2** bind to the metal ion, in tridentate meridional fashion with $N_PN_IO_P$ donor set {N_P = pyridyl–N; N_I = imine–N; O_P = phenolate–O}. The chelate ring formed by N_PN_I atoms is five-membered and that by N_IO_P atoms is six-membered. During synthesis of **1**–**5**, a racemic mixture of **L1H**/**L2H** has been used and all the five compounds have a monochelated dimetallic unit. Compounds **1**, **2** have center of inversion in the dicopper core and are heterochiral. Whereas, in **3**–**5** center of inversion do not lie in the dimetallic core and are homochiral.

Table 1. Crystallographic and refinement parameters

	1	**2**	**3**	**4**	**5**
Formula	$C_{38}H_{32}Cu_2N_6O_8$	$C_{40}H_{38}Cl_2Cu_2N_4O_4$	$C_{38}H_{30}Cu_2N_4O_{13}S$	$C_{29}H_{30}Cu_2N_4O_9S$	$C_{44}H_{41}N_7Ni_2O_6$
CCDC number	831679	831680	831681	831682	831683
Formula weight	827.80	836.74	909.83	737.74	881.22
T (K)	296(2)	296(2)	296(2)	296(2)	296(2)
Wavelength (Å)	0.71073	0.71073	0.71073	0.71073	0.71073
Crystal system	Monoclinic	Monoclinic	Triclinic	Triclinic	Monoclinic
Space group	$P2_1/n$	$P2_1/n$	P-1	P-1	$P\ 2_1/n$
a (Å)	11.8705(3)	9.0248(5)	10.8903(8)	9.7891(15)	15.7499(12)
b (Å)	13.3174(3)	12.1801(6)	13.0500(9)	13.069(2)	17.4273(13)
c (Å)	12.4683(3)	16.9307(9)	16.1451(11)	13.390(2)	16.2398(12)
α (°)			69.523(4)	109.986(11)	
β (°)	113.5240(10)	101.676(3)	70.652(4)	104.239(12)	114.261(3)
γ (°)			86.379(4)	91.103(11)	
V (Å^3)	1807.23(8)	1822.56(17)	2024.5(2)	1550.4(4)	4063.8(5)
Z	2	2	2	2	4
D_{calcd} (g m^{-3})	1.521	1.525	1.492	1.580	1.440
μ (mm^{-1})	1.239	1.362	1.171	1.498	0.985
F(0 0 0)	848.0	860.0	928.0	756.0	1832.0
Reflection collected	3231	4692	7903	7797	9735
Unique reflections	2379	2513	6217	5767	7578
θ_{min}, θ_{max}(°)	1.87, 25.15	2.07, 28.66	1.67, 25.93	1.68, 28.43	1.52, 27.89
Goodness-of-fit (GOF)[a]	1.004	1.045	1.002	1.001	1.002
R_1[b], wR_2[c] ($I \geq 2\sigma(I)$)	0.0428, 0.1213	0.0349, 0.0965	0.0444, 0.1164	0.0874, 0.1898	0.0452, 0.1148
R_1[b], wR_2[c] (all data)	0.0994, 0.1491	0.0456, 0.1041	0.0710, 0.1329	0.1914, 0.2408	0.0778, 0.1384
largest peak/hole (e Å^{-3})	0.693/-0.519	0.358/-0.268	0.757/-0.518	0.862/-0.570	1.136/-0.707

[a]GOF = $[\sum[w(F_0^2 - F_c^2)^2]/ M - N]^{1/2}$ (M =number of reflections, N = number of parameters refined).
[b]$R_1 = \sum \| F_0 | - | Fc \| / \sum | F_0 |$. [c]$wR_2 = [\sum[w(F_0^2 - F_c^2)^2]/ \sum[w(F_0^2)^2]]^{1/2}$.

In compound **1**, the copper center is bound by $N_PN_IO_P$ donor set of nearly-planar **L2** and O2 of nitrate ion, which together form a distorted square-planar arrangement. The O2 atom deviates from the plane containing N1N2O1Cu1 atoms, by a distance of 0.33 Å and an angle of 9.45°. The O2 atom of nitrate ion is further linked to another copper center in a μ–1,1 bridging fashion, leading to a heterochiral dimer around Cu_2O_2 core. To the best of our knowledge this is the third example where such bridging by nitrate ion has been observed [280, 281]. The Cu_2O_2 core has diamond shape having the parameters, Cu1···Cu1A, 3.844(1) Å; Cu1–O2, 2.045(2) Å; Cu1–O2A, 2.559(2) Å; O2–Cu1–O2A, 67.32(8)°; Cu1–O2–Cu1A, 112.68(9)°. The dimer contains *RS* pair of asymmetric carbon–C6 and a center of symmetry is present at the center of Cu_2O_2 core. The distance between two N1N2O1Cu1 planes in the dimer is 1.84 Å. A perspective view of **1** is shown in Fig. 4. The d^9 copper(II) ion is usually severely Jahn-Teller distorted and as a result has a long axial bond. The Cu1–O2A bond having a distance 2.561(2) Å is quite longer than the usual range and deviate by an angle of 31.86° from the axial position, hence orienting along d_{xz}/d_{yz} orbital than the d_z^2. Among the bond distances within the nitrate ion, N3–O2, 1.264(4) Å is longer than other two N3–O3, 1.193(5) Å; N3–O4, 1.204(4) Å which is due to involvement of O2 atom in bridging.

In compound **2**, **L2** and Cl1 are attached to copper(II) center forming a distorted square planar arrangements of donor atoms around it and Cl1 atom deviate by 0.44 Å from the plane containing N1N2O1Cu1 atoms. The Cl1 atom from each of [Cu(**L2**)Cl] unit bridge each other having a distance of 2.881(2) Å, leading to a $[Cu(\mathbf{L2})Cl]_2$ dimeric unit, as shown in Fig. 5. Selected bond distances observed in **1** and **2** are listed in Table 2. A center of symmetry is present at the center of Cu_2Cl_2 core; as a result asymmetric carbons (C6) have a *RS* combination. The Cu_2Cl_2 core has a near rectangular shape with the parameters: Cu1–Cl1, 2.300(1) Å; Cu1–Cl1A, 2.881(2) Å; Cu1–Cl1–Cu1A, 90.92(4)°; Cl1–Cu1–Cl1A, 89.08(4)° and these values are comparable with reported ones [282–286]. The distance between two N1N2O1Cu1 planes in a dimer is 2.40 Å. The O_P is hydrogen bonded to the methanol oxygen with O1···O2 distance of 2.911(6) Å.

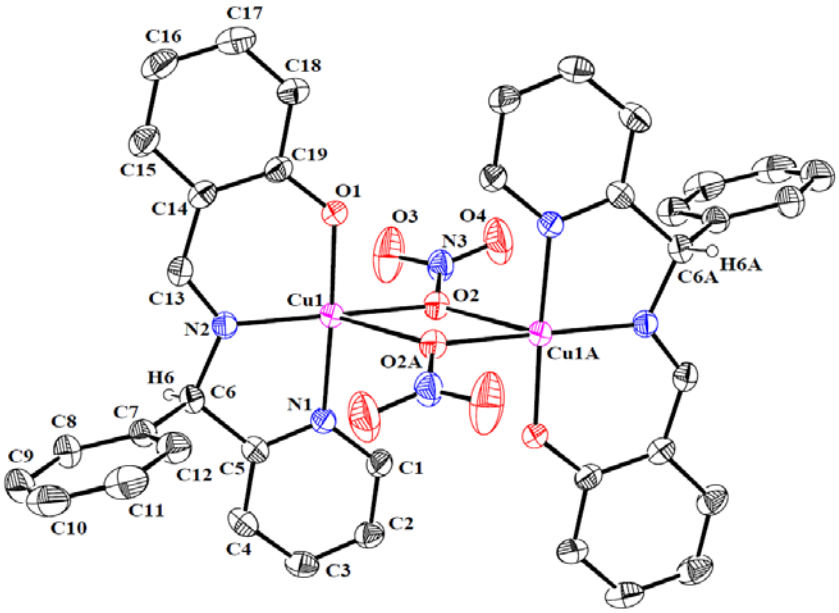

Fig. 4. ORTEP diagram (30% probability ellipsoids) of **1** (All H–atoms except H6 are omitted for clarity) (symmetry code: –x, –y, –z).

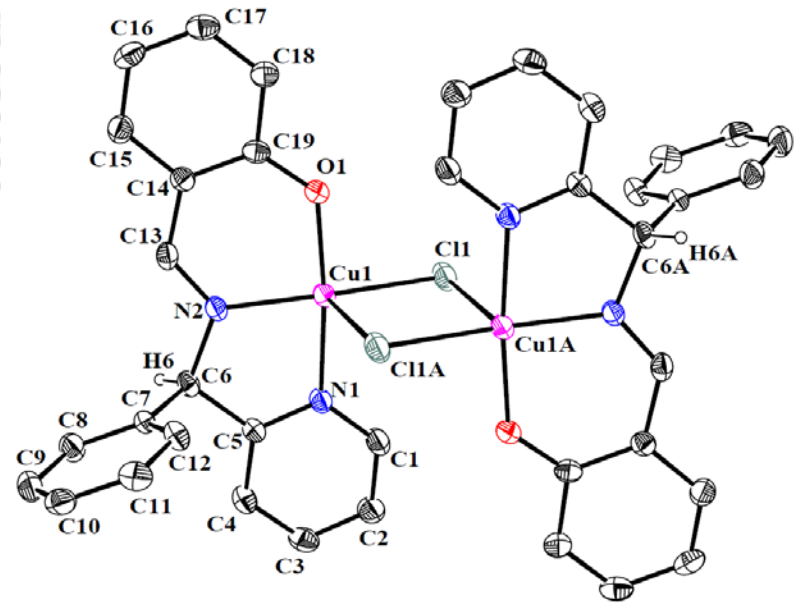

Fig. 5. ORTEP diagram (30% probability ellipsoids) of **2** (All H–atoms except H6 are omitted for clarity) (symmetry code: –x, –y, –z).

Table 2. Selected bond distances (Å) and angles (°) in **1** and **2**.

1		**2**	
Cu1–N1	1.968(2)	Cu1–N1	2.002(4)
Cu1–N2	1.946(2)	Cu1–N2	1.953(4)
Cu1–O1	1.874(2)	Cu1–O1	1.898(4)
Cu1–O2	2.045(2)	Cu1–Cl1	2.300(1)
Cu1–O2A	2.559(2)	Cu1–Cl1A	2.881(2)
Cu1···Cu1A	3.8445(3)	Cu1···Cu1A	3.715(9)
N1–Cu1–N2	82.97(8)	N1–Cu1–N2	82.2(2)
N1–Cu1–O1	177.14(8)	N1–Cu1–O1	173.5(2)
N1–Cu1–O2	94.73(8)	N1–Cu1–Cl1	95.3(1)
N1–Cu1–O2A	90.92(7)	N1–Cu1–Cl1A	88.7(1)
N2–Cu1–O1	94.17(8)	N2–Cu1–O1	92.2(2)
N2–Cu1–O2	170.55(8)	N2–Cu1–Cl1	166.7(1)
N2–Cu1–O2A	121.83(7)	N2–Cu1–Cl1A	103.9(1)
O1–Cu1–O2	88.11(8)	O1–Cu1–Cl1	89.4(1)
O1–Cu1–O2A	90.49(7)	O1–Cu1–Cl1A	95.9(1)
O2–Cu1–O2A	67.24(7)	Cl1–Cu1–Cl1A	89.08(5)

Compounds **3** and **4** crystallized in space group *P*–1, respectively contain a non-centrosymmetric dimeric units of [Cu_2(**L2**)$_2$(μ–1,2–SO_4)] and [Cu_2(**L1**)$_2$(μ–1,2–SO_4)]. In both cases, each copper atom is bound by the mono anionic ligand, one oxygen atom from the sulfate ion which bridge in μ–1,2 fashion [287–300] and by bridging O_P. The ligand has a slight bowl shape and copper center has a distorted square pyramidal geometry, with bridged-O_P being in the axial site. Out of two axial bridged-O_P linkages, Cu1···O2 contact is shorter (2.338(3) Å in **1**; 2.308(4) Å in **2**), than Cu2 ··O1 distance (2.519(3) Å in **1**; 2.517(5) Å in **2**). The O_P bridge leads to a butterfly shaped Cu_2O_2 unit with angle between two planes containing atoms Cu1O2Cu2 and Cu1O1Cu2 planes being 155.98° in **1**; 160.64° in **2**, while between O2Cu1O1 and O2Cu2O1 planes being 157.79° in **1**; 161.44° in **2**. The non-bonded Cu1···Cu2 contact has a distance of 3.1785(6) Å in **1** and 3.112(2) Å in **2**. Within a dimer, the asymmetric carbon atoms have a *RR* or *SS* enantiomeric combinations and since inversion center do not lie within Cu_2O_2 core, such combination has occurred. Perspective views of homochiral dimers, *RR*–[Cu_2(**L2**)$_2$(μ–1,2–SO_4)] and *SS*–[Cu_2(**L1**)$_2$(μ–1,2–SO_4)] are displayed in Fig. 6 and 7

and the selected bond distances are listed in Table 3. The τ parameters calculated for **1** (0.11); **2** (0.12); **3** (0.30, 0.23) and **4** (0.19, 0.13) are imperative of the distorted square pyramidal geometry [269].

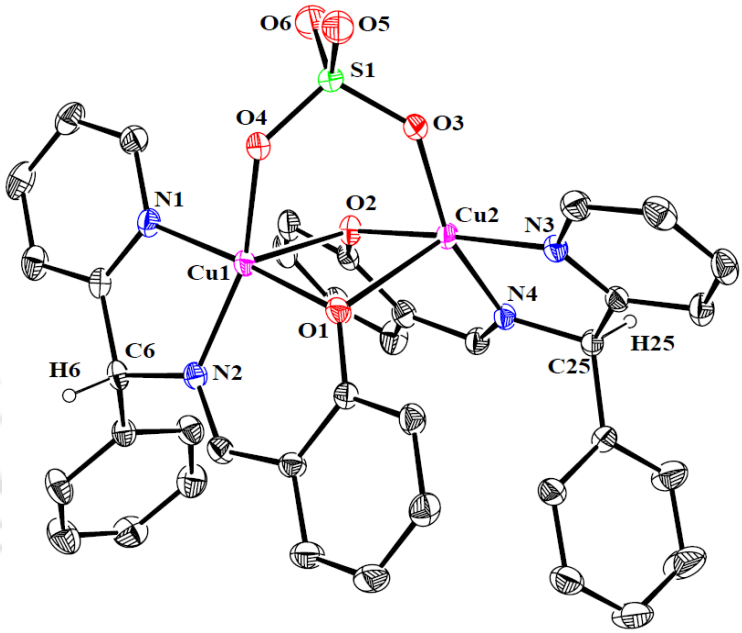

Fig. 6. ORTEP diagram (30% probability ellipsoids) of [Cu_2(**L2**)$_2$(μ–1,2–SO_4)] in **3** (All H–atoms except H6 and H25 are omitted for clarity).

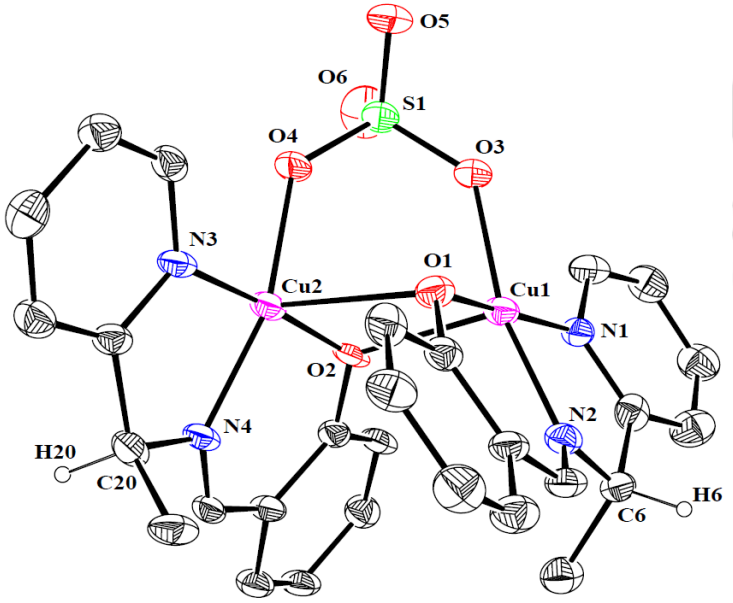

Fig. 7. ORTEP diagram (30% probability ellipsoids) of [Cu_2(**L1**)$_2$(μ–1,2–SO_4)] in **4** (All H–atoms except H6 and H20 are omitted for clarity).

Table 3. Selected bond distances (Å) and angles (°) in **3** and **4**.

	3	**4**		**3**	**4**
Cu1–N1	1.976(3)	1.959(7)	N1–Cu1–N2	82.4(1)	82.6(3)
Cu1–N2	1.939(2)	1.935(7)	N1–Cu1–O1	176.6(1)	173.2(3)
Cu1–O1	1.921(2)	1.924(5)	N1–Cu1–O2	95.6(1)	96.8(2)
Cu1–O2	2.339(3)	2.308(4)	N1–Cu1–O3	92.6(1)	92.6(3)
Cu1–O3	1.971(2)	1.947(6)	N2–Cu1–O1	94.4(1)	93.0(3)
Cu2–N3	1.980(3)	1.956(7)	N2–Cu1–O2	110.2(1)	104.7(3)
Cu2–N4	1.940(3)	1.941(7)	N2–Cu1–O3	158.2(1)	166.1(3)
Cu2–O1	2.515(3)	2.517(5)	N3–Cu2–N4	82.5(1)	82.5(3)
Cu2–O2	1.901(2)	1.882(6)	N3–Cu2–O1	98.8(1)	93.7(2)
Cu2–O4	1.953(3)	1.956(6)	N3–Cu2–O2	176.3(1)	174.4(3)
Cu1···Cu2	3.179(7)	3.112(2)	N3–Cu2–O4	91.0(1)	92.2(3)
			N4–Cu2–O1	112.2(1)	111.3(2)
			N4–Cu2–O2	93.9(1)	93.3(3)
			N4–Cu2–O4	162.0(1)	162.4(3)
			O1–Cu1–O2	86.4(1)	89.4(2)
			O1–Cu1–O3	90.0(1)	90.5(2)
			O2–Cu1–O3	91.4(1)	88.8(2)
			O1–Cu2–O2	82.0(1)	84.3(2)
			O1–Cu2–O4	85.3(1)	85.7(2)
			O2–Cu2–O4	92.6(1)	92.9(2)

In the packing diagram of **3**, dimers having *RR* and *SS* combinations are packed alternatively along the *c*-axis generated by inversion center, but identical *RR* or *SS* combinations are packed over each other along the *a*-axis. The O9, O10 and O11 atoms of water molecules interlink oxygen atoms of sulfate ion, from two *RR* or *SS* units, to a chain along the *a*-axis using hydrogen bonds *viz.*, O5···O10···O9···O11···O6. These are in turn hydrogen bonded to O7, O8, O11, O12 and O13 atoms that are filled up in channels having hydrophilic and hydrophobic environments. The O···O distances are within the range of other reported water chains [301–309]. Two *RR* and *SS* units are cross-linked by hydrogen bonding interactions and notable among them is presence of a planar six-membered ring involving O5 atom of sulfate ion, O7 and O8 atoms of water molecules (Fig. 8). In the packing diagram of **4**, *RR* and *SS* combinations form discrete dimeric units linked by hydrogen-bonding interactions involving solvated water and methanol

molecules, as shown in Fig. 9. The relevant D···A distances found in **3** and **4** are listed in Table 4.

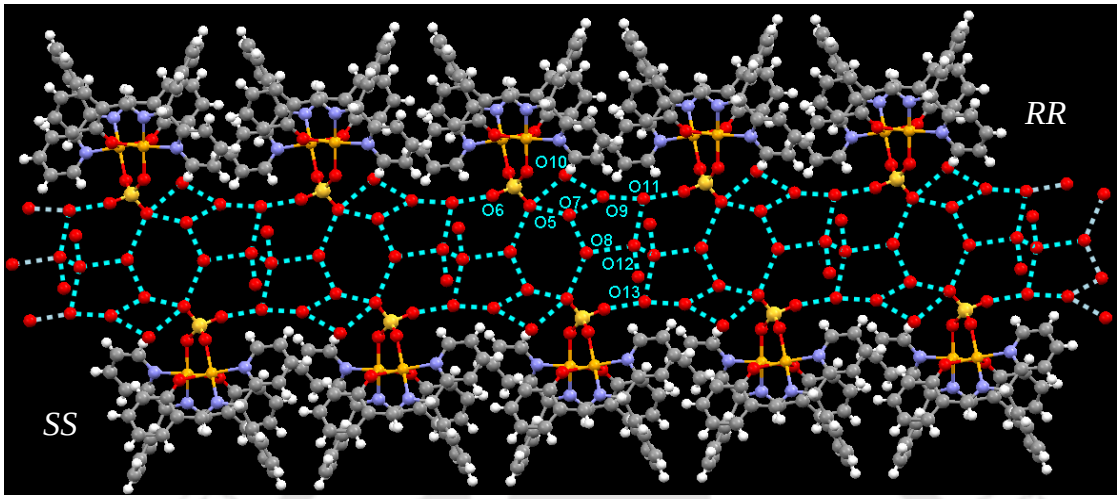

Fig. 8. Packing diagram showing the hydrogen bonding interactions present in **3**, on viewing along *a*-axis.

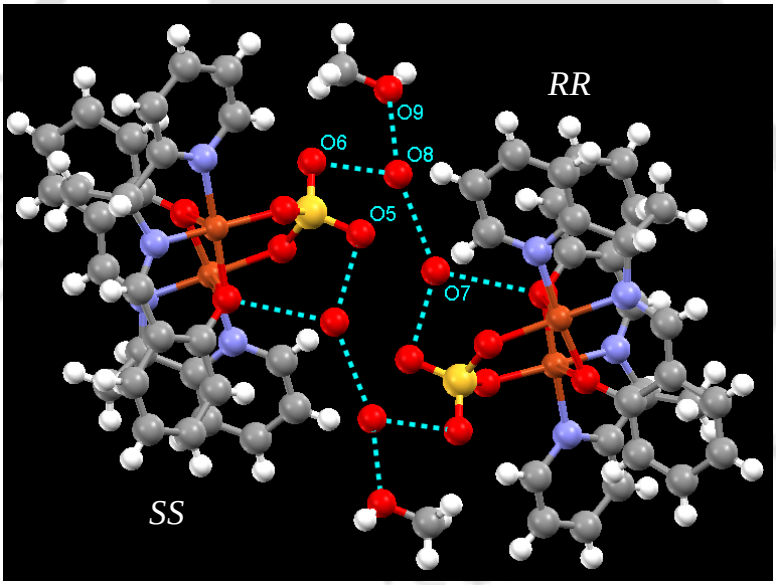

Fig. 9. Existence of discrete dimeric *RR* and *SS* combination linked by H–bonding interactions in **4**.

Table 4. Selected D···A interactions (Å) and their symmetry operators in **3** and **4**.

3		
O5···O7	2.875(5)	x+1, +y, +z
O5···O8	2.865(5)	
O5···O10	3.0(6)	
O6···O11	2.66(12)	
O7···O8	2.736(5)	-x+1, -y+2, -z
O7···O9	2.735(7)	
O8···O12	2.80(1)	x, +y+1, +z
O9···O10	2.89(6)	x-1, +y, +z
O9···O11	2.647(9)	
O11···O12	2.92(2)	x, +y-1, +z
O12···O13	2.71(2)	x, +y-1, +z
4		
O2···O7	2.864(9)	x, +y+1, +z
O5···O7	2.809(8)	x, +y+1, +z
O6···O8	2.99(1)	x, +y, +z-1
O7···O8	2.78(1)	-x+1, -y+1, -z+1
O8···O10	2.67(1)	

Complex **5** crystallizing in the $P2_1/n$ space group, contains a *hexa*-coordinated dinickel complex having $\{Ni_2(\mu\text{–}O_P)_2(\mu\text{–}OAc)\}$ unit, in which two Ni(II) atoms are bridged by an acetate ion and by two phenoxo groups. Coordination by **L2**, acetate ion and O_P bridging brings about the same *penta*-coordination environment around two nickel centers, but differ in the sixth coordination site which is completed by methanol oxygen atom in Ni1 and by cyanide nitrogen atom of dicyanamide ligand in Ni2. Therefore, both nickel centers have distorted *pseudo*-octahedral geometry and a perspective view of *SS*–$[Ni_2(\mathbf{L2})_2(OAc)(DCA)(CH_3OH)]$ homochiral dimer is displayed in Fig. 10. The acetate ion is slightly asymmetrically bridging having Ni–O distances of 2.011(2) and 2.024(2) Å, which is lying within the range 2.01 – 2.07 Å observed in few other cases [310–314]. The Ni_2O_2 core has a butterfly shape with the angles between planes containing Ni1Ni2O1 and Ni1Ni2O2 atoms being 157.45º, while between Ni1O2O1 and O1Ni2O2 atoms being 158.87°. The non-bonded Ni···Ni distance observed in **5** is 3.018(1) Å is considerably shorter by 0.092(1) Å than that reported in a closely related compound [Chapter 2, p 36.].

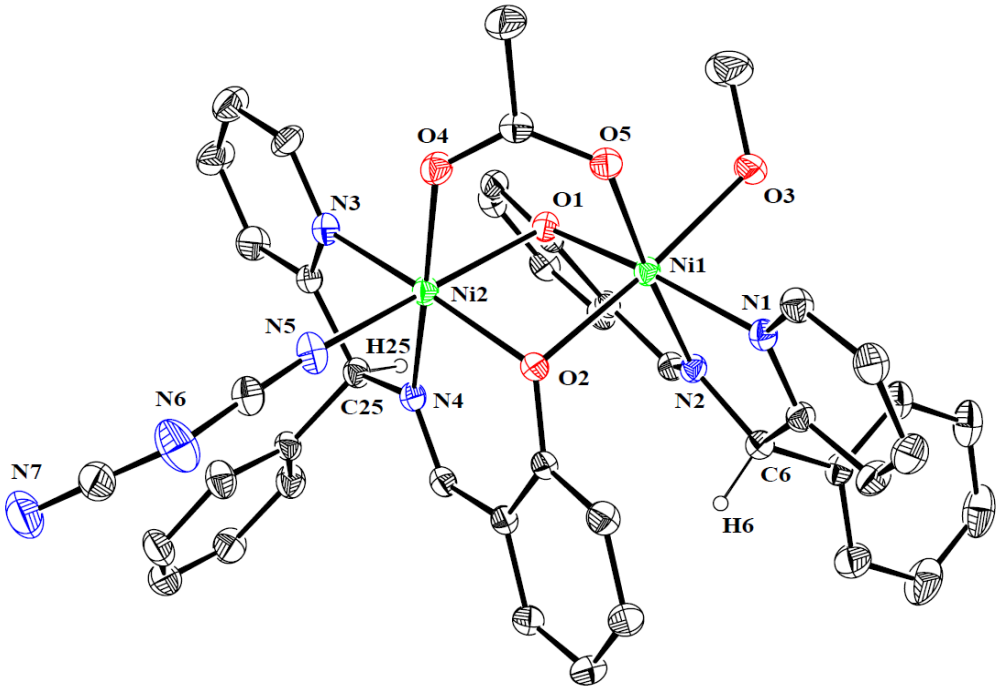

Fig. 10. ORTEP diagram (30% probability ellipsoids) of *SS*–[Ni_2(**L2**)$_2$(OAc)(DCA)(CH_3OH)] in **5** (All H–atoms except H6 and H25 are omitted for clarity).

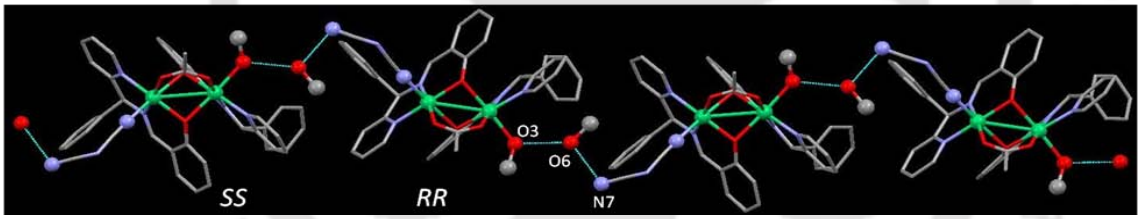

Fig. 11. Chain containing alternating *RR* and *SS* dimers in **5**.

Selected bond distances observed in **5** are listed in Table 5. The four coordination bonds arising from the ligand **L2** is slightly shorter at Ni1 than at Ni2 centers and this may be due to poor coordinating ability of methanol at Ni1. In the packing diagram, *RR* and *SS* dimers are arranged alternatively into chains (Fig. 11) in which two dimers are linked by hydrogen bonding interaction between coordinated methanol, lattice methanol (O3···O6, 2.733(7) Å) and uncoordinated end of the dicyanamide group (O6···N7, 2.820(8) Å). It is also pertinent to note that phenyl group substitution at the asymmetric carbon brings about steric crowding and this probably restricts the formation of dicyanamide ion linked zig-zag coordination chain which was previously observed with sterically less demanding methyl group substitution [Chapter 2, p 38].

Table 5. Selected bond distances (Å) and angles (°) in **5**.

5			
Ni1–N1	2.058(3)	Ni2–N3	2.064(3)
Ni1–N2	2.016(2)	Ni2–N4	2.031(2)
Ni1–O1	1.998(3)	Ni2–O2	2.014(3)
Ni1–O2	2.128(3)	Ni2–O1	2.197(3)
Ni1–O3	2.144(3)	Ni2–N5	2.089(3)
Ni1–O5	2.024(2)	Ni2–O4	2.011(2)
Ni1···Ni2	3.018(1)		
N1–Ni1–N2	80.7(1)	N3–Ni2–N4	80.7(1)
N1–Ni1–O1	171.7(1)	N3–Ni1–N5	92.3(1)
N1–Ni1–O2	94.1(1)	N3–Ni2–O1	91.9(1)
N1–Ni1–O3	88.3(1)	N3–Ni2–O2	170.7(1)
N1–Ni1–O5	97.5(1)	N3–Ni2–O4	93.8(1)
N2–Ni1–O1	91.0(1)	N4–Ni2–N5	92.3(1)
N2–Ni1–O2	94.3(1)	N4–Ni2–O1	92.3(1)
N2–Ni1–O3	89.6(1)	N4–Ni2–O2	90.9(1)
N2–Ni1–O5	176.6(1)	N4–Ni2–O4	173.3(1)
O1–Ni1–O2	86.3(1)	O1–Ni2–N5	174.7(1)
O1–Ni1–O3	91.9(1)	O1–Ni2–O2	84.1(1)
O1–Ni1–O5	90.9(1)	O1–Ni2–O3	175.7(1)
O2–Ni1–O3	175.7(1)	O1–Ni2–O4	84.6(1)
O2–Ni1–O5	88.7(1)	O2–Ni2–N5	92.2(1)
O3–Ni1–O5	87.4(1)	O2–Ni2–O4	94.2(1)

The yield reported here refers to isolated yields of compounds in the crystalline state only. During the isolation, crystalline solid was washed with ice-cold methanol. This resulted in dissolution of some of the product and ultimately led to lesser isolated yields. In order to check the nature of compound in the washings, solvent was removed and combined yield of this compound from washings and crystals were around 90–95%. The powder X-ray pattern of respective crystals of **1–3** (after powdering) and that of isolated powder from washings were examined. Both were identical and matched very well with the calculated pattern from single crystal X-ray data. Hence without doubt, solid isolated from washings were also of the same nature as that of crystals. The powder X-ray pattern of the solid compound isolated from the washings, crystals and calculated pattern from the single crystal X-ray data for complexes **1–3**, were shown in Fig. 12.

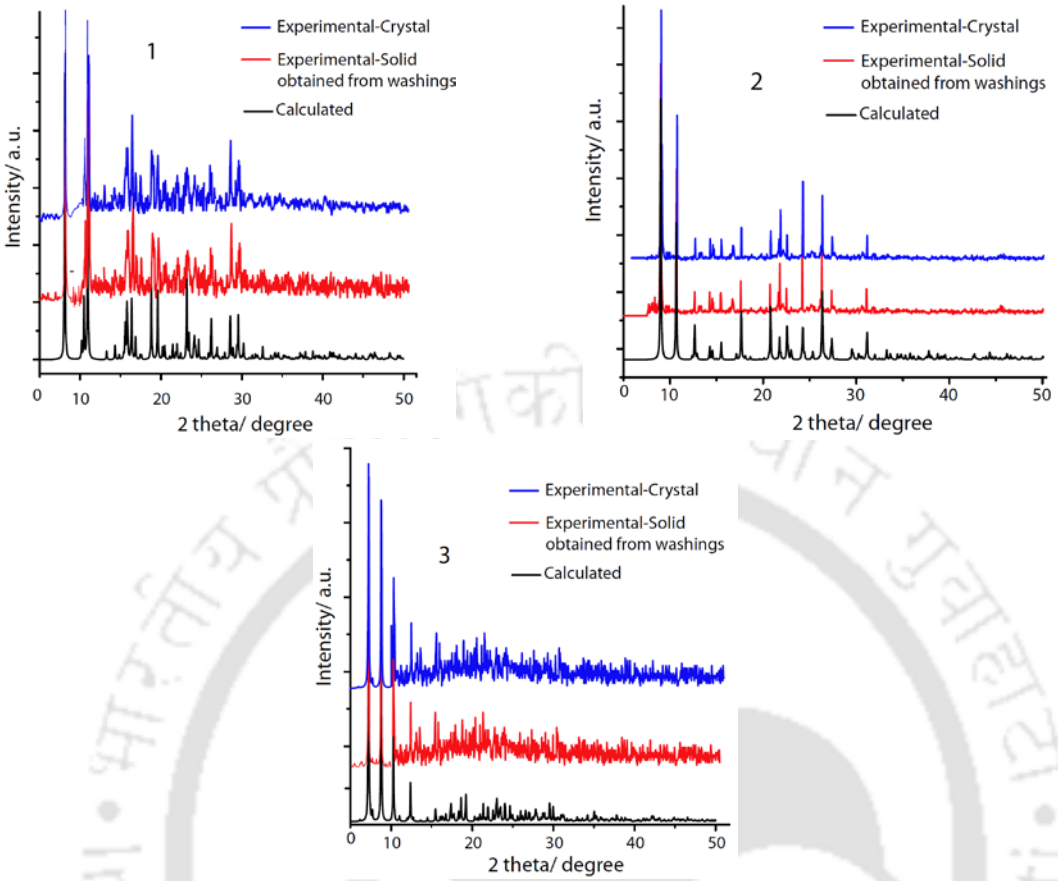

Fig. 12. PXRD patterns of compounds **1**–**3**.

3.4 Conclusion

Five complexes containing a dimetallic core was synthesized using a racemic mixture of end-capping tridentate Schiff base ligand and bridging ligands. Determination of their molecular structures revealed that bridging ligands play a key role in recognizing the chirality of the tridentate ligand. In **1** and **2**, NO_3^- and Cl^- respectively act as a bridge between two copper atoms. Hence dicopper core can have the center of symmetry thus resulting in a *RS* combination (heterochiral dimerization) of chiral tridentate ligands at two metal centers. However in **3**–**5** due to the presence of single sulfate or acetate ion bridges, the dimetallic core cannot have the center of symmetry. Therefore a *RR* and *SS* combinations (homochiral dimerization) of chiral tridentate ligand occur at the two metal centers in equal proportions and thus retain the overall racemic nature. The observed diastereoselectivity in these dimetallic cores refers only to the solid state structures. Also observed in compound **1** is a rare feature of nitrate ion (μ–1,1–NO_3^-) bridge between two copper centers.

Chapter 4

Molecular Structures of Isostructural Dinuclear M(II) (M=Ni, Cu, Zn) Complexes of Chiral Tridentate Ligand

Abstract

Using a racemic mixture of the chiral tridentate ligand, 1–((phenyl(2–pyridyl)methylimino)methyl)–2–naphthol (**L3H**) and $N(CN)_2^-$ as co-ligand, three isostructural complexes having general formula $[M_2(\mathbf{L3})_2(N(CN)_2)_2]\cdot 2MeOH$ (M = Ni(**1**), Cu(**2**) and Zn(**3**)) were prepared and structurally characterized. Determination of molecular structures of **1**–**3** confirmed the presence of dimetallic core constructed by monochelates of the chiral tridentate ligand having end–on–end dicyanamide ion (dca) bridge. Since a racemic mixture of chiral tridentate ligand **L3H** has been used, the self-assembly results in heterochiral dimerization (*RS* combination) of **L3** around the dimetallic core. Compounds **1**–**3** are centrosymmetric in nature as the center of symmetry lies inside the dimeric unit $[M_2(N(CN)_2)_2]$. Compounds **1**–**3** crystallize selectively as methanol solvate and do not crystallize in other polar solvents. In lattice, solvent methanol plays an important role in stabilizing the phenoxo–O of **L3** by strong H–bonding interaction of 2.881(2) Å in **1**, 2.991(5) Å in **2** and 2.800(9) Å in **3** respectively. Also the above complexes exhibits various weak interactions such as C–H···O, C–H···π, lone pair···π and π···π resulting 3D structures. Ligand **L3H** and complex **3** shows solid state photo-luminescence that can be attributed to intraligand transitions.

Molecular Structures of Isostructural Dinuclear M(II) (M=Ni, Cu, Zn) Complexes of Chiral Tridentate Ligand

In this Chapter, synthesis and structural characterization of three isostructural complexes having general formula $[M_2(\mathbf{L3})_2(N(CN)_2)_2]\cdot 2MeOH$ (M = Ni(**1**), Cu(**2**) and Zn(**3**)) derived from the chiral tridentate imine ligand (**L3H**) and $N(CN)_2^-$ as co-ligand has been described. The effect of end–on–end dicyanamide ion on the diastereoselectivity of this ligand around the bimetallic core has been observed. The importance of solvent methanol over other polar solvents for the crystallization of such dimetallic core has also been observed.

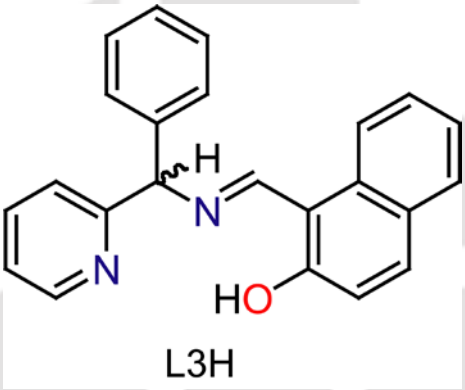

L3H

4.1 Experimental

4.1.1 Syntheses

(*R*, *S*) Phenyl(2–pyridyl)methaneamine is prepared using the same procedure described in Chapter 3.

*4.1.1.1 (R, S) 1–((phenyl(2–pyridyl)methylimino)methyl)–2–naphthol (**L3H**)*

A mixture of phenyl(2–pyridyl)methaneamine (4.5 g, 26.3 mmol) and 2–hydroxy–1–naphthaldehyde (4.2 g, 26.3 mmol) in methanol (100 mL) was stirred for 2 h. Yellow precipitate of **L3H** deposited was collected by suction filtration, washed with cold methanol and dried over $CaCl_2$. Yield: 7.2 g (95%). IR (KBr, cm^{-1}): 3049(w), 2929(w), 1625(s), 1609(m), 1595(m), 1571(w), 1540(s), 1519(w), 1489(s), 1474(m), 1454(m), 1432(m), 1400(s), 1349(s), 1337(s), 1313(m), 1251(w), 1214(s), 1182(s), 1140(m),

1165(w), 1097(w), 1027(s), 993(s), 943(w), 862(m), 837(s), 753(s), 699(s), 609(m), 562(s), 497(m), 470(w). 400 MHz ^{1}H NMR (δ (*J*, Hz), $CDCl_3$): 9.02 (1H, s), 8.52 (1H, d, 4.0), 7.80 (1H, d, 8.4), 7.64 (1H, d, 9.2), 7.58 (1H, d, 8.0), 7.569 (2H, t, 6.6), 7.37 (2H, t, 8.0), 7.30 (1H, t, 8.4), 7.22 (1H, t, 7.4), 7.15 (1H, t, 6.3), 7.01 (1H, t, 5.4), 6.96 (1H, d, 9.2), 5.84 (1H, s), 2.0 (OH, s). 100 MHz ^{13}C NMR (δ, $CDCl_3$): 171.36, 160.5, 159.4, 149.6, 140.7, 137.3, 136.5, 133.5, 129.3, 129.1, 128.1, 128.0, 127.6, 127.0, 123.2, 122.94, 122.8, 121.9, 118.7, 108.1, 74.7.

*4.1.1.2 [Ni_2(**L3**)$_2$(μ–1,5–dca)$_2$]·2MeOH (**1**)*

To **L3H** (0.29 g, 1.0 mmol) dissolved in methanol (30 mL), solid $Ni(NO_3)_2·6H_2O$ (0.21 g, 1.0 mmol) along with $NaN(CN)_2$ (0.076g, 1.0 mmol) were added and the resulting red colored solution was stirred at room temperature for 1 h. The solvent was removed and the green residue was washed with ice-cold methanol. Yield: 0.52 g (52%). Single crystals of **1** suitable for X-ray diffraction study were obtained slow evaporation of methanol solution. *Anal.* Calc. for $C_{52}H_{42}N_{10}Ni_2O_4$: C, 63.19; H, 4.28; N, 14.17%. Found: C, 63.01; H, 4.18; N, 13.87%. IR (KBr, cm^{-1}): 3080(m), 2294(s), 2248(s), 2175(s), 1642(s), 1616(s), 1603(m), 1571(w), 1541(s), 1508(m), 1486(m), 1455(s), 1435(m), 1402(s), 1363(s), 1342(m), 1311(m), 1274(w), 1256(m), 1216(w), 1198(s), 1186(s), 1164(m), 1144(s), 1102(s), 1066(m), 1034(m), 982(s), 949(w), 926(w), 862(m), 832(s), 755(s), 659(m), 644(w), 629(m), 568(s), 514(s), 475(m). μ_{eff}/ Ni (298 K), 2.34 B. M.

Same procedure was followed for the syntheses of **2** and **3** by respectively using $Cu(NO_3)_2·3H_2O$ and $Zn(NO_3)_2·6H_2O$, in 1.0 mmol quantities of each reactant.

*4.1.1.3 [Cu_2(**L3**)$_2$(μ–1,5–dca)$_2$]·2MeOH (**2**)*

Yield: 0.58 g (59%). *Anal.* Calc. for $C_{52}H_{42}Cu_2N_{10}O_4$: C, 62.58; H, 4.24; N, 14.03%. Found: C, 61.92; H, 4.21; N, 13.84%. IR (KBr, cm^{-1}): 3056(w), 2925(w), 2293(m), 2238(m), 2174(s), 1619(s), 1607(s), 1571(m), 1538(s), 1508(w), 1483(w), 1452(m), 1428(m), 1412(m), 1398(m), 1365(m), 1307(w), 1251(m), 1187(s), 1165(w), 1142(w), 1094(w), 1053(w), 1030(m), 968(w), 829(s), 758(s), 746(m), 705(s), 676(w), 630(w), 566(m), 510(s). EPR (solid): g_{av}= 2.05, μ_{eff}/ Cu (298 K), 1.82 B. M.

*4.1.1.4 [Zn_2(**L3**)$_2$(μ–1,5–dca)$_2$]·2MeOH (**3**)*

Yield: 0.652 g (71%). *Anal.* Calc. for $C_{52}H_{42}Zn_2N_{10}O_4$: C, 62.35; H, 4.23; N, 13.98%. Found: C, 62.31; H, 3.84; N, 13.64%. IR (KBr, cm^{-1}): 3058(w), 2967(w), 2924(w), 2225(w), 2171(w), 2089(s), 1620(s), 1572(m), 1547(s), 1511(s), 1480(m), 1458(m), 1433(w), 1416(s), 1382(m), 1364(m), 1335(s), 1295(s), 1248(s), 1184(s), 1159(m), 1144(m), 1122(w), 1103(m), 1016(m), 988(m), 962(w), 857(m), 824(s), 776(m), 746(s), 731(w), 638(w), 563(m), 486(m).

4.2 Results and discussion

4.2.1 Synthesis and spectroscopic studies

The racemic mixture of the Schiff base (**L3H**) was synthesized by stirring (*R*, *S*)–phenyl(2–pyridyl)methaneamine and 2–hydroxy–1–naphthaldehyde (1:1 ratio) in methanol at room temperature. This ligand has unsymmetrical N_2O chromophore and a chiral carbon. A 1:1:1 mixture of metal nitrate, **L3H** and Na(dca) on stirring in methanol afforded the neutral *penta*-coordinated dimer [Ni_2(**L3**)$_2$(dca)$_2$]·2MeOH (**1**), [Cu_2(**L3**)$_2$(dca)$_2$]·2MeOH (**2**) and [Zn_2(**L3**)$_2$(dca)$_2$]·2MeOH (**3**) respectively, in good yields. The three complexes were characterized using microanalyses and spectroscopic studies. The micro analytical results are in good agreement with the formulations. All the complexes are stable over a long period in powdery or in crystalline form and are soluble in common organic solvents. The IR spectra of **1**–**3** exhibit strong absorptions in the range 2130 – 2200 cm^{-1} and weak to medium bands in the range 2230 – 2360 cm^{-1}. These bands originate from the coordinated dca ion and since frequencies of these bands are shifted to higher values than that observed in the free dca, presence of μ–1,5 bridging mode can be inferred [315–320]. Presence of coordinated **L3H** in these complexes can be inferred from the bands due to $\nu_{C=N}$ and $\nu_{C=C}$ stretches in the region 1620 – 1595 cm^{-1}. Room-temperature solid phase magnetic susceptibility of **1** has been determined. The experimentally observed μ_{eff} value of 2.34 B. M. is less than calculated spin only value which is suggestive of presence of antiferromagnetic coupling through dca ion. Compound **2** shows one-electron paramagnetism with μ_{eff} = 1.82 B. M. which is closer to

spin only value. Complex **3** is diamagnetic as expected for a metal ion having d^{10} electronic configurations.

4.3 Molecular structures

The molecular structures of **1**–**3** were determined using single crystal X-ray diffraction techniques. The crystal data and refinement parameters are listed in Table 1. Selected bond distances and angles are listed in Table 2. All the three complexes crystallized in *P*–1 space group and have the isostructural $[M_2(\mathbf{L3})_2(\mu\text{–}1,5\text{–dca})_2]$ entity. The binuclear molecule is centrosymmetric in nature. Perspective views of heterochiral dimers are displayed in Fig. 1 (**1**), Fig. 2 (**2**) and Fig. 3 (**3**). In addition, two methanol molecules are present in the lattice. In each case the bivalent metal ion is bound by the tridentate end-cap ligand **L3**. One end of dca is linked to the metal ion in the square plane and the other end occupies the axial site of second metal center. Thus the central metal ions have a distorted square pyramidal geometry and the τ parameters (0.03 in **1**; 0.03 in **2** and 0.13 in **3**) concur this [269]. The ligand **L3** is bound to the bivalent metal ions by a five-membered and a six-membered chelate rings. The ligand framework is nearly planar and the metal ions deviate slightly (Ni, 0.25; Cu, 0.15; Zn, 0.37 Å) from the plane containing the donor atoms (N1MO1) and are shifted towards the axial site.

A racemic mixture of Schiff base ligand has been used and compounds **1**–**3** contain equal mixture of *R* and *S* isomers. Since the $[M_2(\mathbf{L3})_2(\mu\text{–}1,5\text{–dca})_2]$ unit is centrosymmetric, *RS* combination (heterochiral dimerization) of Schiff base is present in the dimeric unit. In all the cases, the M–O_P {O_P = phenolate–O; N_Y = pyridyl–N; N_I = imine–N; N_C = dicyanamide–N and O_M = methanol–O} distance is shorter than the M–N distances. The M–O_P distance follow the trend Ni > Cu < Zn, which is in accordance with the relative sizes of the metal ions. The same trend is also observable in the M–N_Y and M–N_I distances. The M–N_C distances in the equatorial plane are marginally shorter by 0.023(2) Å than the axial bond in Ni but more pronounced in Cu by 0.404(3) Å, which is the result of Jahn-Teller distortion. But in **3**, the M–N_C distances in the equatorial plane is marginally longer by 0.046(5) Å than the axial bond. The chelate bite angle for the five-membered ring N1–M–N2 lie in the range 79.1(1) – 82.7(1)º and for the six-membered ring N2–M–O1 lie in the range 88.2(2) – 91.6(1)°. The *cisoid* angles deviate from their

ideal values of 90° and are in the range 88.96(7) – 104.58(7)° (in Ni); 89.17(8) – 99.16(8)° (in Cu) and 89.7(2) – 112.0(2)° (in Zn) respectively.

Table 1. Crystallographic and refinement parameters for **1**–**3**.

	1	**2**	**3**
Formula	$C_{52}H_{42}N_{10}O_4Ni_2$	$C_{52}H_{42}N_{10}O_4Cu_2$	$C_{52}H_{42}N_{10}O_4Zn_2$
Formula weight	988.34	998.06	1001.74
T (K)	293(2)	293(2)	293(2)
Wavelength (Å)	0.71073	0.71073	0.71073
Crystal system	Triclinic	Triclinic	Triclinic
Space group	*P*–1	*P*–1	*P*–1
a (Å)	7.8555(3)	7.8619(7)	7.8390(10)
b (Å)	10.6916(4)	10.6309(10)	10.5604(13)
c (Å)	15.2206(8)	15.3210(19)	15.551(3)
α (°)	101.829(3)	101.984(8)	102.301(11)
β (°)	99.708(3)	100.042(8)	101.278(12)
γ (°)	110.408(2)	110.246(6)	108.883(8)
V (Å^3)	1131.78(9)	1132.1(2)	1140.3(3)
Z	1	1	1
D_{calcd} (g m^{-3})	1.450	1.464	1.459
μ (mm^{-1})	0.892	0.999	1.111
F(0 0 0)	512	514	516
Reflection collected	5172	5669	5208
Unique reflections	5167	4964	5205
Goodness-of-fit (GOF)[a] on F^2	1.000	1.002	1.002
R [$I > 2\sigma(I)$]	[b]R_1 = 0.0223 [c]wR_2 = 0.1457	[b]R_1 = 0.0388 [c]wR_2 = 0.0917	[b]R_1 = 0.0665 [c]wR_2 = 0.1890
R indices (all data)	[b]R_1 = 0.0223 [c]wR_2 = 0.1457	[b]R_1 = 0.0598 [c]wR_2 = 0.1010	[b]R_1 = 0.0665 [c]wR_2 = 0.1890

[a]GOF = $[\sum[w(F_0^2 - F_c^2)^2]/ M - N]^{1/2}$ (M =number of reflections, N = number of parameters refined).

[b]$R_1 = \sum \| F_0 | - | Fc \| / \sum | F_0 |$.

[c]$wR_2 = [\sum[w(F_0^2 - F_c^2)^2]/ \sum[w(F_0^2)^2]]^{1/2}$.

Table 2. Selected bond distances (Å) and angles (°) in **1**–**3**.

	1	**2**	**3**
M1–N1	2.036(1)	2.001(1)	2.106(3)
M1–N2	1.969(2)	1.935(2)	2.064(3)
M1–N3	2.022(2)	1.977(3)	2.077(5)
M1–N4	2.045(2)	2.381(3)	2.031(5)
M1–O1	1.945(1)	1.912(1)	1.977(3)
N1–M1–N2	81.53(6)	82.67(8)	79.1(1)
N2–M1–O1	90.55(6)	91.63(7)	88.2(1)
N1–M1–N3	94.48(7)	90.79(8)	92.1(2)
N1–M1–N4	94.57(7)	94.74(9)	98.8(2)
N3–M1–N4	92.72(8)	92.58(9)	98.3(2)
O1–M1–N3	100.53(7)	98.15(8)	89.7(2)
O1–M1–N4	88.96(7)	89.17(8)	102.9(2)
N2–M1–N3	104.58(7)	99.16(8)	149.3(2)
N2–M1–N4	162.47(7)	168.0(9)	112.0(2)
N1–M1–O1	164.40(6)	170.08(7)	157.7(1)

Two solvated methanol molecules are selectively interacting with two O_P atoms each forming a strong H–bonding interaction having a non-bonded $O_M\cdots O_P$ distance of 2.880(3) Å (in Ni); 2.898(4) Å (in Cu) and 2.783(7) Å (in Zn). Here methanol serve as H–donor and phenoxide oxygen acts as H–acceptor. It exhibits various weak interaction such as C–H$\cdots O_M$, {3.210(4) Å in **1**; 3.202(4) Å in **2**; 3.198(9) Å in **3**} C–H$\cdots\pi$, {3.532(3) Å in **1**; 3.584(4) Å in **2**; 3.542(9) Å in **3**} and $O_M\cdots\pi$, {3.213(3) Å in **1**; 3.252(4) Å in **2**; 3.328(6) Å in **3**}. The pictorial representation of various weak interactions present between methanol and $[M_2(\mathbf{L3})_2(\mu\text{–}1,5\text{–dca})_2]$ in **1** is displayed in Fig. 4. It seems that $[M_2(\mathbf{L3})_2(\mu\text{–}1,5\text{–dca})_2]$ unit crystallizes only as methanol solvate and attempts to crystallize in other polar solvents including different alcohols failed to yield crystals. In addition, in a mixture of polar solvents that include methanol, crystals of **1**–**3** could not be obtained. Therefore dimer $[M_2(\mathbf{L3})_2(\mu\text{–}1,5\text{–dca})_2]$ crystallizes selectively as methanol solvate using pure methanol as solvent.

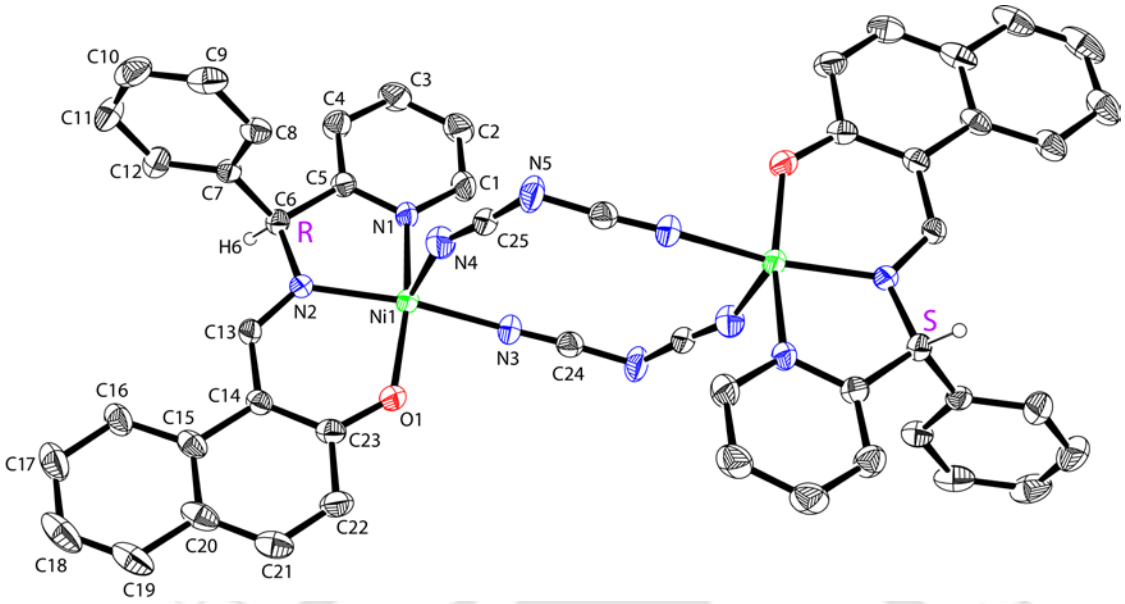

Fig. 1. ORTEP diagram (30%) and atom labeling scheme in $[Ni_2(\mathbf{L3})_2(\mu\text{–}1,5\text{–dca})_2]$ (All H– atoms except H6 are omitted for clarity).

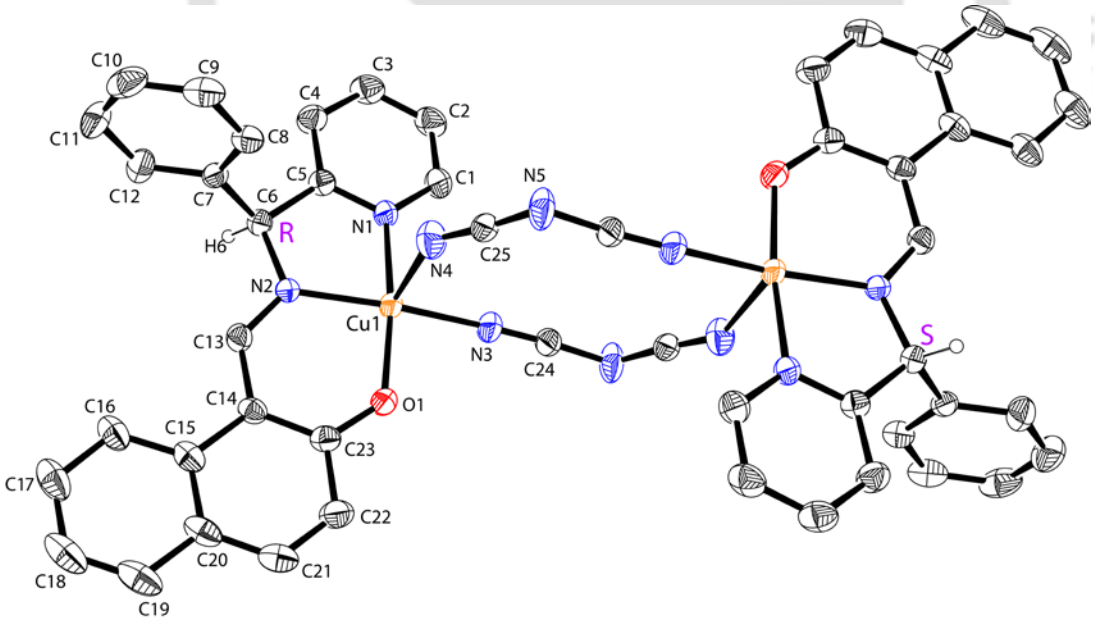

Fig. 2. ORTEP diagram (30%) and atom labeling scheme in $[Cu_2(\mathbf{L3})_2(\mu\text{–}1,5\text{–dca})_2]$ (All H–atoms except H6 are omitted for clarity).

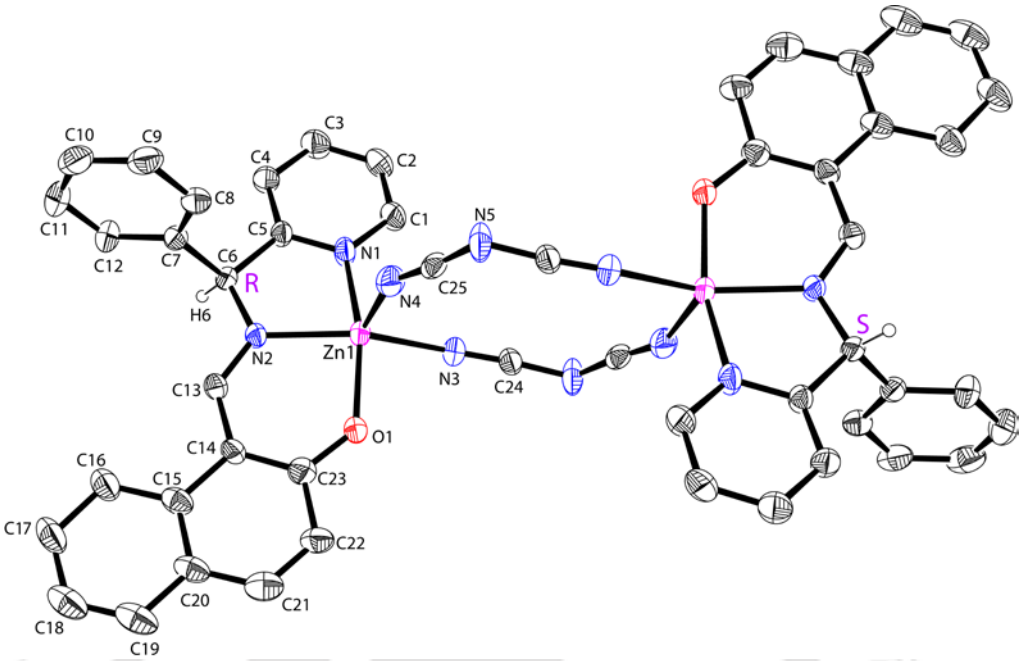

Fig. 3. ORTEP diagram (30%) and atom labeling scheme in $[Zn_2(\mathbf{L3})_2(\mu\text{–}1,5\text{–dca})_2]$ (All H– atoms except H6 are omitted for clarity).

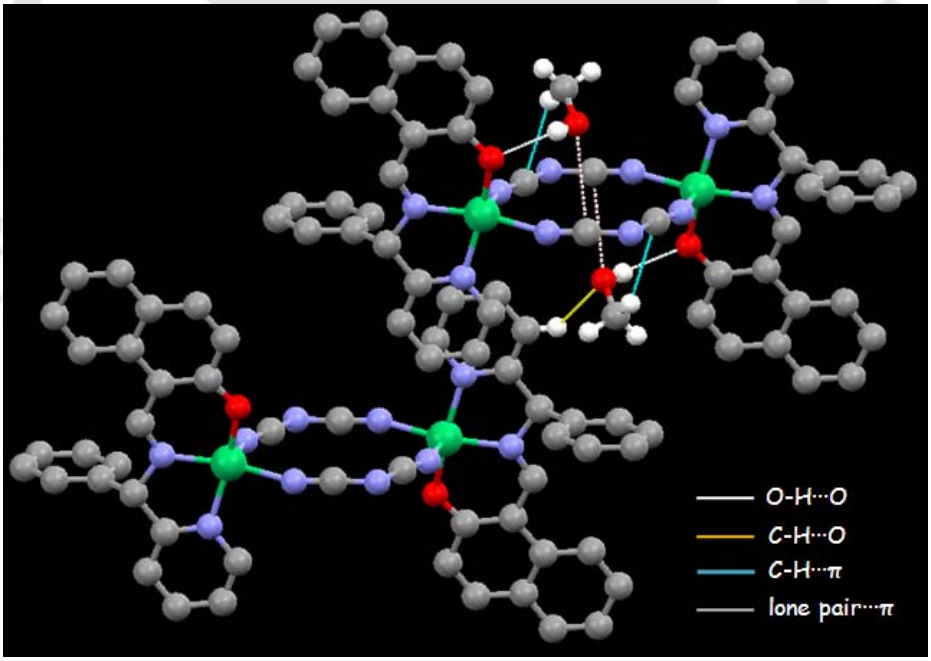

Fig. 4. Various interactions exhibited by solvent methanol in **1**.

In packing diagram, apart from H–bonding and weak interaction of methanol molecule, other weak interactions present between $[M_2(\mathbf{L3})_2(\mu\text{–}1,5\text{–dca})_2]$ are C6–H6···π, {3.551(2)

Å in **1**; 3.567(4) Å in **2**; 3.560(4) Å in **3**} C19–H19···π, {3.734(2) Å in **1**; 3.691(4) Å in **2**; 3.690(7) Å in **3**} and C10–H10···O_P {3.487(2) Å in **1**; 3.519(4) Å in **2**; 3.198(9) Å in **3**}. The extended 3D structure of **1** representing H–bonding interaction between solvent methanol and phenoxo–O of **L3** is displayed in Fig. 5. The π stacking interaction is present between the aromatic rings and distance between two planes containing carbon atoms of napthyl rings are 3.28 Å (in **1**), 3.31 Å (in **2**) and 3.41Å (in **3**).

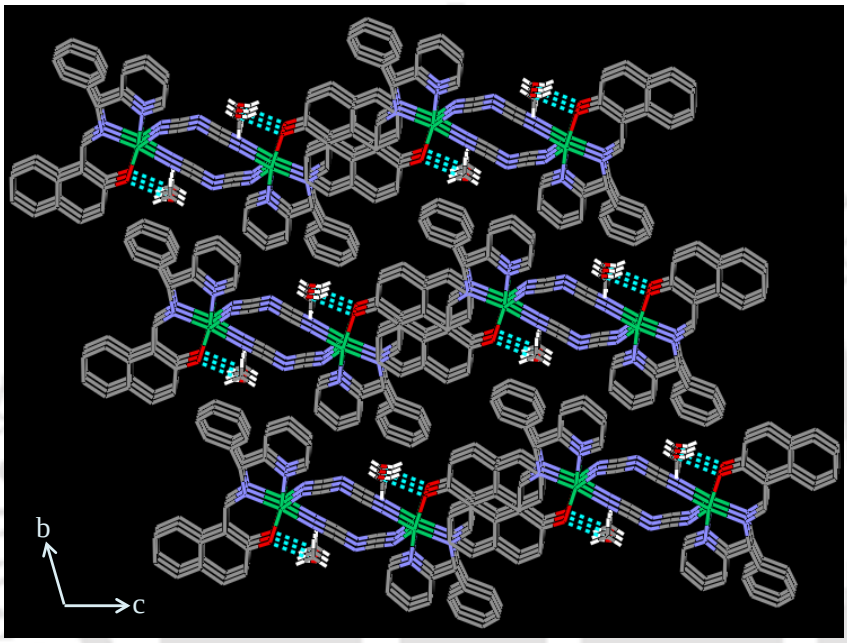

Fig. 5. Packing diagram representing H–bonding interaction between solvent methanol(O_M) and phenoxo-O(O_P) in **1**.

4.3.1. $M_2(dca)_2$ units

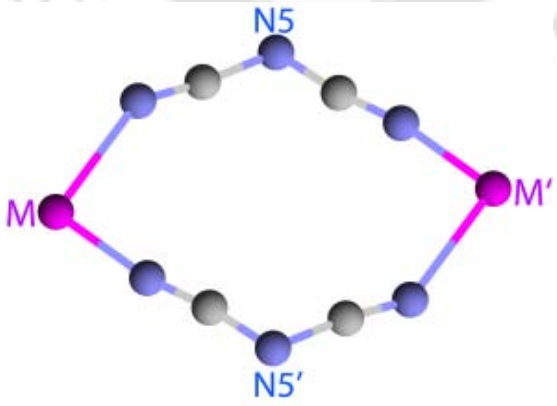

Fig. 6. Schematic view of $M_2(dca)_2$ units in **1**–**3**.

In **1**–**3**, the double μ–1,5 dca ion bridge brings about dinuclear $M_2(dca)_2$ units due to *cis* orientation of two dca units around the metal center and sp^2 hybridization on amide nitrogen N5 that imparts a ‘‘V’’ shape to dca. A schematic view of such unit is shown in Fig. 6 and relevant parameters are listed in Table 3. The bond angles subtended at the metal center and at N5 lie in the ranges 71.20(5) – 73.74(1)° and 106.26(1) – 108.10(5)°, respectively

Table 3. Selective bond parameters around $M_2(dca)_2$ units in **1**–**3**.

Link	**1**	**2**	**3**
M···N5	4.407(2)	4.384(3)	4.368(6)
M···N5′	4.413(2)	4.591(3)	4.422(6)
N5···N5′	5.168(2)	5.227(4)	5.27(1)
M···M′	7.148(4)	7.299(1)	7.032(1)
N5···M···N5′	71.74(3)	71.20(5)	73.74(1)
M···N5···M′	108.26(3)	108.80(5)	106.26(1)

The bond angles related to the bridging dca ligands such as M1–N3–C24 and M1–N4–C25 are 153.8(1) Å and 159.2(1) Å for **1**, 165.9(2) Å and 141.4(2) Å for **2** and 153.4(5) Å and 149.7(5) Å for **3** respectively, that means **2** deviate more in comparison to **1** and **3** from linearity. The M–N3 (M1′–N3′) and M1–N4 (M1′–N4′) bond distances in **1**, **2** and **3** are 2.045(1) Å and 2.021(1) Å, 1.977(2) Å and 2.379(3) Å, 2.073(6) Å and 2.031(6) Å, respectively, that means in **2** elongation and compression of M–N3/N4 bonds are more in comparison to **1** and **3**. The M1–NCNCN–M1′ bridging array in **1**, **2** and **3** adopts a ‘‘V’’ shape conformation due to sp^2 hybridization of the middle nitrogen N5 atom of dca, where the C–N–C angle are 120.2(1)° for **1**, 122.7(2)° for **2** and 120.7(6)° for **3** respectively. An approximate C_{2v} symmetry is observed for the dca ligands in **1**, **2** and **3**, where the average C–N and C=N bond lengths are of 1.302(2) and 1.146(2) Å, respectively, as commonly observed in $[N(CN)_2]^-$ anions. A small degree of p conjugation within $[N(CN)_2]^-$ results in longer N5–C24 and N5–C25 bond distances.

4.4 Thermal analyses

The thermogravimetric analyses of **1**–**3** were carried out on freshly prepared samples. The profiles recorded in the temperature range 30 – 700°C in a static atmosphere of

nitrogen are displayed in Fig. 7. The weight loss of 6.38% (calcd. 6.47%) for **1**, 6.40% (calcd. 6.41%) for **2** and 6.35% (calcd. 6.38%) for **3**, corresponding to the loss of two methanol molecules were observed in the temperature range 64 – 112°C (midpoint temperature, 98°C) for **1**, 52 – 118°C (midpoint temperature, 102°C) for **2** and 61 – 115°C (midpoint temperature, 101°C) for **3** respectively.

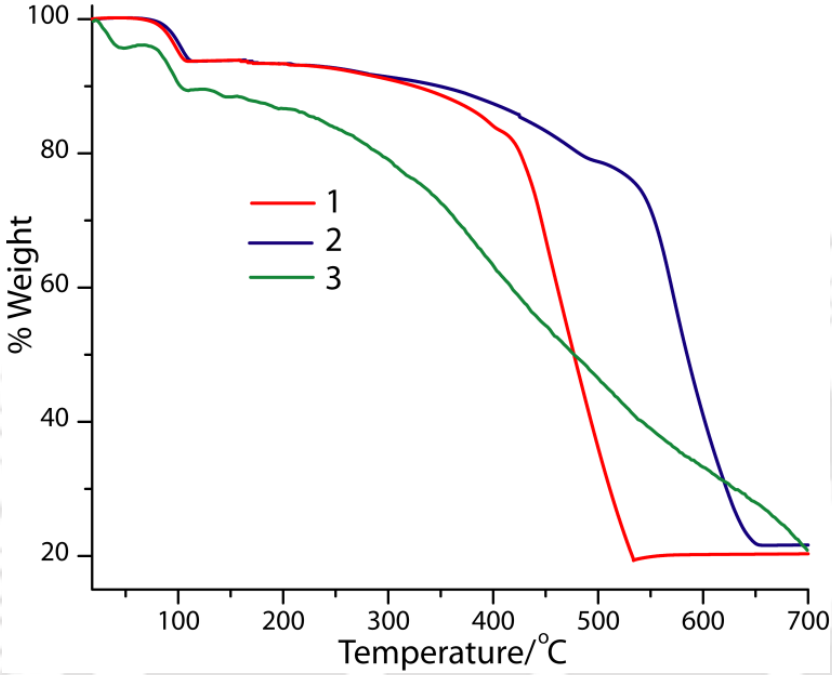

Fig. 7. TG profiles of **1**–**3**.

4.5 Luminescence properties

Solid-state emission spectra of **1**–**3** complexes were recorded and compared with the ligand **L3H**. On coordination, the conformational flexibility of the ligand is restricted and metal ions having d^{10} configuration exhibit interesting luminescence properties [321–324]. The emission spectra of compounds **1**–**3** and **L3H** obtained by using excitation wavelength (λ_{ex}) in the range 390 – 410 nm are depicted in Fig. 8. The ligand itself exhibits a luminescence with peak maxima 475 nm which is slightly red shifted by about 7 nm on complexation with divalent zinc. The luminescence is of intra-ligand ($\pi^* - \pi$) fluorescence in origin. However the other two metal ions *viz.*, Cu^{2+} partially quench the luminescence while Ni^{2+} does completely. This observation is expected for the metal ions having partially filled *d*–orbitals. The solution state luminescence of **L3H** and **1–3** has

been recorded in methanol and indeed quenching by Cu^{2+} and Ni^{2+} has been observed. However partial quenching that has been observed in solid state emission spectra may be due to inefficient decay of the excited state through the internal conversion mechanism with surrounding, but is very efficient in solution state with the solvent matrix.

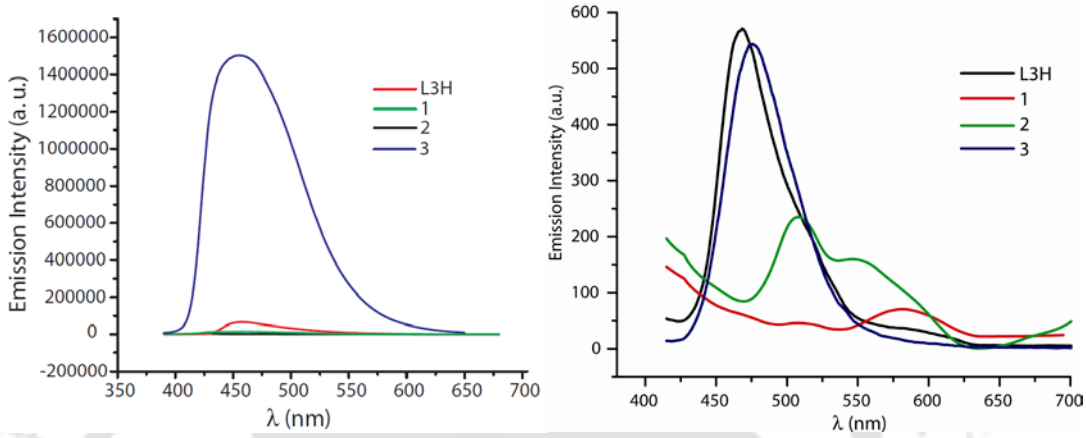

Fig. 8. Luminescence spectra of **L3H** and **1**–**3** in methanol (left) and in the solid state (right).

4.6 Conclusion

Three isostructural complexes having general formula $[M_2(\mathbf{L3})_2(N(CN)_2)_2]\cdot 2MeOH$ (M = Ni(**1**), Cu(**2**) and Zn(**3**)) were prepared by using chiral tridentate Schiff base ligand (**L3H**) and $N(CN)_2^-$ ion as co-ligand. Determination of molecular structures of **1**–**3** reveals the presence of centrosymmetric dimetallic cores based on a pair of *R* and *S* enantiomers of **L3**. Hence the self-assembly prefers heterochiral dimerization (*RS*) of **L3** around the dimetallic core linked by long V-shaped μ–1,5–dca bridge. Since compounds **1**–**3** do not crystallize in other polar solvents, dimer $[M_2(\mathbf{L3})_2(\mu\text{–}1,5\text{–}dca)_2]$ crystallizes selectively as methanol solvate only. In lattice, solvent methanol plays an important role in stabilizing the phenoxo–O of **L3** by strong H–bonding interaction of 2.881(2) Å in **1**, 2.991(5) Å in **2** and 2.800(9) Å in **3** respectively. These complexes are particularly interesting because of their bimetallic core having long dca bridge; specifically **1** and **2** in magnetic point of view whereas **3** due to its luminescence properties in the solid-state.

Chapter 5

Structural Variations in Copper Complexes Containing a Chiral Tridentate Ligand and Dicyanamide Ion

Abstract

Using a racemic mixture of chiral tridentate ligand 2–((1–(2–pyridyl)ethylimino)methyl)phenolate ion (**L1**), different Cu(II) salts and sodium dicyanamide, complexes having formulae $[Cu_4(\mathbf{L1})_2(dca)_4]_n$ (**1**), $[Cu(\mathbf{L1})(dca)(OH_2)]$ (**2**), $[Cu_2(\mathbf{L1})_2(dca)_2]_n$ (**3**) and $[Cu_2(\mathbf{L1})_2(dca)_2]$ (**4**) were synthesized and characterized. The formation of these compounds clearly depends upon the nature of copper(II) salt and amount of sodium dicyanamide employed in the reaction. By using either $Cu(ClO_4)_2{\cdot}6H_2O$ or $CuCl_2{\cdot}2H_2O$, **1** was isolated. On the other hand by using $CuSO_4{\cdot}5H_2O$, $Cu(NO_3)_2{\cdot}3H_2O$ and $Cu(OAc)_2{\cdot}H_2O$, compounds **2**, **3**, and **4** were isolated respectively. Compounds **1**, **3** and **4** have center of symmetry with in Cu_2O_2 core. Complex **1** is a mixed valent Cu(II)Cu(I) polymer having zipper like structure whereas complex **3** exhibits 2D grid structure. In **2**, coordinated H_2O molecule forms enantioselective and diastereoselective hydrogen-bonding interaction with dca ion and phonoxo–O atom respectively. In **4**, dca ion involves in strong C–H···N interaction which restricts the formation of dca ion bridged dimer or polymer as found in **1** and **3**. Since the Schiff base used is a racemic mixture, each dimeric unit result in a heterochiral dimerization of **L1**.

Structural Variations in Copper Complexes Containing a Chiral Tridentate Ligand and Dicyanamide Ion

In this chapter, synthesis and structural characterization of copper complexes derived from the chiral tridentate Schiff base ligand (**L1H**) and Na(dca) are described. The formation of these compounds clearly depends on nature of copper(II) salt and amount of sodium dicyanamide employed used in the reaction. That is compound **1** was isolated either by using $Cu(ClO_4)_2 \cdot 6H_2O$ or $CuCl_2 \cdot 2H_2O$; **2** by using $CuSO_4 \cdot 5H_2O$; **3** by using $Cu(NO_3)_2 \cdot 3H_2O$ and **4** by using $Cu(OAc)_2 \cdot H_2O$. All compounds formed are specific on identity of copper(II) salt and amount of sodium dicyanamide employed in the reaction.

5.1 Experimental

5.1.1 Syntheses

*5.1.1.1 $[Cu^{II}Cu^{I}(\mathbf{L1})(N(CN)_2)_2]_n$ (**1**)*

A methanolic solution (40 mL) of (*R*, *S*) 1–(2–pyridyl)ethylamine (0.122 g, 1 mmol) and salicylaldehyde (0.122 g, 1 mmol) was heated at reflux for 4 hour. To this $Cu(ClO_4)_2 \cdot 6H_2O$ (0.372 g, 1 mmol) dissolved in methanol was added and was stirred for 4 h. Finally, an aqueous solution (2 mL) of $NaN(CN)_2$ (0.180 g, 2 mmol) was added drop wise to the above mixture with stirring and the resulting solution was then filtered. After few days, the green solution deposited dark green crystals suitable for X-ray crystallographic analysis and were collected by filtration and dried in desiccators. A suitable crystal was selected for X-ray crystallographic analysis. Yield: 0.280 g (56%). *Anal*. Calc. for $C_{18}H_{13}Cu_2N_8O$: C, 44.63; H, 2.70; N, 23.13%. Found: C, 44.21; H, 2.56; N, 22.84%. IR (KBr, $c\bar{m}^{1}$): 3069(w), 2980(s), 2320(w), 2278(s), 2208(s), 2166(s), 1627(s), 1602(s), 1572(w), 1541(w), 1443(s), 1399(s), 1337(s), 1294(s), 1282(w), 1255(w), 1200(w), 1147(w), 1131(s), 1103(s), 1058(w), 991(s), 769(s), 752(s), 740(s), 656(w), 602(w), 519(s), 505(w). UV–Vis [λ_{max}, nm (ε, $M^{-1}cm^{-1}$), CH_3OH solution]: 637(326); 375(12700); 269(41120); 242(50070); 219(57780). μ_{eff}/ Cu = 1.84 B. M. EPR (CH_3OH solution, 298 K): g_{av} = 2.091, A = 73 G.

*5.1.1.2 [Cu(**L1**)(N(CN)$_2$)(H$_2$O)] (**2**)*

Compound **2** was synthesized by following the procedure described for **1** by using $CuSO_4 \cdot 5H_2O$ (0.250 g, 1 mmol) instead of $Cu(ClO_4)_2 \cdot 6H_2O$. Yield: 0.231 g (62%). *Anal.* Calc. for $C_{16}H_{15}CuN_5O_2$: C, 51.54; H, 4.05; N, 18.78%. Found: C, 51.23; H, 3.89; N, 18.45%. IR (KBr, cm^{-1}): 3062(w), 2926(w), 2285(s), 2232(s), 2179(s), 1629(s), 1600(s), 1573(w), 1540(s), 1468(s), 1445(s), 1404(s), 1377(w), 1351(s), 1304(s), 1197(w), 1147(w), 1130(w), 1103(s), 1052(w), 1030(s), 903(s), 858(w), 764(s), 754(s), 741(s), 601(w), 563(w), 518(s), 460(w). UV–Vis [λ_{max}, nm (ε, $M^{-1}cm^{-1}$), CH_3OH solution]: 631(175); 376(5980); 269(22120); 242(26900); 219(31510). μ_{eff}/ Cu = 1.86 B. M. EPR (CH_3OH solution, 298 K): g_{av} = 2.110, A = 73 G

*5.1.1.3 [Cu$_2$(**L1**)$_2$(N(CN))$_2$]$_n$ (**3**)*

Compound **3** was synthesized by following the procedure described for **1** by using $Cu(NO_3)_2 \cdot 3H_2O$ (0.241 g, 1 mmol) instead of $Cu(ClO_4)_2 \cdot 6H_2O$ and by using 0.5 mmol of $NaN(CN)_2$ (0.044 g). Yield: 0.386 g (54%). *Anal.* Calc. for $C_{32}H_{26}Cu_2N_{10}O_2$: C, 54.16; H, 3.69; N, 19.74%. Found: C, 54.08; H, 3.25; N, 19.25%. IR (KBr, cm^{-1}): 3061(w), 2969(w), 2884(w), 2298(s), 2252(m), 2199(s), 2182(s), 1646(s), 1597(s), 1571(m), 1546(s), 1470(m), 1443(m), 1396(m), 1358(s), 1315(w), 1281(s), 1251(w), 1195(m), 1153(w), 1130(m), 1103(w), 1052(w), 921(m), 898(s), 855(w), 816(w), 767(s), 738(m), 653(w), 586(m), 548(m), 509(m), 445(m). UV–Vis [λ_{max}, nm (ε, $M^{-1}cm^{-1}$), CH_3OH solution]: 630(217); 375(7810); 270(28890); 242(37750); 218(42240). μ_{eff}/ Cu = 1.92 B. M. EPR (CH_3OH solution, 298 K): g_{av}= 2.128, A = 74 G.

*5.1.1.4 [Cu$_2$(**L1**)$_2$(N(CN)$_2$)$_2$]* (**4**)

Compound **4** was synthesized by following the procedure described for **1** by using $Cu(OAc)_2 \cdot H_2O$ (0.199 g, 1 mmol) instead of $Cu(ClO_4)_2 \cdot 6H_2O$. Yield: 0.411 g (58%). *Anal.* Calc. for $C_{32}H_{26}Cu_2N_{10}O_2$: C, 54.16; H, 3.69; N, 19.74%. Found: C, 54.92; H, 3.39; N, 19.15%. IR (KBr, cm^{-1}): 3055(w), 2958(w), 2285(s), 2236(s), 2148(s), 1629(s), 1600(s), 1567(s), 1507(w), 1445(s), 1489(w), 1345(s), 1304(s), 1295(s), 1249(w), 1158(w), 1108(s), 1037(s), 980(s), 910(s), 874(s), 794(s), 621(s), 524(s), 487(w). UV–Vis [λ_{max}, nm (ε, $M^{-1}cm^{-1}$), CH_3OH solution]: 625(123); 493(140); 463(187); 373(3625);

299(2800); 270(13690); 242(17580); 219(23790). μ_{eff}/ Cu = 1.84 B. M. EPR (CH_3OH solution, 298 K): g_{av} = 2.092, A = 76 G.

5.2 Results and discussion

5.2.1 Synthesis and spectroscopic studies

The racemic mixture of the Schiff base (**L1H**) with a chiral carbon having a unsymmetrical N_2O donor set of atoms was synthesized by refluxing (4 h) a 1:1 molar ratio of racemic 1–(2–pyridyl)ethylamine and salicyldehyde in methanol. One-pot synthesis using a 1:1:1 molar ratio of hydrated copper(II) salts, **L1H** and Na(dca) in methanol at room temperature, afforded the neutral phenoxo bridged polymeric (by having μ–1,5–dca bridge) and dimeric (by having μ–1–dca) complexes such as, $[Cu_4(\mathbf{L1})_2(dca)_4]_n$ (**1**), $[Cu(\mathbf{L1})(dca)(OH_2)]$ (**2**), $[Cu_2(\mathbf{L1})_2(dca)_2]_n$ (**3**) and $[Cu_2(\mathbf{L1})_2(dca)_2]$ (**4**) in good yields. The formation of these compounds clearly depends on the nature of copper(II) salt and amount of sodium dicyanamide used in the reaction. That is compound **1** was isolated either by using $Cu(ClO_4)_2{\cdot}6H_2O$ or $CuCl_2{\cdot}2H_2O$; **2** by using $CuSO_4{\cdot}5H_2O$; **3** by using $Cu(NO_3)_2{\cdot}3H_2O$ and **4** by using $Cu(OAc)_2{\cdot}H_2O$. All the compounds formed are specific on the identity of copper(II) salt and amount of sodium dicyanamide employed in the reaction. In compound **1**, dicyanamide ion may act as reducing agent. Although such reduction was not observed in the formation of **2**–**5**, hence serendipity may play a major role in the formation of **1**. Compound **3** can be synthesized by using either $Cu(ClO_4)_2{\cdot}6H_2O$ or $CuCl_2{\cdot}4H_2O$. The crystallographic cell parameters of **3** obtained from $CuCl_2{\cdot}4H_2O$ was identical with that from $Cu(ClO_4)_2{\cdot}6H_2O$.

The IR spectra of **1**–**4** exhibit strong absorptions in the range 2150 – 2210 cm^{-1} and weak to medium bands in the range 2235 – 2320 cm^{-1}. These bands originate from the coordinated dca ion and since frequencies of these bands are shifted to higher values than that observed in the free dca, presence of μ–1,5 and/or μ–1 bridging modes can be inferred [325–327]. Presence of coordinated **LH** in these complexes can be inferred from the bands due to $\nu_{C=N}$ and $\nu_{C=C}$ stretches in the region 1620 – 1595 cm^{-1}. The electronic spectra of the complex **1**–**4** have been measured in dry methanolic solution. Three higher energy bands around 295 – 220 nm corresponds to the n→π* and π→π* transition of the Schiff base ligand (ILCT). An intense band around 375 nm can be assigned to charge

transfer M→L (MLCT) bands. A relatively weak band appears at around 630 nm for all complexes can be assigned to $d_z^2 \rightarrow d_{x^2-y^2}$ transition (Fig. 1). Room-temperature solid phase magnetic susceptibility measurement of **1**–**4** is in agreement with d^9 electronic configuration with μ_{eff} = 1.84–1.86 B. M. which is greater than spin only value (1.73 B. M.). X-band EPR spectrum of **1**–**4** in methanol recorded at room-temperature show four line spectra in accordance with isotropic nature of copper center with hyperfine splitting (Fig. 2).

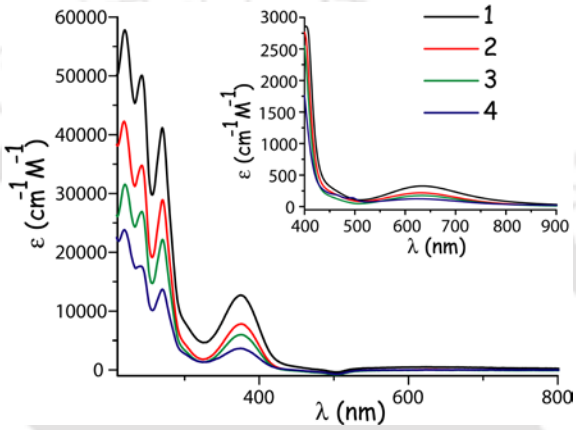

Fig. 1. UV–Vis spectra of **1**–**4** in CH_3OH at 298 K (insert shows the d – d transition).

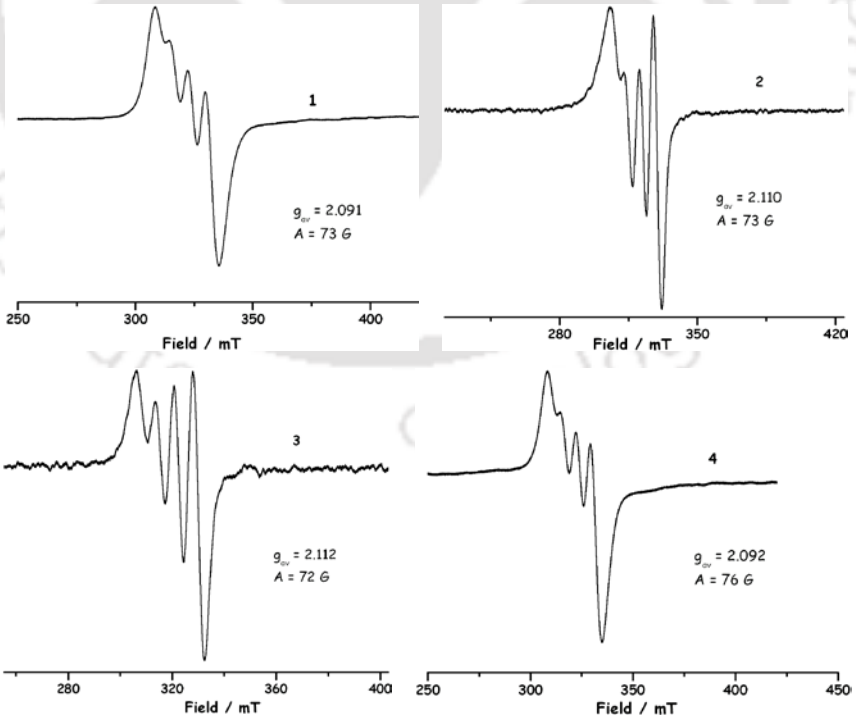

Fig. 2. EPR spectra of **1**–**4** in CH_3OH at 298 K.

5.3 Molecular Structures

The molecular structures of **1**–**4** were determined using single crystal X-ray diffraction techniques. The crystal data and refinement parameters are listed in Table 1. Selected bond parameters are listed in Table 2 (for **1** and **2**) and selected bond distances and angles are in Table 3 and 4, respectively (for **3** and **4**). In all cases the bivalent copper is coordinated by tridentate end-cap ligand **L1** (**L1** = 2–((1–(2–pyridyl)ethylimino)methyl)-phenolate ion). In compounds **1**, **3** and **4**, O_P bridge is present which creates a Cu_2O_2 core, while in **2** such O_P bridge is absent {O_P = phenolate–O; N_Y = pyridyl–N; N_I = imine–N; and N_D = dicyanamide–N}. As a consequence of the O_P bridge the coordinated ligand is non-planar and the two aromatic rings are bent away from the metal center having a butterfly shape. However, in **2** due to the lacking of O_P bridge the ligand is nearly planar in nature.

Complex **1** crystallized in space group $P2_1/n$ and its ORTEP diagram with the atom numbering scheme is displayed in Fig. 3. The molecular structure of **1** consists of neutral dinuclear [Cu_2(**L1**)$_2$(dca)$_2$] and mononuclear [Cu(dca)] complex units. These two units are further linked to a 1D polymer by μ–1,5–dca bridges. There are two types of dca bridges: one that links a copper(II) with a copper(I) center and the other that interconnects two copper(I) centers. The respective non-bonded distances are 7.8915(9) Å and 7.7364(7) Å for Cu1···Cu2 and Cu2···Cu2. Copper(II) center is *penta*-coordinated and has a distorted square pyramidal geometry as it is evident from the Addison's τ parameter of 0.12 [269]. The basal plane of copper(II) ion is occupied by N_2O donor atoms set of the tridentate ligand **L1** and terminal nitrogen atom of dca ligand. Two such copper(II) centers further form a dimeric structure as a result of O_P bridge, which fill up the apical site with a Cu1···O1 bond distance of 2.418(3) Å. This generates a rectangular Cu_2O_2 core having the Cu1···Cu1 non -bonded distance of 3.2709(7) Å. In this dimeric structure the asymmetric–C6 atom of the pair of **L1** has opposite chirality (i.e. *RS* combination or heterochiral dimerization of **L1**) and is a consequence of the rectangular Cu_2O_2 core having the center of symmetry at its center. The Cu–N bond distances follow the order Cu–N_Y > Cu–N_D > Cu–N_I. The *trans* angles for N2–Cu1–N3 = 166.2(1)° and O1–Cu1–N1 = 173.7(1)° are smaller than expected in a regular square pyramid.

Chelation of **L1** to Cu(II) atom occurs by a nearly planar five-membered and a puckered six-membered chelate ring. The O_P atom of **L1** is slightly asymmetrically bridging to Cu(II) center having Cu–O_P distances of 1.925(3) and 2.418(3) Å and makes the ligand non-planar.

The copper(I) center has a distorted trigonal planar coordination geometry with terminal N atoms of dca occupying three corners. The bond distances and bond angles around metal center are, Cu2–N5, 1.922(5); Cu2–N6, 1.960(4); Cu2–N7, 1.899(4) Å and N5–Cu2–N6, 109.6(2); N5–Cu2–N7, 127.7(2); N6–Cu2–N7, 122.0(2)° respectively. Thus, the sum of the bond angles around Cu2 center deviate by 0.7(2)° from the ideal value of 360° and also the Cu(I) atom lie 0.093(1)° above the plane formed by N5N6N7 atoms. Two of the angles deviate largely from ideal value of 120° for a regular trigonal plane, while the other to a smaller extent. Such a stereochemistry is usual for Cu(I) ion since trigonal planar is the preferred geometry of three-coordinate d^{10} metal complexes, and this distortion might represent a compromise between idealness and the limits of stretching ability of the dca ligand. The observed bond distances around Cu(I) center are lying on the lower side of the range of 1.890(8) – 2.295(7) Å reported for $[CuN_3]^+$ type complexes [328].

The packing diagram of **1** exhibits a zipper like 1D polymeric chain in which the end–on–end dca bridge between the copper(I) forms a planar zig-zag chain and other dca bridge between copper(I) and copper(II) behaving like the tether. The distance between the center of the two Cu_2O_2 cores (or Cu2···Cu2) is 7.7364(7) Å. The bridge between Cu1 and Cu2 centers connects to a zipper like 1D coordination polymer having two ···Cu1···dca···Cu1···dca···Cu1··· strings that link Cu_2O_2 cores. A view of the zipper like 1D coordination polymer as well as its schematic representation is displayed in Fig. 4 and 5. Weak interaction such as C–H···π; 2.884(4) and 2.874(6), lone pair···π; 3.186(5) and π···π; 3.315(6) Å were also present.

Table 1. Crystallographic and refinement parameters.

	1	**2**	**3**	**4**
Chemical formula	$C_{18}H_{13}Cu_2N_8O$	$C_{16}H_{15}CuN_5O_2$	$C_{32}H_{26}Cu_2N_{10}O_2$	$C_{32}H_{26}Cu_2N_{10}O_2$
Formula weight	484.46	372.88	709.73	709.73
Temperature (K)	296(2)	296(2)	296(2)	296(2)
Crystal system	Monoclinic	Triclinic	Triclinic	Monoclinic
Space group	$P2_1/n$	$P\bar{1}$	$P\bar{1}$	$P2_1/c$
a (Å)	15.1517(7)	7.9794(4)	11.4696(4)	12.4158(8)
b (Å)	7.7364(3)	10.2330(5)	11.6432(5)	13.4904(9)
c (Å)	16.9881(8)	11.0680(6)	13.4883(5)	21.0951(12)
α (°)	-	65.518(3)	84.488(2)	-
β (°)	101.387(2)	73.305(4)	82.801(2)	120.849(3)
γ (°)	-	76.036(3)	61.108(2)	-
V (Å^3)	1952.14(15)	780.03(7)	1563.33(10)	3033.4(3)
Z	4	2	2	4
μ (mm^{-1})	2.209	1.420	1.408	1.451
ρ_{calcd} (g cm^{-3})	1.648	1.588	1.508	1.554
No. of rflns collected	22006	9199	25635	33665
No. of unique rflns	4889	3895	7754	5729
No. of rflns ($I \geq 2\sigma(I)$)	3007	2700	4258	3971
No. of params	269	223	417	417
R_1[a], wR_2[b] ($I \geq 2\sigma(I)$)	0.0459, 0.0793	0.0378, 0.0789	0.0558, 0.1427	0.0354, 0.0832
R_1[a], wR_2[b] (all data)	0.1566, 0.1784	0.0613, 0.0869	0.1153, 0.1674	0.0629, 0.0933
Goodness of fit (F^2)	1.008	1.000	1.003	1.003

[a]GOF = $[\sum[w(F_0^2 - F_c^2)^2] / M - N]^{1/2}$ (M =number of reflections, N = number of parameters refined).

[a]$R_1 = \Sigma||F_o| - |F_c||/\Sigma|F_o|$

[b]$wR_2 = [\Sigma w(F_o^2 - F_c^2)^2/\Sigma w(F_o^2)^2]^{1/2}$

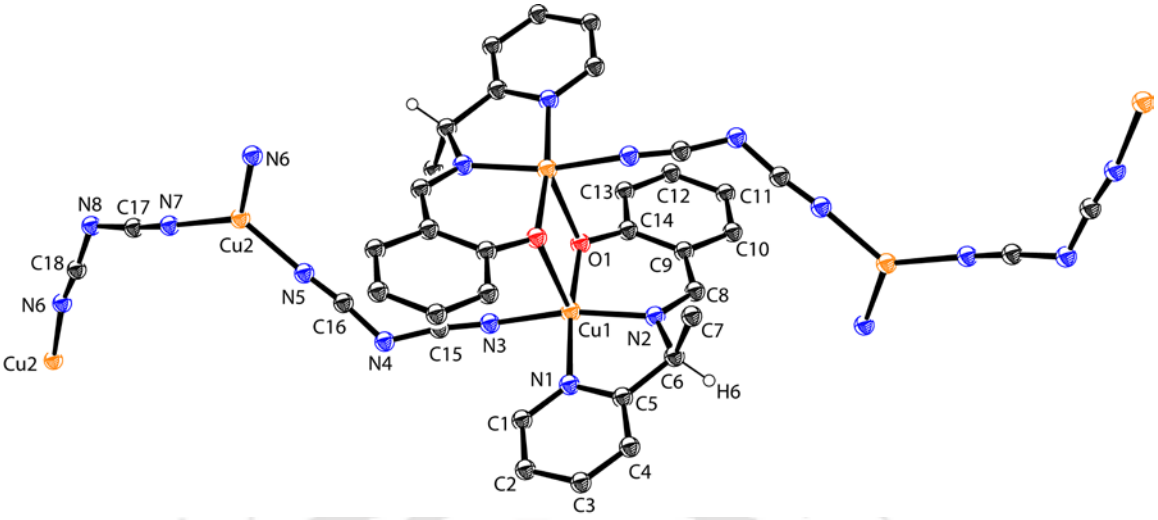

Fig. 3. ORTEP diagram (30%) and atom labeling scheme in **1** (All H–atoms except H6 are omitted for clarity).

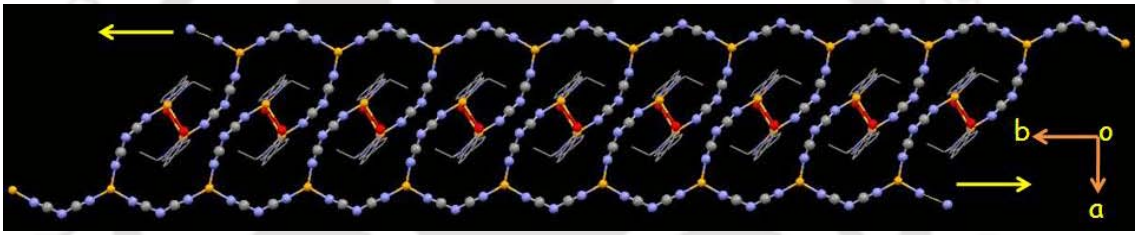

Fig. 4. Packing diagram of **1** having zipper like 1D coordination polymer.

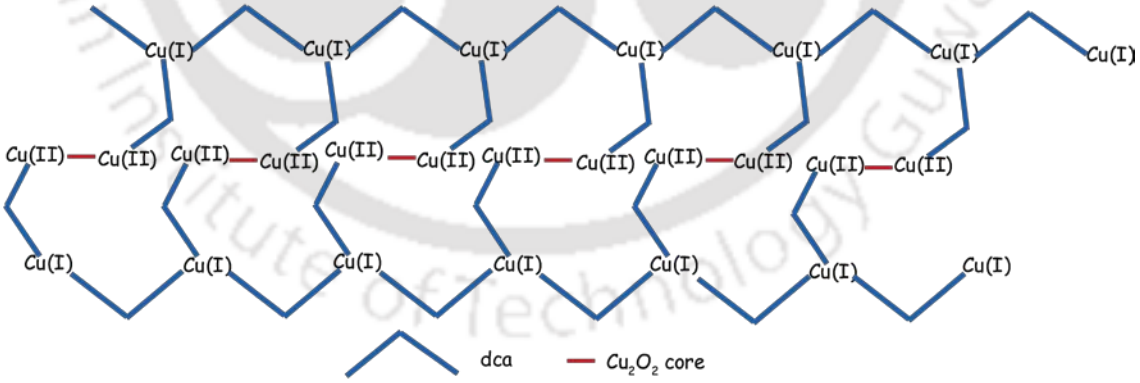

Fig. 5. Schematic representation of dca bridged 1D coordination polymer in **1**.

Complex **2** crystallized in space group *P*–1. ORTEP diagram of **2** with the atom numbering scheme is displayed in Fig. 6. The molecular structure of **2** contain a neutral mononuclear complex [Cu(**L1**)(dca)(OH_2)] in which the copper(II) ion is coordinated by **L1**, μ–1–dca in the basal plane and a water molecule in the axial site. Hence the metal

center has a nearly square pyramidal geometry (τ = 0.09). The coordinated water molecule acts as a H–donor to O_P (O2–H···O1, 2.791(3) Å) of the adjacent molecule. Thus, the dimeric Cu_2O_2 unit is obtained having a Cu···Cu distance of 4.886(5) Å that bear the center of symmetry at it and hence lead to the formation of a heterochiral dimer having a *RS* combination for the asymmetric–C6 atom.

Table 2. Selected bond distances (Å) and angles (°) in **1** and **2**.

1		**2**	
Cu1–N1	2.035(3)	Cu1–N1	2.017(2)
Cu1–N2	1.938(3)	Cu1–N2	1.944(2)
Cu1–N3	1.957(3)	Cu1–N3	1.980(2)
Cu1–O1	1.925(3)	Cu1–O1	1.923(2)
Cu1–O1A	2.418(3)	Cu1–O2	2.296(3)
Cu2–N5	1.922(5)		
Cu2–N6	1.960(4)		
Cu2–N8	1.899(4)		
N1–Cu1–N2	81.9(1)	N1–Cu1–N2	81.67(9)
N1–Cu1–N3	93.9(1)	N1–Cu1–N3	93.95(9)
N1–Cu1–O1	173.7(1)	N1–Cu1–O1	171.12(8)
N1–Cu1–O1A	97.4(1)	N1–Cu1–O2	90.17(8)
N2–Cu1–N3	166.2(1)	N2–Cu1–N3	165.67(9)
N2–Cu1–O1	91.9(1)	N2–Cu1–O1	93.06(9)
N2–Cu1–O1A	102.9(1)	N2–Cu1–O2	101.43(9)
N3–Cu1–O1A	92.4(1)	N3–Cu1–O1	89.44(8)
O1–Cu1–N3	90.7(1)	N3–Cu1–O2	92.17(9)
O1–Cu1–O1A	82.9(1)	O1–Cu1–O2	97.91(8)
N5–Cu2–N7	127.7(2)		
N6–Cu2–N7	122.0(2)		

A perspective view of coordinated water bridged dimer in **2** is displayed in Fig. 7. **L1** is bound to the Cu1 atom by a five-membered and a six-membered chelate ring and both the chelate rings are planar. The trend in length of coordination bonds Cu–N_Y > Cu–N_D > Cu–N_I is also observed here and the longer axial Cu1–O2 bond distance of 2.296(3) Å is consistent with the expectation from Jahn-Teller distortions. The *trans* angles N2–Cu1–N3, 165.67(9)° and O1–Cu1–N1, 171.12(8)° are smaller than expected in a regular square pyramid.

It is interesting to note that in **2**, axial water coordination is preferred over O_P bridging which has been observed in **1**. This O_W–H···O_P hydrogen bonding is diasteroselective in the sense that if O_W is bound to the metal ion having the ligand ^{R}**L1**, the O_P is from the adjacent complex with ^{S}**L1**. In addition to this, coordinated water molecule is also involved in H–bonding interaction with the terminal N_D (O2–H···N5, 2.909(5) Å) and this O_W–H···N_D hydrogen bonding is enantioselective [329, 330]. That is if the copper(II) ion is bound by the ^{R}**L1** and the coordinated water O_W forms O_W–H···N_D hydrogen bond with the adjacent complex having the configuration for the ligand as ^{R}**L1** and *vice versa*.

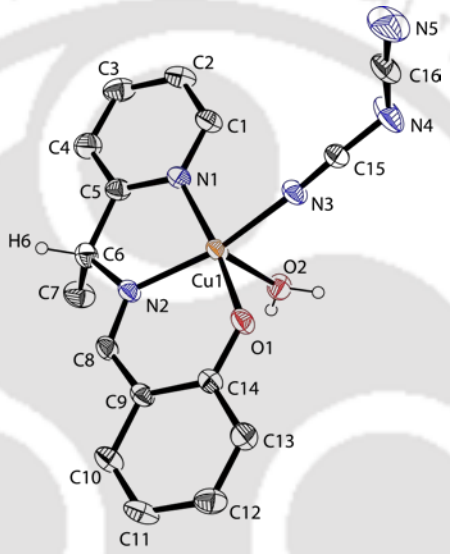

Fig. 6. ORTEP diagram (30%) and atom labeling scheme of **2** (All H–atoms except those attached at C6 and O2 are omitted for clarity).

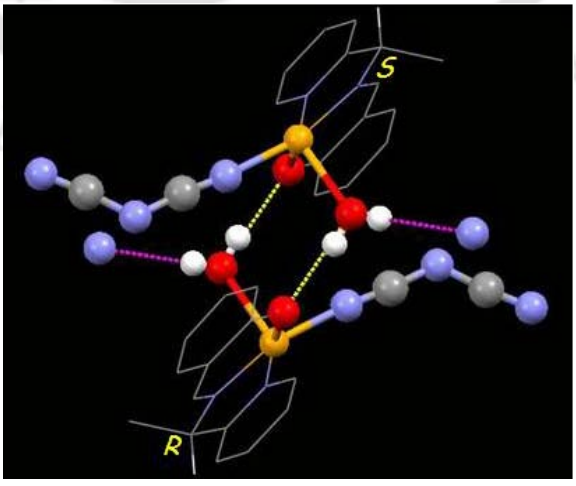

Fig. 7. A perspective view of H–bonded centrosymmetric dimer in **2**.

These enantioselective O_W–H···N_D and diasteroselective O_W–H···O_P H–bonding interaction leads to the existence of 1D supramolecular assembly of double stranded chain along the *b*–axis and a perspective view is shown in Fig. 8. Weak interaction such as C–H···π; 3.703(4) and C–H···O; 3.389(3) Å between dca and **L1** are also present.

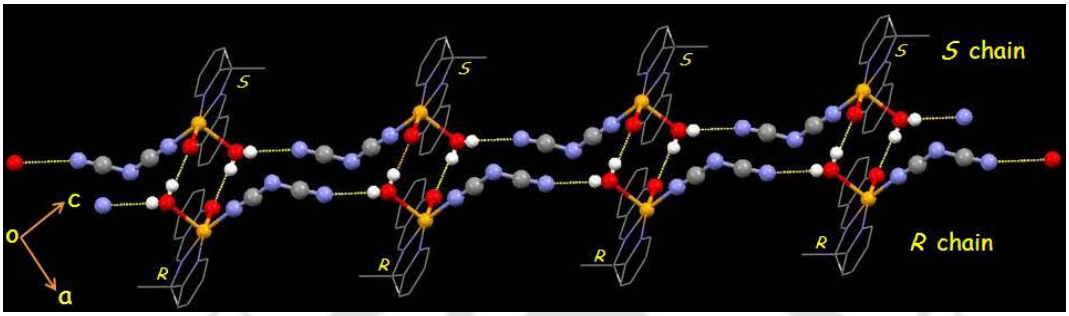

Fig. 8. Schematic figure representing enantioselective and diastereoselective H–bonded 1D polymer found in **2.**

Complex **3** crystallized in space group *P*–1. ORTEP diagram of **3** with the atom numbering scheme is displayed in Fig. 9. The molecular structure of **3** is made up of copper(II) monochelates of **L1** bound by two *μ*–1,5–dca bridges. The N_2O donor set of **L1** and one N_D of dca occupy the square plane. The two axial sites are occupied by another N_D and bridging O_P and *hexa*-coordinated copper centers have distorted octahedral geometry. The two copper centers have a stereochemistry of *cis*,*cis*,*cis*-$(O_P)_2(N_D)_2(N_YN_I)$. The O_P bridge results in a dimeric structure having the Cu_2O_2 core. There are two different but structurally very similar Cu_2O_2 cores and both having a center of symmetry lying in it and a diamond shape. The parameters within the cores are Cu1···Cu1, 3.182(1); O1···O1, 2.719(5); Cu1–O1, 2.037(4) and 2.147(3) Å; and the angles at Cu1 and O1 respectively are 81.0(1) and 99.0(1)°; Cu2···Cu2, 3.148(1); O2···O2, 2.736(4); Cu1–O1, 2.029(4) and 2.140(3) Å; and the angles at Cu2 and O2 respectively are 82.0(1) and 98.0(1)°. The angle between adjacent planes containing the atoms $Cu2_2O2_2$ and $Cu1_2O1_2$ are 55.8°. The angle N5–Cu1–N8 between the two N_D atoms being 86.1(2)° and a pair of these *cis* orientated N_D linkages brings about a *μ*–1,5–dca bridged grid-like structure (Fig. 10). The copper-copper separations across the dca ion bridged 2D grid structures are 8.315(1), 8.281(1) Å and are lying within the range (7.56 – 8.37 Å) of such reported end–to–end dca bridged grids [331–334].

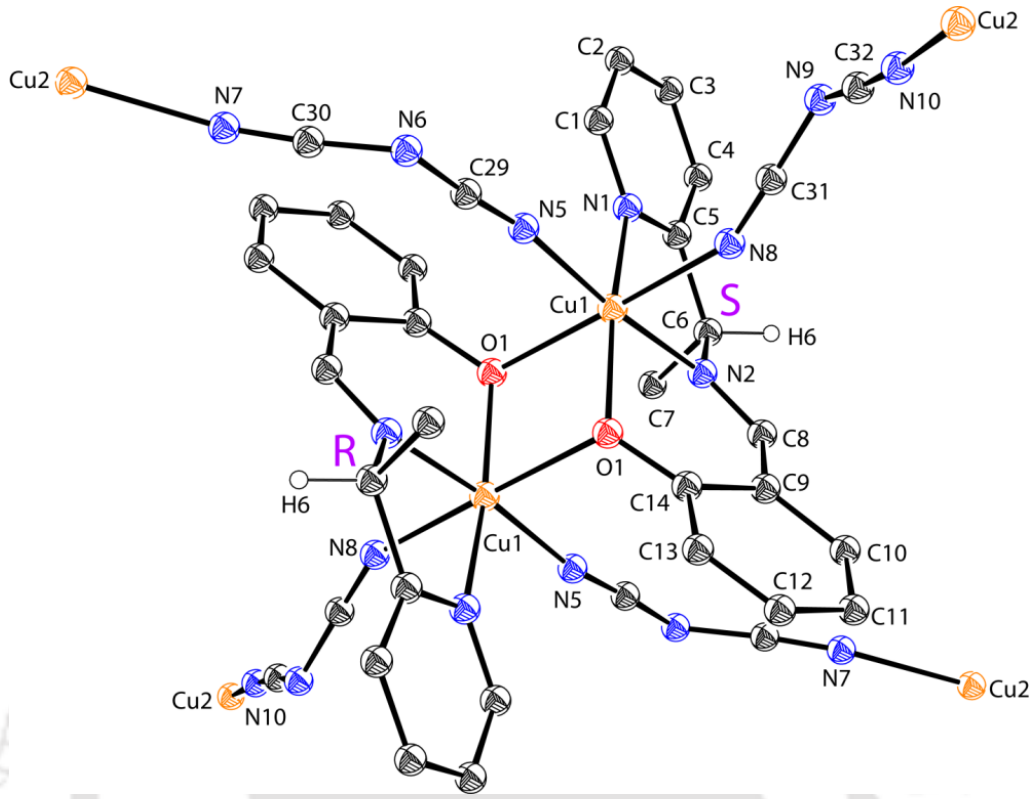

Fig. 9. ORTEP diagram (30%) and atom labeling scheme of **3** (All H–atoms except H6 are omitted for clarity).

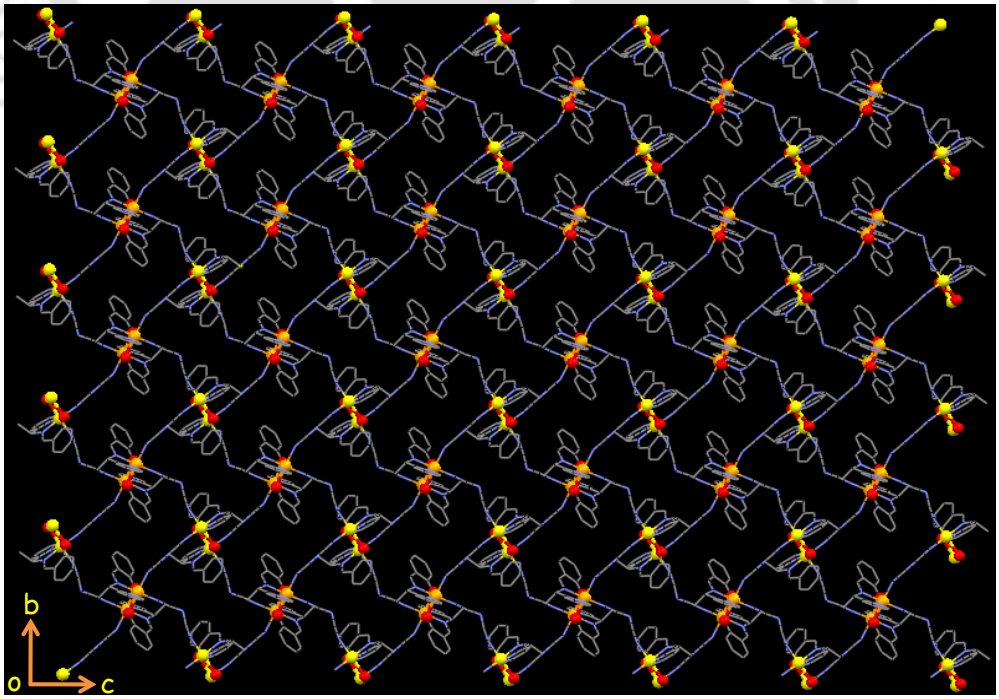

Fig. 10. Packing diagram of **3** having 2D grid structure along *a*-axis.

The ligand **L1** is bound to the copper centers by a five-membered and a six-membered chelate ring and both the chelate rings are puckered. The Cu–N_Y bond distances are longer than the Cu–N_D distances by ~0.055 Å and the two longer axial bonds Cu–O_P, ~2.15(1) Å; Cu–N_D, ~2.10(1) Å, is consistent with the expectation from Jahn-Teller distortions. The *trans* angles at Cu1 center are N(2)–Cu(1)–N(5) = 174.6(2)°, O(1)–Cu(1)–N(1) = 166.9(1)° and O(1A)–Cu(1)–N(8) = 175.1(2)° and at Cu2 centers are N(4)–Cu(2)–N(10) = 174.0(1)°, O(2)–Cu(2)–N(3) = 166.2(1)° and O(2A)–Cu(2)–N(7) = 175.1(2)° are smaller than expected value of 180°. The O_P atom of **L1** is slightly asymmetrically bridging to Cu(II) centers having Cu–O_P distances of 2.037(4); 2.147(3) Å around Cu1 center and 2.029(4); 2.140(3) Å around Cu2 center. The rectangular phenoxo bridged Cu_2O_2 cores in **3** has the center of symmetry residing inside the rectangular unit and hence lead to the formation of a heterochiral dimer having asymmetric carbon atom combinations as *RS*.

Complex **4** crystallized in space group $P2_1/c$ and the asymmetric unit contains two nearly identical $[Cu_2(\mathbf{L1})_2(dca)_2]$ molecules. The ORTEP diagram of one of the $[Cu_2(\mathbf{L1})_2(dca)_2]$ units with the atom numbering scheme is displayed in Fig. 11. In both the molecules the copper centers are five-coordinated having distorted square pyramidal geometry (τ = 0.10, 0.04). In addition to **L1**, the basal plane is occupied by terminal nitrogen atoms of μ–1–dca ligand and the apical site is occupied by O_P. The non-bonded Cu1···Cu1A and Cu2···Cu2A distances are 3.166(3) and 3.247(1) Å respectively. Both the Cu_2O_2 cores have a rectangular shape and the center of symmetry inside it, hence lead to the formation of a heterochiral dimer having a *RS* combination for the asymmetric–C6 atom. Ligand **L1** is bound to the copper centers by a five-membered and a six-membered chelate ring and both the chelate rings are puckered. The trend in length of coordination bonds Cu–N_Y > Cu–N_D > Cu–N_I is also observed at the copper centers. The *trans* angles around Cu1 center are N(2)–Cu(1)–N(3) = 168.4(1)° and O(1)–Cu(1)–N(1) = 174.83(9)° and Cu2 centers are N(6)–Cu(2)–N(8) = 171.1(1)° and O(2)–Cu(2)–N(6) = 173.74(9)°. The O_P atom of **L1** is slightly asymmetrically bridging having Cu–O_P distances of 1.913(2) and 2.529(2) Å at Cu1 center and 1.916(2) and 2.520(2) Å at Cu2 center respectively.

Compound **4** exhibits C–H···N interaction of C3–H3···N5; 2.719(4), C4–H4···N5; 2.680(4), C8–H8···N10; 3.540(4), C10–H10···N9; 3.501(4) and C24–H24···N4; 3.476(6) Å respectively (Fig. 12). Thus the terminal dca–N participates in C–H···N interaction with adjacent molecule instead of bridging in end–on–end fashion to form a 1D coordination polymer as observed in **1** and **3**. Weak interaction such as C–H···π, 3.322(4) and 3.301(4), C–H···C; 3.623(6) Å between dca and **L1** were also observed.

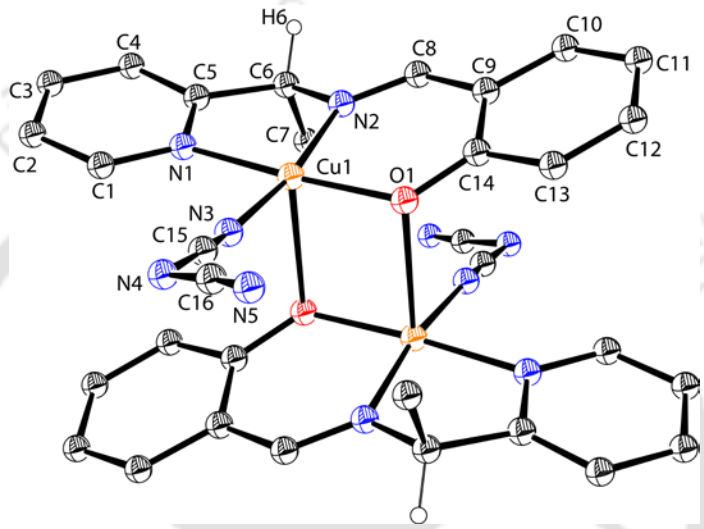

Fig. 11. ORTEP diagram (30%) and atom labeling scheme of **4** (All H–atoms except H6 are omitted for clarity).

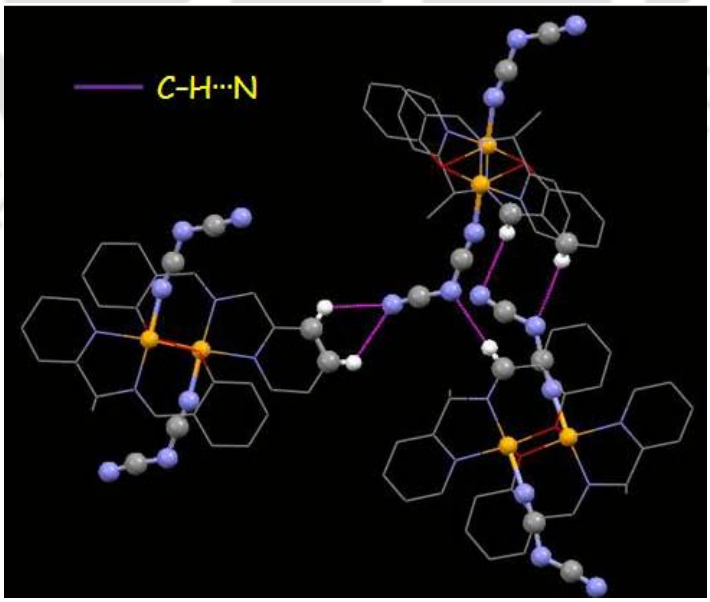

Fig. 12. C–H···N interaction between dca–N and **L1** in **4**.

Table 3. Selected bond distances (Å) in **3** and **4**.

3		**4**	
Cu1–N1	2.089(4)	Cu1–N1	1.995(1)
Cu1–N2	2.021(4)	Cu1–N2	1.933(2)
Cu1–N5	2.037(4)	Cu1–N3	1.958(3)
Cu1–N8	2.110(3)	Cu1–O1	1.913(2)
Cu1–O1	2.037(4)	Cu1–O1A	2.529(2)
Cu1–O1A	2.147(3)	Cu2–N6	2.010(2)
Cu2–N3	2.083(4)	Cu2–N7	1.936(3)
Cu2–N4	2.029(3)	Cu2–N8	1.950(3)
Cu2–N7	2.090(4)	Cu2–O2	1.916(2)
Cu2–N10	2.057(4)	Cu2–O2A	2.520(2)
Cu2–O2	2.029(4)	Cu1···Cu1A	3.176(5)
Cu2–O2A	2.140(3)	Cu2···Cu2A	3.246(6)
Cu1···Cu1A	3.182(1)		
Cu2···Cu2A	3.148(1)		

Table 4. Selected bond angles (°) in **3** and **4**.

3		**4**	
N1–Cu1–N2	79.3(1)	N1–Cu1–N2	82.5(1)
N1–Cu1–N5	96.1(2)	N1–Cu1–N3	94.9(1)
N1–Cu1–N8	88.6(2)	N1–Cu1–O1	174.83(9)
N1–Cu1–O1	166.9(1)	N1–Cu1–O1A	90.48(8)
N1–Cu1–O1A	94.8(1)	N2–Cu1–N3	168.4(1)
N2–Cu1–N5	174.6(2)	N2–Cu1–O1	92.30(9)
N2–Cu1–N8	90.9(2)	N2–Cu1–O1A	95.80(8)
N5–Cu1–N8	86.1(2)	N3–Cu1–O1	90.2(1)
N2–Cu1–O1	88.4(1)	N3–Cu1–O1A	95.55(9)
N2–Cu1–O1A	93.2(1)	O1–Cu1–O1A	89.79(1)
N5–Cu1–O1	96.4(2)	N6–Cu2–N7	81.8(1)
N5–Cu1–O1A	90.1(2)	N6–Cu2–N8	93.7(1)
N8–Cu1–O1	96.4(2)	N6–Cu2–O2	95.52(8)
N8–Cu1–O1A	175.1(2)	N6–Cu2–O2A	92.33(9)
O1–Cu1–O1A	81.0(1)	N7–Cu2–N8	171.1(1)
N3–Cu2–N4	79.6(1)	N7–Cu2–O2	92.33(9)
N3–Cu2–N7	92.3(2)	N7–Cu2–O2A	93.59(9)
N3–Cu2–N10	95.3(2)	N8–Cu2–O2	91.9(1)
N3–Cu2–O2	166.2(1)	N8–Cu2–O2A	94.49(9)

N3–Cu2–O2A	92.5(1)	O2–Cu2–O2A	86.89(8)
N4–Cu2–N7	86.8(2)	Cu1–O1A–Cu1A	90.21(7)
N4–Cu2–N10	174.0(1)	Cu2–O2A–Cu2A	93.11(8)
N4–Cu2–O2	88.0(1)		
N4–Cu2–O2A	92.8(1)		
N7–Cu2–N10	90.3(2)		
N7–Cu2–O2	93.1(2)		
N7–Cu2–O2A	175.1(2)		
N10–Cu2–O2	97.4(1)		
N10–Cu2–O2A	90.5(1)		
O2–Cu2–O2A	82.0(1)		
Cu1–O1–Cu1A	99.0(1)		
Cu2–O2–Cu2A	98.0(1)		

5.3.1 Dicyanamide ion and structural diversity:

In compounds **1**–**4**, dca plays a major role in stabilizing the Cu_2O_2 core containing the racemic Schiff base, by coordination through either μ–1 or μ–1,5 bridging modes. The composition of compounds **1**–**4** depends on the identity of copper(II) salt used in the reaction. In the sense that dicyanamide ion metathesis with ClO_4^- or Cl^- ions yield compound **1**, while with SO_4^{2-} ion yield **2**, with NO_3^- ion yield **3** and with OAc^- ion yield **4**. Dca ion exhibits H–bonding interaction and various other weak interaction such as C–H···N, C–H···O, C–H···π and π···π with **L1**. In **1**, end–on–end dca ion bridges the Cu(II) and Cu(I) center in a zipper like 1D coordination polymer wherein two ···Cu(I)···dca···Cu(I)···dca···Cu(I)··· chains are being connected to each other by phenoxo bridged *RS*–[Cu^{II}_2(**L1**)$_2$(dca)$_2$] backbone. Dca ion separates Cu(II) and Cu(I) so nicely, such that all Cu(I) are on the strip whereas Cu(II) are on the back bone forming a zipper structure. In **2**, the axial coordinated H_2O plays a crucial role in enantioselective and diastereoselective H–bonding interaction. In **3**, dca ion bridges the Cu_2O_2 core in a rectangle shape resulting 2D grid structure. In **4**, dca ion acts as terminal ligand in phenoxo bridged dimer having *R* and *S* isomer of the racemic Schiff base. Another terminal dca–N participates in C–H···N interaction with adjacent molecule and unable to form a 1D coordination polymer as observed in **1**, **2** and **3**. Although *R* and *S* isomers of racemic Schiff base are segregated in different chain bridged by dca ion, in overall all the complexes are racemic in nature.

5.3 Conclusion

In this Chapter, the synthesis and structural characterization of four Cu(II) complexes, using a chiral tridentate Schiff base (**L1H**), different Cu(II) salts, and Na(dca) have been reported. The compositions of the isolated complex are dependent on the nature of copper(II) salt and amount of sodium dicyanamide used in the reaction. In compounds **1**, **3** and **4**, O_P bridge is present which creates a Cu_2O_2 core, while in **2** such O_P bridge is absent. As a consequence of the O_P bridge the coordinated ligand is non-planar and the two aromatic rings are bent away from the metal center having a butterfly shape. However in **2** due to the absence of O_P bridge the ligand is nearly planar in nature. Compound **1**, **3** and **4** are centrosymmetric in nature having center of symmetry with in Cu_2O_2 core. Compound **1** is a mixed valent Cu(II)Cu(I) polymer having zipper like structure whereas complex **3** exhibits 2D grid structure. In **2**, coordinated H_2O molecule is involved in enantioselective and diastereoselective hydrogen-bonding interaction with dicyanamide ion (dca) and phonoxo–O atom respectively. Since the Schiff base used is racemic in nature, the isolated complexes contain equal amount of *R*(*S*) enantiomers of the racemic Schiff base. Hence all the complexes are racemic nature.

Chapter 6

Molecular Structures of Dinuclear Zinc(II) Complexes of Chiral Tridentate Imine and Amine Ligands: Effect of Ligand Geometry on Diastereoselectivity†

Abstract

Racemic mixtures of Schiff bases (**L1H** and **L2H**) were reduced to respective amines (**L1′H** and **L2′H**). Compounds of composition $[Zn_2(\mathbf{L1})_2(NCO)_2]$ (**1**), $[Zn(\mathbf{L1})N_3]_n$ (**2**), $[Zn_2(\mathbf{L2})_2(NCO)_2]$ (**3**), $[Zn_2(\mathbf{L1'})_2(NCO)_2]$ (**1′**), $[Zn_2(\mathbf{L1'})_2(N_3)_2]\cdot 2DMF$ (**2′**·2DMF) and $[Zn_2(\mathbf{L2'})_2(NCO)_2]\cdot DMF$ (**3′**·DMF) were synthesized using these ligands, $Zn(NO_3)_2\cdot 6H_2O$ and NCO^- or N_3^- ions. Molecular structures of all six compounds have been established. Both imine and amine ligands have N_2O donor set, but coordinate respectively in *meridional* and *facial* fashions. First four complexes are monochelates and last two are bis-chelates. The Zn_2O_2 unit in **1**–**3** has *RS* combination of imine whereas, **1′** has *RR*(*SS*) combinations of amine. In **2′** and **3′**, zinc(II) bis-chelates have *cis*,*cis*,*trans*-$(O_P)_2(N_A)_2(N_Y)_2$ stereochemistry and *cis*-$(O_P)_2$ disposition further coordinate to tetrahedral zinc. Compound **1′** exhibits 1D hydrogen-bonded polymer by enantioselective H–bonding interaction. In **2′**, DMF molecules assemble *RR* and *SS* bis-chelates through N–H···O interactions.

† This work has been submitted for publication.

H. S. Jena, V. Manivannan, Submitted

Molecular Structures of Dinuclear Zinc(II) Complexes of Chiral Tridentate Imine and Amine Ligands: Effect of Ligand Geometry on Diastereoselectivity

In this Chapter, synthesis and structural characterization of six zinc(II) complexes derived from the chiral tridentate imine (**L1H** and **L2H**), amine (**L1′H** and **L2′H**) ligands (Scheme 1) and co-ligands such as N_3^- and NCO^- has been described. The role of ligand geometry on the diastereoselectivity of these ligands has been observed around the bivalent zinc center.

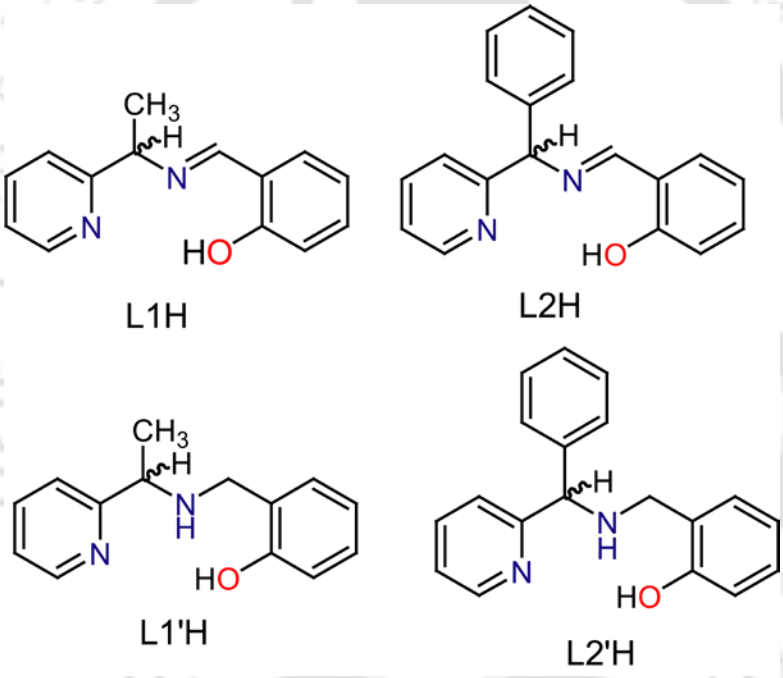

Scheme 1. Chiral tridentate imine and amine ligands used in this Chapter.

6.1 Experimental

6.1.1 Syntheses

(*R*, *S*) 1–(2–pyridyl)ethylamine, (*R*, *S*) 2–((1–(2–pyridyl)ethylimino)methyl)phenol (**L1H**) are prepared using the same procedure described in Chapter 2. Similarly (*R*, *S*)

Phenyl(2–pyridyl)methaneamine and (*R, S*) 2–((phenyl(2–pyridyl)methylimino)methyl) phenol (**L2H**) are prepared using the same procedure described in Chapter 3.

*6.1.1.1 (R, S) 1–(2–pyridyl)ethylamino)methyl)phenol (**L1′H**)*

(*R, S*) 1–(2–pyridyl)ethylamine (0.6 g, 5 mmol) and 2–hydroxybenzaldehyde (0.6 g, 5 mmol) in MeOH (50 mL) were stirred for 1 h at ambient conditions. The resultant yellow solution was cooled in an ice bath and solid $NaBH_4$ (0.57 g, 10 mmol) was added with stirring, which turned the color of the solution to colorless and stirring was continued overnight. The volatiles were removed in vacuum and the residue was dissolved in water (50 mL), extracted with CH_2Cl_2 (3 × 20 mL), dried over anhydrous Na_2SO_4 and **L1′H** was obtained as colorless oil after removal of the solvent. Yield: 1.08 g (95%), *Anal.* Calc. for $C_{14}H_{16}N_2O$: C, 73.66; H, 7.06; N, 12.27%. Found: C, 73.52; H, 6.96; N, 12.01%. ESI-MS: *m/z* calcd. for $C_{14}H_{16}N_2O^+$ 228.13. Found (M^++H) 229.14. IR (KBr, cm^{-1}): 3285(w), 3048(w), 3009(w), 2970(m), 2926(w), 2855(w), 2720(w), 2637(w), 1614(w), 1590(s), 1572(w), 1488(w), 1471(w), 1455(w), 1434(m), 1372(w), 1257(s), 1185(m), 1150(m), 1103(s), 1035(s), 993(w), 977(s), 932(s), 842(m), 788(s), 752(s), 720(w), 627(s), 553(w), 500(s). 400 MHz ^{1}H NMR (δ (*J*, Hz), $CDCl_3$): 13.23 (OH, s), 8.56 (1H, d, 2.8), 7.61 (1H, t, 7.8), 7.17 (1H, t, 8.4), 7.12 (1H, t, 7.6), 7.10 (1H, d, 7.6), 6.85 (1H, d, 6.0), 6.82 (1H, d, 6.0), 6.71 (1H, t, 7.2), 3.86 (1H, q, 9.8), 3.64 (2H, d, 6.2), 3.23 (NH, b), 1.39 (2H, d, 5.6). 100 MHz ^{13}C NMR (δ, $CDCl_3$): 161.7, 157.9, 149.1, 136.2, 128.1, 122.5., 121.8, 121.6, 118.5, 115.9, 56.7, 53.2, 49.6, 22.0.

*6.1.1.2 (R, S) 2–((phenyl(2–pyridyl)methane)aminomethyl)phenol (**L2′H**)*

L2′H was synthesized by following the procedure described for **L1′H** by using (*R, S*)–phenyl(2–pyridyl)methaneamine (0.755 g, 4 mmol) and 2–hydroxybenzaldehyde (0.5 g, 4 mmol) in MeOH (50 mL). Yield of the solid product: 1.12 g (97%), *Anal.* Calc. for $C_{19}H_{18}N_2O$: C, 78.59; H, 6.25; N, 9.65%. Found: C, 78.34; H, 6.11; N, 9.42%. ESI-MS: *m/z* calcd. for $C_{19}H_{18}N_2O^+$ 290.14. Found (M^++H) 291.13. IR (KBr, cm^{-1}): 3328(s), 3263(w), 3058(w), 3043(w), 3008(s), 2916(w), 2902(w), 2854(m), 2717(w), 1614(w), 1588(s), 1570(w), 1492(w), 1471(m), 1455(w), 1443(w), 1415(w), 1362(s), 1342(w), 1318(m), 1253(s), 1190(s), 1148(m), 1121(m), 1104(m), 1096(w), 1076(w), 1047(m), 988(m), 977(s), 930(s), 896(s), 869(w), 842(s), 801(s), 752(s), 716(w), 702(s), 667(m),

633(m), 608(m), 567(m), 543(s), 470(s). 400 MHz ^{1}H NMR (δ (*J*, Hz), $CDCl_3$): 11.23 (OH, s), 8.59 (1H, d, 4.8), 7.55 (1H, d, 8.0), 7.31 (2H, d, 6.8), 7.23 (1H, t, 4.6), 7.13 (1H, t, 8.0), 7.11(1H, d, 7.6), 6.86 (2H, t, 7.4), 6.73 (1H, t, 8.4), 4.90 (1H, s), 3.86 (2H, s), 3.42 (NH, b). 100 MHz ^{13}C NMR (δ, $CDCl_3$): 160.3, 158.2, 149.3, 141.3, 136.8, 128.9, 128.7, 127.8, 123.0, 122.9, 122.5, 119.1, 116.5, 66.0, 50.43.

*6.1.1.3 [Zn_2(**L1**)$_2$$(NCO)_2$] (**1**)*

To **L1H** (0.226 g, 1.0 mmol) dissolved in DMF (10 mL), solid $Zn(NO)_3 \cdot 6H_2O$ (0.300 g, 1.0 mmol) was added and stirred for 10 min. To this colorless solution, aqueous (5 mL) NaNCO (0.65 g, 1.0 mmol) was added and stirred for another 30 min. Colorless single crystals of **1** suitable for X-ray diffraction study were obtained from this DMF–H_2O solution on standing for about one week time. Yield: 0.58 g (87%). *Anal.* Calc. for $C_{30}H_{26}N_6O_4Zn_2$: C, 54.16; H, 3.94; N, 12.63%. Found: C, 53.84; H, 3.51; N, 11.92%. IR (KBr, cm^{-1}): 3022(w), 2981(w), 2906(w), 2873(w), 2187(s), 1649(s), 1606(w), 1597(m), 1575(w), 1548(s), 1470(s), 1448(s), 1397(s), 1380(w), 1337(w), 1316(w), 1287(s), 1198(m), 1146(w), 1130(m), 1101(m), 1072(w), 1052(m), 1026(w), 1015(w), 969(w), 901(s), 857(w), 814(w), 785(m), 759(s), 746(m), 676(w), 647(m), 620(w), 581(w), 543(w), 517(w), 468(w).

Same procedure was followed for the synthesis of **2**–**3** and **1′**–**3′** by using appropriate ligand and co-ligand in the same molar ratio.

*6.1.1.4 [Zn(**L1**)$(N_3)]_n$ (**2**)*

Yield: 0.652 g (71%). *Anal.* Calc. for $C_{14}H_{13}N_5OZn$: C, 50.54; H, 3.94; N, 21.05%. Found: C, 50.12; H, 3.12; N, 20.54%. IR (KBr, cm^{-1}): 2866(w), 2066(s), 1650(s), 1596(s), 1549(s), 1481(w), 1469(m), 1447(m), 1389(s), 1284(s), 1198(s), 1130(m), 1101(m), 1052(m), 900(m), 854(m), 784(m), 759(s), 747(m), 657(m), 517(m).

*6.1.1.5 [Zn_2(**L2**)$_2$$(NCO)_2$] (**3**)*

Yield: 0.65 g (82%). *Anal.* Calc. for $C_{40}H_{30}N_6O_4Zn_2$: C, 60.85; H, 3.83; N, 10.64%. Found: C, 59.48; H, 3.04; N, 9.87%. IR (KBr, cm^{-1}): 3295(s), 3063(w), 2925(m), 2221(s), 2189(s), 1668(s), 1627(s), 1599(s), 1572(m), 1549(m), 1483(s), 1442(s),

1405(m), 1331(w), 1291(w), 1277(m), 1197(m), 1151(m), 1127(m), 1046(m), 1019(m), 906(w), 871(s), 789(m), 757(s), 743(w), 701(s), 640(s), 620(s), 587(s), 547(m), 468(m).

*6.1.1.6 $[Zn_2(\mathbf{L1'})_2(NCO)_2]$ (**1'**)*

Yield: 0.55 g (82%). *Anal.* Calc. for $C_{30}H_{30}N_6O_4Zn_2$: C, 53.83; H, 4.52; N, 12.55%. Found: C, 52.86; H, 4.21; N, 11.84%. IR (KBr, cm^{-1}): 3330(s), 3057(w), 2982(w), 2920(w), 2862(w), 2210(s), 1609(m), 1595(m), 1572(w), 1482(s), 1467(w), 1451(s), 1355(w), 1310(s), 1289(w), 1271(s), 1156(m), 1130(w), 1095(m), 1054(s), 1023(s), 971(w), 941(w), 927(s), 892(m), 873(s), 814(w), 785(m), 757(s), 731(s), 645(m), 623(m), 582(m), 556(w), 545(s).

*6.1.1.7 $[Zn_2(\mathbf{L1'})_2(N_3)_2]\cdot 2DMF$ (**2'**·2DMF)*

Yield: 0.71 g (87%). *Anal.* Calc. for $C_{34}H_{44}N_{12}O_4Zn_2$: C, 50.07; H, 5.44; N, 20.61%. Found: C, 49.25; H, 5.13; N, 19.87%. IR (KBr, cm^{-1}): 3252(s), 3069(w), 2922(w), 2857(w), 2076(s), 1662(s), 1596(s), 1573(m), 1484(s), 1450(s), 1381(w), 1348(m), 1284(m), 1260(s), 1154(m), 1135(w), 1096(m), 1054(m), 1021(s), 998(w), 936(m), 872(s), 781(m), 757(s), 735(s), 644(m), 617(w), 581(m), 541(m), 502(m).

*6.1.1.8 $[Zn_2(\mathbf{L2'})_2(NCO)_2]\cdot DMF$ (**3'**·DMF)*

Yield: 0.72 g (83%). *Anal.* Calc. for $C_{43}H_{40}N_7O_5Zn_2$: C, 59.66; H, 4.66; N, 11.33%. Found: C, 58.72; H, 4.01; N, 10.93%. IR (KBr, cm^{-1}): 3295(s), 3064(w), 2926(w), 2866(w), 2243(s), 2220(s), 1668(s), 1596(s), 1572(m), 1484(s), 1452(m), 1441(m), 1331(m), 1274(s), 1194(m), 1155(m), 1089(m), 1063(w), 1046(m), 1015(s), 984(s), 906(s), 871(s), 860(w), 773(w), 756(s), 743(m), 728(w), 700(s), 676(w), 640(m), 617(s), 586(m), 562(w), 534(m).

6.2 Results and discussion

6.2.1 Synthesis and spectroscopic studies

Condensation of racemic 1–(2–pyridyl)ethylamine or phenyl(2–pyridyl)methaneamine with salicyladehyde afforded imine ligands **L1H** and **L2H**, which on reduction with $NaBH_4$ gave the corresponding amine ligands **L1′H** and **L2′H**. By reacting the racemic mixture of these two Schiff bases with $Zn(NO_3)_2\cdot 6H_2O$ and co-ligands such as cyanate

and azide ions, compounds of composition $[Zn_2(\mathbf{L1})_2(NCO)_2]$ (**1**), $[Zn(\mathbf{L1})(N_3)]_n$ (**2**) and $[Zn_2(\mathbf{L2})_2(NCO)_2]$ (**3**), were isolated. In a similar manner, $[Zn_2(\mathbf{L1'})_2(NCO)_2]$ (**1′**), $[Zn_2(\mathbf{L1'})_2(N_3)_2]\cdot 2DMF$ (**2′**) and $[Zn_2(\mathbf{L2'})_2(NCO)_2]\cdot DMF$ (**3′**) were isolated from their reduced bases (Scheme 2). These reactions yielded complexes in which zinc(II) ion are being shown to have coordination numbers ranging from 4–6 having distorted tetrahedral, square pyramidal, trigonal bipyramidal and octahedral geometries (*vide infra*). Imine function is planar due to the sp^2 hybridization for the nitrogen atom, hence ligands **L1H** and **L2H** bind to the metal ion in *meridional* fashion whereas amine function is pyramidal due to the sp^3 hybridization for the nitrogen atom and as a consequence ligands **L1′H** and **L2′H** span the *facial* positions around the metal center. Thus by isolating racemic mixtures of a pair of tridentate ligands containing a chiral carbon atom that can bind the metal ion in *meridional* and *facial* fashions, an opportunity exists to explore the nature of their coordinating behaviors. In addition phenolate group has the potential to bridge two metal centers and as result, Zn_2O_2 core can be anticipated. In order to satisfy the coordination environment around M_2O_2 core, a chiral imine/ amine interact with another molecule either of same chirality (homochiral dimer) or of opposite chirality (heterochiral dimer) leaving some vacant sites for solvent or coligands to occupy [54, 60, 155, 193, 335]. This preferred interaction between components of the same or opposite chirality leads to spontaneous selection of enantiomers from the racemic mixture. Thus the self-assembly of racemic imines or amines will be very important for self-sorting processes.

In IR spectra, conversion of **L2H** to **L2′H** can be inferred by the presence of a strong and sharp ν_{N-H} peak at 3328 cm^{-1} in **L2′H**. However in **L1′H**, the ν_{N-H} peak is obscured by a broad band of ν_{O-H} probably due to involvement of O–H and N–H groups in hydrogen bonding interactions. In imine ligands, the $\nu_{C=N}$ for imine group is present as a strong and sharp peak at ~1623 cm^{-1}. This peak was replaced by a weak ν_{N-H} deformation peak at ~1614 cm^{-1}, in amine ligands. In amine ligands a new strong peak due to the ν_{C-N} was observed at ~1255 cm^{-1}. The cyanato complexes show $\nu_{C\equiv N}$ peak in the range 2187 – 2243 cm^{-1}. Presence of coordinated azide in **2** and **2′** can be inferred by a peak in the range 2066 – 2076 cm^{-1}.

6.3 Molecular Structures

The molecular structures of **1**–**3**, **1′**, **2′·2DMF** and **3′·DMF** were determined using single crystal X-ray diffraction techniques. The crystallographic data and refinement parameters are listed in Table 1. Selected bond parameters are listed in Table 2 (for **1**–**3**) and Table 3 (for **1′**, **2′·2DMF** and **3′·DMF**). The conventions followed in discussions are: **L1** = 2–((1–(2–pyridyl)ethylimino)methyl)phenolate ion; **L2** = 2–((phenyl(2–pyridyl)methylimino)-methyl)phenolate ion; **L1′** = 2–((1–(2–pyridyl)ethylamino)methyl)phenolate ion; **L2′** = 2–((phenyl(2–pyridyl)methane)aminomethyl)phenolate ion; O_P = phenolate–O; N_Y = pyridyl–N; N_I = imine–N; N_A = amine–N; N_C = cyanate–N and N_Z = azide–N.

Compound **1** crystallized in space group $P2_1/n$ and ORTEP diagram of the centrosymmetric dimeric unit, $[Zn_2(\mathbf{L1})_2(NCO)_2]$, is displayed in Fig. 1. The zinc(II) ion is bound by mono anionic end-cap ligand **L1** and nitrogen end of ambidentate cyanate ion, in the square plane. The axial site is occupied by bridging O_P from another [Zn(**L1**)(NCO)] unit. Thus *penta*-coordination around zinc centers can be described as distorted square pyramidal geometry based on the calculated τ value of 0.38 [269]. The two *trans* angles N(2)–Zn(1)–N(3), 140.06(7)° and N(1)–Zn(1)–O(1), 163.25(6)°, in the square plane are smaller than expected for a regular square base. As a consequence of the O_P bridge, a Zn_2O_2 unit exists which has a planar rectangular shape having Zn–O distances of 2.016(1) and 2.105(1) Å. This implies that O_P bridge is unsymmetrical in nature with non-bonded distances of Zn···Zn, 3.108(1) Å and O1 ···O1, 2.707(2) Å. The Zn_2O_2 unit has a center of symmetry in it and as a consequence exists as heterochiral dimer. The O_P bridge also brings about a butterfly shape to the overall ligand moiety. In the coordination sphere, the trend Zn–N_Y > Zn–N_I > Zn–N_C, in bond lengths was observable. The cyanate ion is slightly bent at the carbon atom with the angle subtended at C13 being 177.6(3)° and coordinate through nitrogen atom in a bent fashion with an angle of 137.0(2)° at N3. Both the five- and six- membered chelate rings are puckered with the former having a near-envelope shape. The asymmetric–C6 atom, lie in flap at a distance of 0.32 Å from the slightly twisted plane containing other four atoms N2Zn1N1C5. In the six-membered ring Zn1 atom lies at a distance of 0.51Å from the slightly twisted plane containing the atoms N2C8C9C14O1.

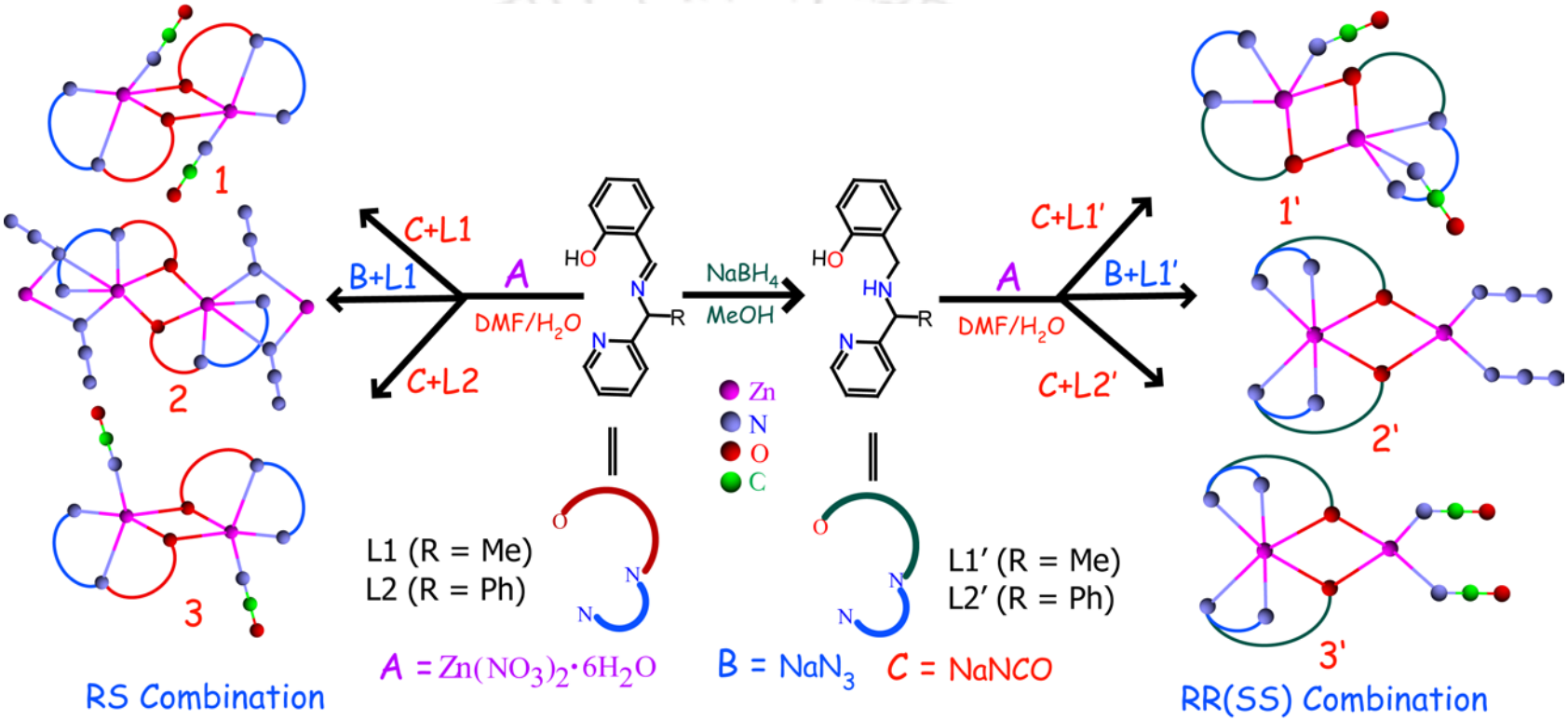

Scheme 2. Schematic representation for the synthesis of **1**–**3** and **1′**–**3′**.

Table 1. Crystallographic and refinement parameters of **1**–**3** and **1′**–**3′**.

	1	**2**	**3**	**1′**	**2′·2DMF**	**3′·DMF**
CCDC Number	863807	863808	863809	863810	863811	863812
Chem formula	$C_{30}H_{26}N_6O_4Zn_2$	$C_{14}H_{13}N_5OZn$	$C_{40}H_{30}N_6O_4Zn_2$	$C_{30}H_{30}N_6O_4Zn_2$	$C_{34}H_{44}N_{12}O_4Zn_2$	$C_{43}H_{40}N_7O_5Zn_2$
Formula weight	665.35	332.66	789.48	669.38	815.59	865.60
Temperature (K)	296(2)	296(2)	296(2)	296(2)	296(2)	296(2)
Crystal system	Monoclinic	Triclinic	Monoclinic	Monoclinic	Monoclinic	Triclinic
Space group	$P2_1/n$	P–1	$P2_1/c$	$P2_1/n$	$P2_1/c$	P–1
a (Å)	8.6765(12)	6.2073(11)	8.6555(4)	9.039(2)	11.8857(9)	9.0463(3)
b (Å)	16.646(2)	10.5477(19)	11.6319(6)	11.126(4)	19.1656(14)	11.3639(4)
c (Å)	10.0095(14)	11.406(2)	17.4024(9)	31.323(10)	18.9389(12)	20.4068(8)
α (°)		67.647(12)				97.960(2)
β (°)	94.381(7)	87.400(13)	94.858(3)	91.162(19)	116.113(4)	92.802(2)
γ (°)		79.832(12)				102.032(2)
V (Å^3)	1441.4(3)	679.6(2)	1745.78(15)	3149.2(16)	3873.9(5)	2025.43(13)
Z	2	2	2	4	4	2
μ (mm^{-1})	1.711	1.813	1.426	1.566	1.291	1.238
ρ_{calcd} (g cm^{-3})	1.533	1.626	1.502	1.412	1.398	1.419
no. of unique rflns	3588	3098	3037	5518	7752	7060
no. of rflns ($I \geq 2\sigma(I)$)	2755	3097	2752	3755	5644	6197
R_1[a], wR_2[b] ($I \geq 2\sigma(I)$)	0.0274, 0.0733	0.0398,	0.0365, 0.0817	0.0434, 0.0918	0.0402, 0.1083	0.0366, 0.0918
R_1[a], wR_2[b] (all data)	0.0381, 0.0799	0.0398,	0.0627, 0.0950	0.0715, 0.1031	0.0627, 0.1255	0.0636, 0.1052
goodness of fit (F^2)	1.005	1.000	1.087	1.022	1.030	1.042
largest peak/hole (e Å^{-3})	0.243 /-0.239	0.442/-0.897	0.393/-0.219	0.307/-0.307	0.882/-0.930	0.542/-0.319

[a]GOF = $[\sum[w(F_0^2 - F_c^2)^2] / M - N]^{1/2}$ (M =number of reflections, N = number of parameters refined).
[b]$R_1 = \sum \| F_0 | - | Fc \| / \sum | F_0 |$. [c]$wR_2 = [\sum[w(F_0^2 - F_c^2)^2] / \sum[w(F_0^2)^2]]^{1/2}$.

In the packing diagram of **1**, C–H···π interaction, C10–H10···C13 (3.690(3) Å) and C–H···O interaction, C2–H2···O2 (3.187(3) Å) are significant.

Compound **2** crystallized in space group *P*–1 and the molecular structure consists of neutral 1D coordination polymer having the formula $[Zn(\mathbf{L1})(N_3)]_n$. This polymer is formed from a $[Zn(\mathbf{L1})]_2$ dimer in which each zinc(II) ion is coordinated by **L1**, and both O_P atoms are involved in bridging the two metal ions. These $[Zn(\mathbf{L1})]_2$ units are further bridged by two azide ions in a μ–1,1 fashion to a 1D coordination polymer. The ORTEP diagram with atom numbering scheme of the repeating unit is displayed in Fig. 2 and a representative view of the polymer in Fig. 3. The bivalent zinc is *hexa*-coordinated and has a distorted pseudo octahedral geometry. The coordination environment around bivalent zinc is $N_IN_Y(N_Z)_2(O_P)_2$ and the stereochemistry for $(N_IN_Y)(N_Z)_2(O_P)_2$ being *cis*,*cis*,*cis*. Thus, the polymer contains rectangular shaped planar Zn_2O_2 and Zn_2N_2 units, each having center of symmetry residing in the unit. As a consequence, heterochiral dimer is formed from a racemic pair of **L1**. The coordination polymer is formed by edge-sharing of two octahedral $\{ZnN_IN_Y(N_Z)_2(O_P)_2\}$ units and the shared edges are *cis* to each other with an angle at zinc atom being 134.38(2)°. In Zn_2O_2 units, bridging by O_P is unsymmetrical and the bond parameters in it are: Zn1–O1, 2.067(3) and 2.131(3); Zn1···Zn1, 3.198(1) and O1···O1, 2.720(5) Å. The N_Z linked Zn_2N_2 unit is also unsymmetrical having the bond parameters Zn1–N3, 2.086(3) and 2.388(3), Zn1···Zn1, 3.534(1); N3···N3, 2.759(4) Å. The trend, $Zn–N_Y > Zn–N_I > Zn–N_Z$ in the metal ligand bonds is also observed. The **L1** is bound to Zn(II) ion by a puckered five- and six-membered chelate rings with the ligand being twisted. The asymmetric carbon atom deviates from the five-membered chelate ring having dihedral angle of 18.17° between C5C6N2 and C5N1Zn1N2 planes. The dihedral angle of 35.82° between the planes formed by N2Zn1O1 and O1C14C9C8N2 suggests an out of plane displacement of zinc from the envelope shaped six membered rings.

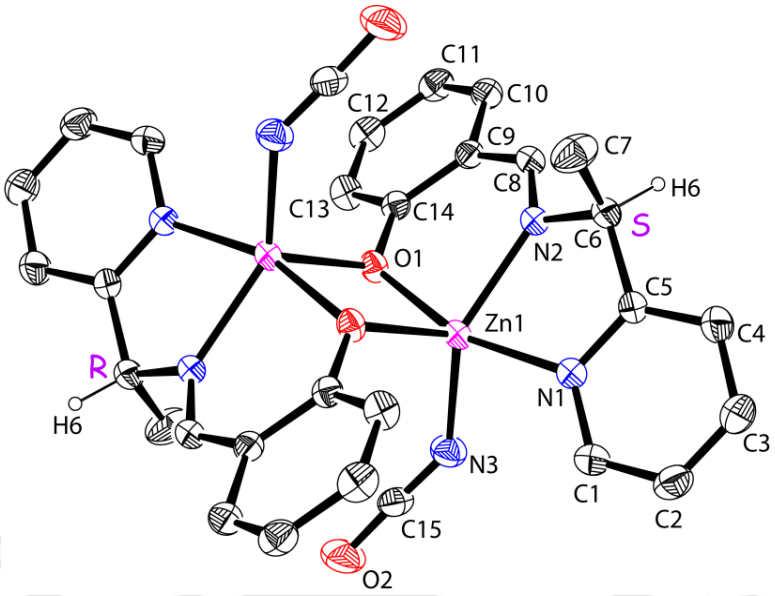

Fig. 1. ORTEP diagram (30%) and atom labeling scheme in **1** (All H–atoms except H6 are omitted for clarity).

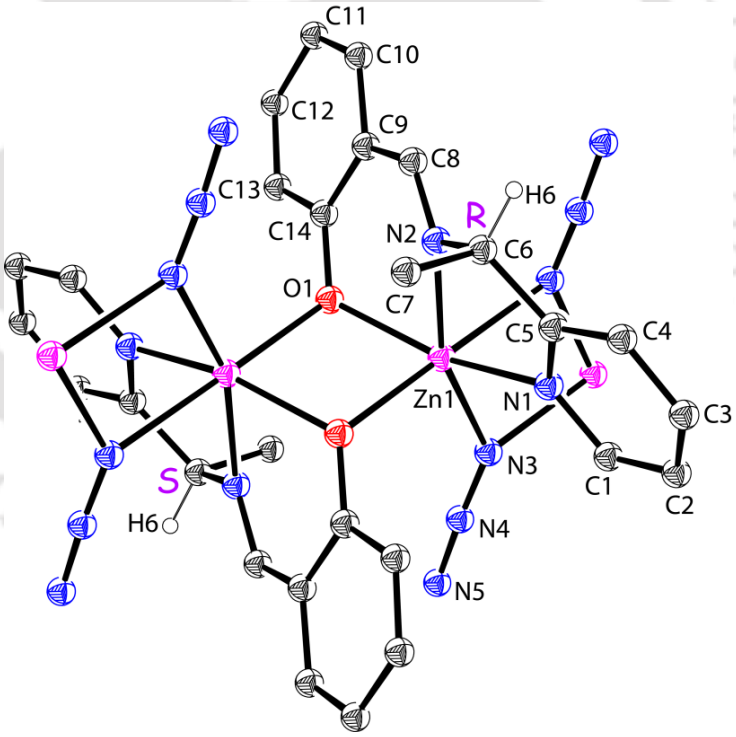

Fig. 2. ORTEP diagram (30%) and atom labeling scheme in **2** (All H–atoms except H6 are omitted for clarity).

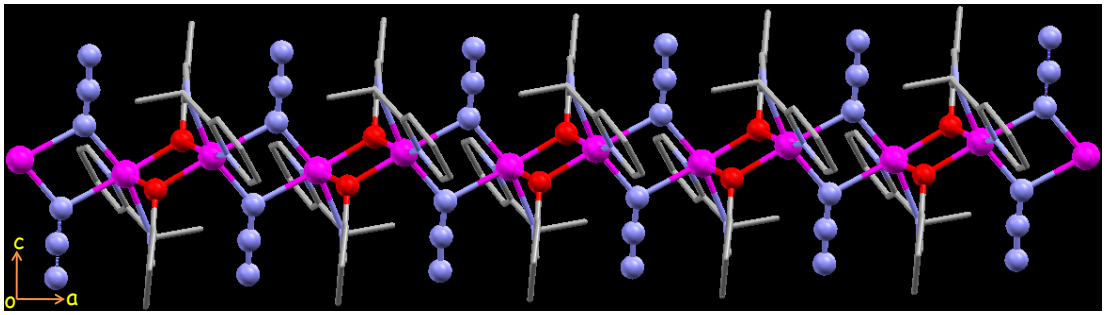

Fig. 3. 1D coordination polymeric structure in **2**.

Table 2. Selected bond lengths (Å) and bond angles (°) in **1**–**3**.

	1	**2**	**3**
Zn1–N1	2.159(2)	2.167(4)	2.155(4)
Zn1–N2	2.065(2)	2.124(3)	2.066(3)
Zn1–N3/N3A	1.969(2)	2.086(3)/2.388(3)	1.954(5)
Zn1–O1	2.105(1)	2.067(3)	2.128(3)
Zn1–O1A	2.016(1)	2.131(3)	1.999(3)
Zn1···Zn1A	3.108(1)	3.199(1)	3.193(1)
N1–Zn1–N2	77.78(6)	76.2(1)	77.8(1)
N1–Zn1–N3/N3A	94.37(7)	88.5(1)/94.1(1)	100.2(2)
N1–Zn1–O1	163.25(6)	158.2(1)	160.2(1)
N1–Zn1–O1A	106.14(6)	94.3(1)	102.4(1)
N2–Zn1–N3/N3A	140.06(7)	88.2(1)/161.6(1)	125.2(2)
N2–Zn1–O1	85.57(6)	83.0(1)	84.3(1)
N2–Zn1–O1A	113.48(6)	95.2(1)	118.4(1)
O1–Zn1–N3/N3A	97.26(7)	97.6(1)/107.7(1)	97.0(2)
O1A–Zn1–N3/N3A	106.35(7)	176.0(1)/101.1(1)	115.5(2)
O1–Zn1–O1A	82.09(5)	80.8(1)	78.7(1)
N3–Zn1–N3A		75.8(1)	
Zn1–O1–Zn1A	97.91(6)	99.2(1)	101.3(1)

Compound **3** crystallized in space group $P2_1/c$ and ORTEP diagram with the atom labeling scheme is displayed in Fig. 4. Ligands **L1** (R = Me) and **L2** (R = Ph) differ in the substitution at the asymmetric carbon atom but the coordination environment remain identical. Hence compounds **1** and **3** are isostructural, but with subtle differences. Five-coordinated zinc centers are highly distorted having a calculated τ value of 0.58, but the

coordination geometry can be best described as distorted trigonal bipyramid. The trigonal plane is formed by $O_PN_IN_C$ donor set with its angles lying in the range 115.5(2) – 125.2(2)° and the axial O1–Zn1–N1 angle has a value of 160.2(1)°. The Zn_2O_2 unit has a planar rectangular shape having Zn–O distances of 1.999(3) and 2.128(3) Å, implying that O_P bridge is unsymmetrical in nature having the non-bonded contacts Zn·Zn, 3.193(1) Å and O1···O1, 2.618(3) Å. Since the unit also has the center of symmetry in it, exists as heterochiral dimer. Among the coordination bonds, the trend $Zn–N_Y > Zn–N_I > Zn–N_C$ in bond lengths was observable. Ligand **L2** is bound to the zinc atom by a five-membered and a six-membered chelate ring and both rings are puckered, resulting in an open book shape for the ligand moiety. The asymmetric carbon atom deviates from the puckered five-membered chelate ring and dihedral angle between the two planes C5C6N2 and C5N1Zn1N2 being 8.8°. The dihedral angle of 29.36° between the planes formed by N2Zn1O1 and O1C14C9C8N2 suggests an out of plane displacement of zinc from envelope shaped six membered rings. In the packing diagram, C12–H12···O2 (3.478(6) Å) and C16–H16···π (C20) (3.668(7) Å) interactions connects the dimers in head-to-tail fashion to a 1D structure (Fig. 5) in which an isotactic arrangement of the asymmetric carbon centers are present.

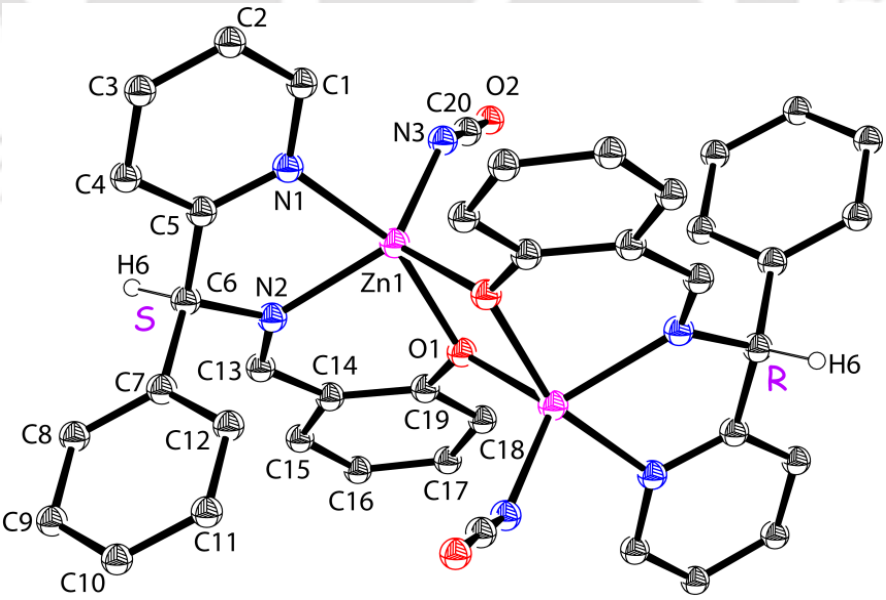

Fig. 4. ORTEP diagram (30%) and atom labeling scheme in **3** (All H–atoms except H6 are omitted for clarity).

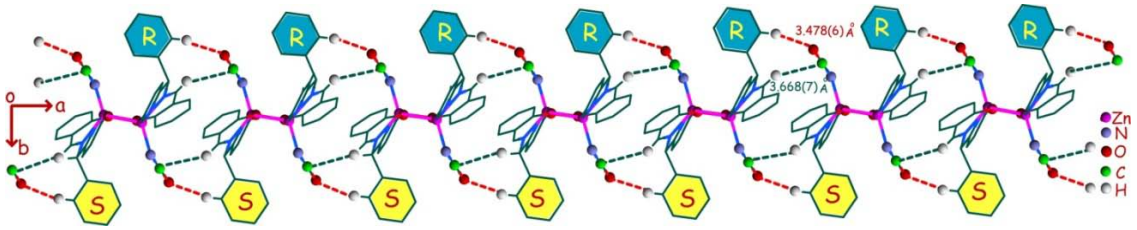

Fig. 5. 1D chains formed by C–H···O and C–H···π interactions with an isotactic arrangement of the asymmetric carbon centers present in **3**.

Compound **1′** crystallized in space group $P2_1/n$ and asymmetric unit contains the neutral dinuclear complex $[Zn_2(\mathbf{L1'})_2(NCO)_2]$. The molecule is non-centrosymmetric in nature and ORTEP diagram with the atom labeling scheme is displayed in Fig. 6. Both the zinc centers are *penta*-coordinated and each bound by a mono anionic tridentate ligand in *facial* fashion. Other two coordination sites are occupied by N_C and bridging O_P. Coordination geometry around both zinc centers is highly distorted as evident from calculated τ values of 0.56 and 0.50.

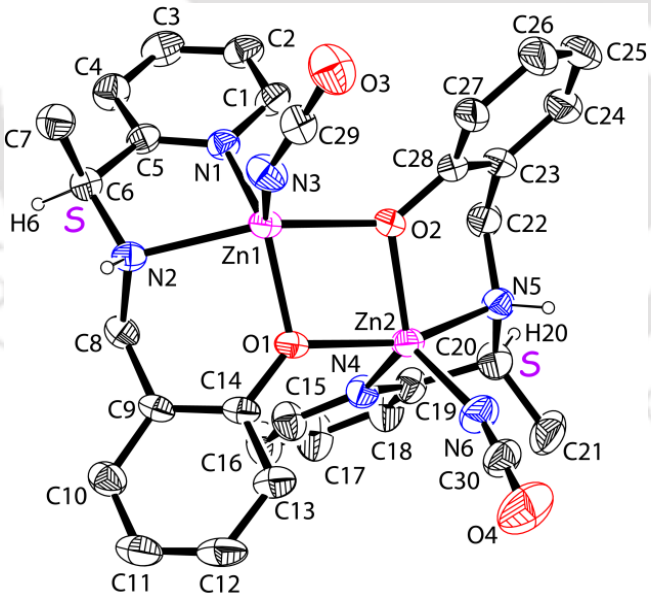

Fig. 6. ORTEP diagram (30%) and atom labeling scheme in **1′** (All H–atoms except H6 and H20 are omitted for clarity).

However, the geometry around both zinc centers can be regarded as distorted trigonal bipyramidal with $N_C N_Y$ and coordinated–O_P forming the trigonal plane while N_A and bridged–O_P atoms occupying axial sites. The sum of three angles in the trigonal planes at Zn1 and Zn2 are 359.7(2)° and 359.8(2)°, respectively. But the *trans* angles at Zn1 and Zn2 are respectively 154.1(1)° and 156.8(1)°, deviate largely from linearity. The Zn_2O_2 unit is slightly non planar with the dihedral angle between O1Zn1O2 and O1Zn2O2 planes being 6.9° and that between Zn1O1Zn2 and Zn1O2Zn2 being 8.7°. The unit has an oblique/diamond shape as can be inferred from the bonding and non-bonding distances: Zn1–O1, 1.980(3), Zn1–O2, 2.127(3), Zn2–O1, 2.084(3), Zn2–O2, 2.002(3), Zn1···Zn2, 3.218(1) and O1···O2, 2.531(5) Å. The Zn_2O_2 unit in **1′** doesn't have the center of symmetry inside the dimeric form and hence lead to the formation of a homochiral dimer having the combination as either *RR* or *SS* for the asymmetric carbon atom. However the crystal lattice, in overall has an equal mixture of dimers containing *RR* and *SS* combinations, due to the center of symmetry that lies outside the molecule. On complexation, nitrogen atom of the secondary amine group in **L1′** also becomes chiral. In **1′**, if the absolute configurations of both the N_A centers are *RR* then *C*–centers are *SS* and *vice versa*.

The trend Zn–N_A (Zn1–N2 = 2.233(4) Å; Zn2–N5 = 2.189(4) Å) > Zn–N_Y (Zn1–N1 = 2.081(4) Å; Zn2–N4 = 2.121(5) Å) > Zn–N_C (Zn1–N3 = 1.938(5) Å; Zn2–N6 = 1.933(5) Å) in the metal ligand bond distances is observed. The ligand forms a five-membered chelate ring with bite angle of ~77.7(2)° and six-membered chelate ring with bite angles of 88.6(1), 90.0(2)° and both rings are puckered. However, other *cis* angle having the values of 122.7(2) and 124.1(2)° is much wider. Two cyanato groups are oriented at torsional angle of 28.1(3)°. The packing diagram of **1′** reveals the presence of H–bonding interaction N5–H5···O4, 2.984(7) Å between the secondary amine hydrogen and cyanato oxygen atoms. This occurs at N5O4Zn2O4 having a torsional angle of 24.4(3)°. This N5–H5···O4 interaction selectively links adjacent heterochiral dimers to 1D H–bonded polymer {such as ···*RR*···*RR*···*RR*··· or ···*SS*···*SS*···*SS*···} as shown in Fig. 7. This type of H–bonding interaction has been termed as enantioselective H–bonding interactions [329, 330]. In addition, two adjacent heterochiral dimers are also associated by C17–H17···O4; 3.40(1) and C17–H17···π; 3.69(1) Å interactions.

Table 3. Selected bond lengths (Å) and bond angles (°) in **1′**–**3′**.

	1′	**2′·2DMF**	**3′·DMF**
Zn1–N1	2.081(4)	2.141(3)	2.157(2)
Zn1–N2	2.233(4)	2.148(3)	2.154(2)
Zn1–N3	1.938(5)	2.138(4)	2.140(2)
Zn1–N4		2.155(3)	2.158(2)
Zn1–O1	1.980(3)	2.180(2)	2.131(1)
Zn1–O2	2.127(3)	2.127(2)	2.107(1)
Zn2–N4	2.121(5)		
Zn2–N5	2.189(4)	1.973(4)	1.931(2)
Zn2–N6	1.933(5)		1.915(2)
Zn2–N8		1.963(4)	
Zn2–O1	2.084(3)	1.969(2)	1.992(1)
Zn2–O2	2.002(3)	1.961(2)	1.990(1)
Zn1···Zn2	3.218(1)	3.142(1)	3.096(1)
N1–Zn1–N2	77.6(2)	79.0(1)	78.36(6)
N1–Zn1–N3	114.1(2)	176.0(1)	177.1(1)
N1–Zn1–N4		98.7(1)	97.91(6)
N1–Zn1–O1	124.1(2)	88.70(9)	89.99(5)
N1–Zn1–O2	93.7(2)	93.17(9)	92.29(6)
N2–Zn1–N3	98.8(2)	98.6(1)	101.69(6)
N2–Zn1–N4		106.1(1)	100.30(6)
N2–Zn1–O1	88.6(1)	88.9(1)	90.70(5)
N2–Zn1–O2	154.1(1)	163.3(1)	166.28(6)
N3–Zn1–N4		78.8(1)	79.18(6)
N3–Zn1–O1	121.5(2)	94.5(1)	92.94(5)
N3–Zn1–O2	107.0(2)	90.0(1)	88.16(6)
O1–Zn1–O2	76.0(1)	76.08(8)	85.38(5)
N4–Zn1–O1	93.7(2)	164.3(1)	167.53(6)
N4–Zn2–N5	77.7(2)		
N4–Zn2–N6	117.3(2)		
N4–Zn2–O2	122.7(2)	89.6(1)	90.85(6)
N5–Zn2–N6	98.1(2)		114.6(1)
N5–Zn2–N8		110.0(1)	
N5–Zn2–O1	156.8(1)	113.0(1)	116.34(8)
N5–Zn2–O2	90.0(2)	119.0(1)	109.23(8)
N6–Zn2–O1	105.0(2)		109.58(7)
N6–Zn2–O2	119.8(2)		118.68(8)
N8–Zn2–O1		117.6(1)	
N8–Zn2–O2		110.7(1)	
O1–Zn2–O2	76.5(1)		
O1–Zn2–O2		84.96(9)	85.38(5)
Zn1–O1–Zn2	104.7(2)	98.34(9)	97.28(5)
Zn1–O2–Zn2	102.3(1)	100.42(9)	98.13(6)

The adjacent *RR* and *SS* H–bonded polymers are interlinked by H–bonding interaction N2–H2···N3, 3.435(6) Å and other weak interaction such as: C3–H3···O3, 3.470(8); C10–H10···O3, 3.392(8); and C10–H10···π, 3.554(9) Å, to a 2D sheet structure along *a*-axis.

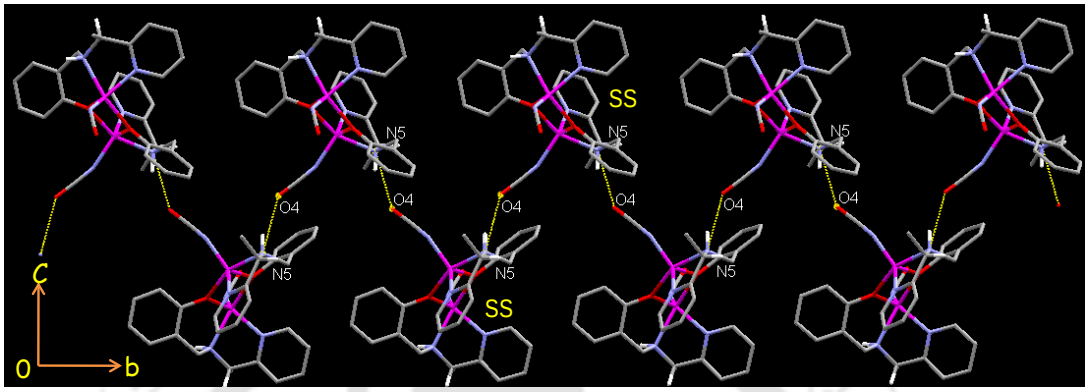

Fig. 7. 1D H–bonded polymer representing ···*SS*···*SS*···*SS*··· sequence in **1′**.

Compound **2′·2DMF** crystallized in space group $P2_1/c$ and ORTEP diagram with atom labeling scheme of **2′**, is displayed in Fig. 8. The molecular structure of **2′** consists phenoxo bridged neutral molecule having the formula $[Zn_2(\mathbf{L1'})_2(N_3)_2]$.

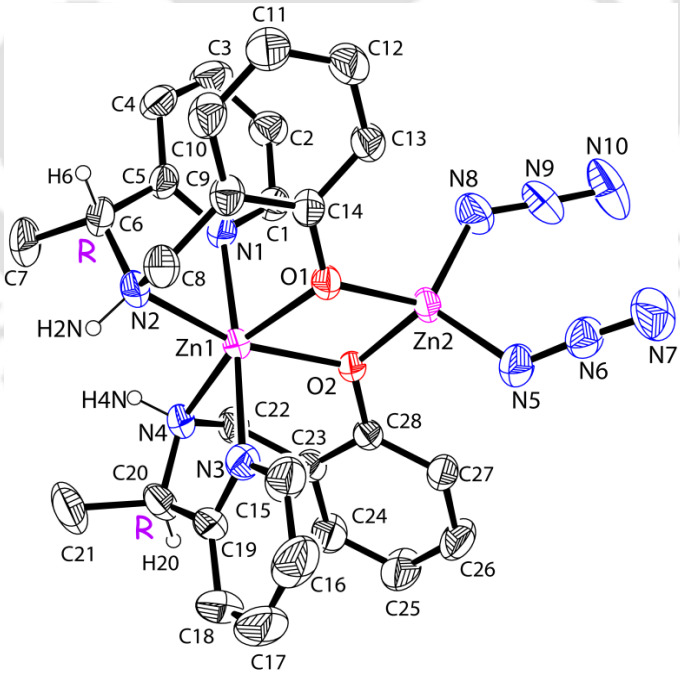

Fig. 8. ORTEP diagram (30%) and atom labeling scheme in **2′** (All H–atoms except H6, H20, H2N and H4N are omitted for clarity).

There are two zinc centers: (*i*) a *hexa*-coordinated bis-chelate {Zn(**L1′**)$_2$}, in which zinc(II) ion being coordinated by the *facial* tridentate ligand **L1′**, resulting in overall *cis*,*cis*,*trans*-$(O_P)_2(N_A)_2(N_Y)_2$ stereochemistry around the metal ion; (*ii*) a *tetra* coordinated zinc center in which the bivalent zinc is coordinated by two end-on azide ions and by the {Zn(**L1′**)$_2$}-unit through two O_P atoms. It is relevant to note that formation of such bimetallic centers using *cis*-$(O_P)_2$ disposition has been reported [324].

Compound **2′** is completely different from **1′**, although it contains the same base **L1′**, but the effect of changing the co-ligand from cyanate ion (**1′**) to azide ion (**2′**), is reflected in a drastic change in the coordination environment. The *hexa*- and *tetra*- coordinated zinc centers respectively have distorted octahedral and tetrahedral geometries. In the *hexa*-coordinated center the *cis* angles lie in the range 76.1(1) – 106.1(1)° while the *trans* angles lie in the range 163.3(1) – 176.0(1)°. The three angles around the metal center in *tetra*-coordinated zinc center are in the range 110.0(1) – 119.0(1)° but the O1–Zn2–O2 (85.0(1)°) being acute which is due to their bridging nature. The edge sharing between the *hexa*- and *tetra*-coordinated zinc centers forms a rectangular Zn_2O_2 unit in which the two planes containing the atoms O1Zn1O2 and O1Zn2O2 angle by 4.4°. Since the center of symmetry do not lie at zinc atom of *hexa*-coordinated center, the asymmetric carbon atom in both **L1′** have the same absolute configuration. As observed in **1′**, if the absolute configurations of both the N_A centers are *RR* then *C*–centers are *SS* and *vice versa*. The Zn–N_A bond lengths (Zn1–N2 = 2.148(3) Å; Zn1–N4 = 2.155(3) Å) are longer than that of Zn–N_Y (Zn1–N1 = 2.141(3) Å; Zn1–N3 = 2.138(4) Å). And the Zn–N_Z bond distances (Zn2–N5 = 1.973(4) Å; Zn2–N8 = 1.963(4) Å) found in the *tetra*-coordinated zinc atom are shorter than Zn–N_I and Zn–N_Y bond distances found in *hexa*-coordinated zinc atom. Solvent DMF molecules play an important role in assembling *RR* and *SS* bis-chelates, by involving its oxygen atom in H–bonding interaction with each of the two N_A atom of the reduced Schiff bases {N2–H2···O3, 2.80(1); N4–H4···O4, 2.966(5) Å}. Other significant weak interactions (Fig. 9) that occur between DMF and **2′** are: N2–H2···O3; 2.80(1), C21–H21···O3; 3.36(1), C29–H29···N5; 3.582(3) and C29–H29···N6; 3.485(8) Å. The packing diagram of **2′**, reveals weak interactions such as: C6–H6···O10, 3.497(8) and C29–H29···π, 3.77(1) Å exist between *RR* and *SS* bis-chelates. The C4–H4···N7, 3.580(6);

C7–H7···O4, 3.581(6) and C33–H33···C11; 3.691(7) Å interactions occur between two identical *RR*(*SS*) bis-chelates.

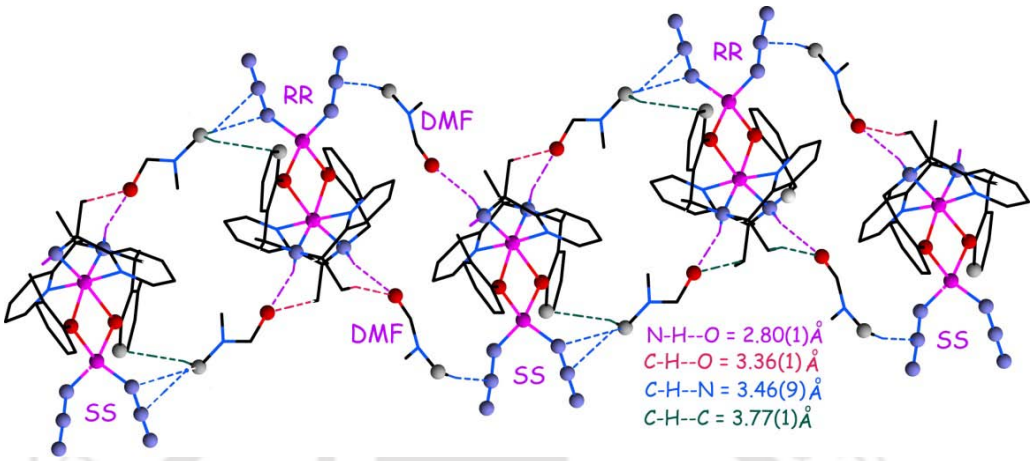

Fig. 9. Interaction of DMF with *RR* and *SS* bis-chelates in **2′**.

Compound **3′·DMF** crystallized in space group *P*–1 and ORTEP diagram with the atom labeling scheme of **3′**, is displayed in Fig. 10. The molecular structure of **3′** consists O_P bridged neutral dinuclear complex $[Zn_2(\mathbf{L2'})_2(NCO)_2]$.

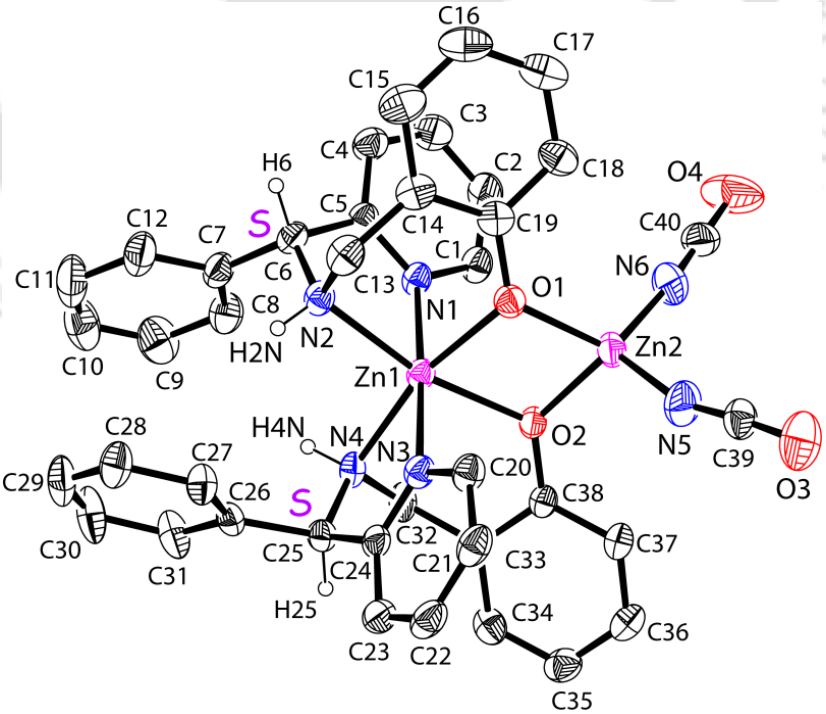

Fig. 10. ORTEP diagram (30%) and atom labeling scheme in **3′** (All H–atoms except H6, H25, H2N and H4N are omitted for clarity).

As observed in **2′**, there are two zinc centers in **3′** as well: (*i*) a *hexa*-coordinated bis-chelate {Zn(**L2′**)$_2$}, in which zinc(II) ion being coordinated by the *facial* tridentate ligand **L2′** resulting in overall *cis*,*cis*,*trans*-$(O_P)_2(N_A)_2(N_Y)_2$ stereochemistry around the metal ion; (*ii*) a *tetra*-coordinated zinc center in which the bivalent zinc is coordinated by two N_C atoms of cyanate ions and by the {Zn(**L2′**)$_2$}-unit through two O_P atoms.

Compound **3′** is completely different from **3**, as a result of changing **L2** to **L2′** and with the same co-ligand. It is also different from **1′** (similar ligand and same co-ligand) but similar to **2′** (similar ligand and different co-ligand). The *hexa*- and *tetra*- coordinated zinc centers respectively have distorted octahedral and tetrahedral geometries. In the *hexa*-coordinated center the *cis* angles lie in the range 78.36(6) – 101.69(6)° while the *trans* angles lie in the range 166.28(6) – 177.07(6)°. The three angles around the metal center in *tetra*-coordinated zinc center are in the range 109.3(1)–114.6(1)° but the O1–Zn2–O2 (85.4(1)°) being acute which is due to their bridging nature. The edge sharing between the *hexa*- and *tetra*- coordinated zinc centers form a rectangular Zn_2O_2 unit in which the two planes containing the atoms O1Zn1O2 and O1Zn2O2 angle by 2.0°. Since the center of symmetry do not lie at zinc atom of *hexa*-coordinated center, the asymmetric carbon atom in both the **L2′** have the same absolute configuration and the bis-chelates have *RR* or *SS* combinations. As observed in **1′** and **2′**, if the absolute configurations of both the N_A centers are *RR* then *C*–centers are *SS* and *vice versa*. The Zn–N_A bond lengths (Zn1–N2 = 2.154(2) Å; Zn1–N4 = 2.158(2) Å) are comparable that of Zn–N_Y (Zn1–N1=2.157(2) Å; Zn1–N3 = 2.140(2) Å) lengths. And the Zn–N_Z bond distances (Zn2–N5 = 1.931(2) Å; Zn2–N6 = 1.915(2) Å) found in the *tetra*-coordinated zinc atom are shorter than Zn–N_I and Zn–N_Y bond distances found in *hexa*-coordinated zinc atom. The Zn–O_P bond distances (Zn1–O1 = 2.131(1); Zn1–O2 = 2.107(1) Å) in the *hexa*-coordinated zinc atoms are longer (Zn2–O2 = 1.990(2); Zn2–O1 = 1.992(1) Å) than that found in the *tetra*-coordinated zinc atom. Solvent DMF molecules do not involve in H–bonding interaction but show some C–H···O interactions {C23–H23···O4, 3.247(3); C41–H41···O4, 3.55(5); C25–H25···O5, 3.574(5)} that include oxygen and carbon atoms of DMF (Fig. 11).

The *hexa*-coordinated zinc centers in **2′** and **3′** are intrinsically asymmetric in nature due to orientation of chelate rings. By viewing through the opposite $N_YN_AO_P$ pair of triangular faces, the *RR* bis-chelates have a Δ configuration for the complex molecule and the *SS* bis-chelates have Λ configuration. Since the overall crystal lattice has an equal proportions of *RR* and *SS* bis-chelates, Δ and Λ isomers are also in equal amounts.

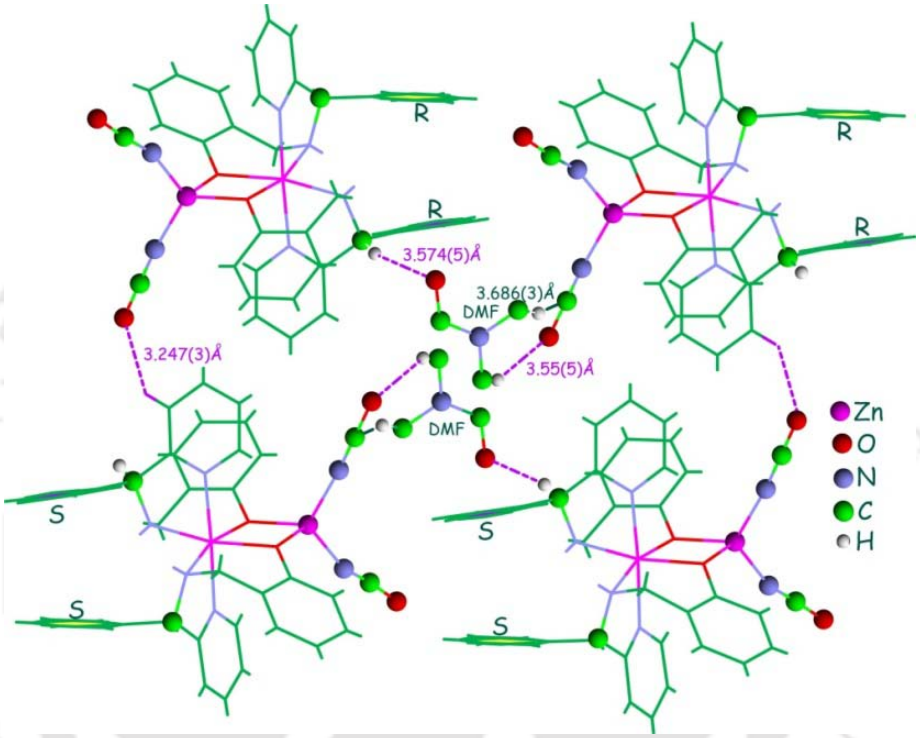

Fig. 11. C–H···O interactions of DMF with *RR* and *SS* bis-chelates in **3′**.

6.3.1 Role of ligand geometry, coligands and weak interactions:

From compound **1**–**3** synthesized from the Schiff base ligands and **1′**–**3′** containing the reduced base ligands, the following points can be compared: (*a*) nature of the ligand (imine or amine) (*b*) nature of co-ligands (azide or cyanate) (*c*) nature of weak interaction such as N–H···O, N–H···N, C–H···O, C–H···N, C–H···C, C–H···π and π···π.

(*a*) *Nature of Ligand*: Imine ligands are coordinated in meridional fashion and forms O_P bridged centrosymmetric binuclear structures, hence compounds **1**–**3** have a *RS* combination of the ligand. Amine ligands span *facial* positions and form a non-centrosymmetric Zn_2O_2 unit in **1′** resulting in a *RR* or *SS* combination of amine. However

in **2′** and **3′**, amine bis-chelates are present and two O_P groups occupy the *cis* positions which further act as bidentate ligand towards $\{Zn(NCO)_2\}$ and $\{Zn(N_3)_2\}$ units. This leads to binuclear zinc complexes with edge-shared octahedron and tetrahedron of zinc centers. Since center of symmetric do not reside at zinc, a *RR* and *SS* bis-chelates are formed and respectively has Δ and Λ configurations. On complexation, the N–atom of secondary amine becomes *N*–centered chirality as well, which remain opposite in chirality with respect to *C*–center. The metal to ligand bond lengths follow different trend in imine and amine types. The $Zn–N_Y$ bonds in imine compounds are longer than $Zn–N_I$ bonds, but are shorter than $Zn–N_A$ bonds in the amine complex. The amine ligands show a wide range of $N_Y–Zn–O_P$ angles (88.2(1) – 124.1(2)°). The observed angles, 122.7(2)–124.1(2)° (in **1′**) and 88.2(1) – 90.0(1)° (in **2′** and **3′**), are respectively necessary for the demands of trigonal bipyramidal and octahedral geometries. This is consistent with the flexible nature of the secondary amine function on coordination to transition metal ions [336–338]. Hence simple changing the ligand system from imine to amine, affect a lot in their orientation around metal center and the self-assembly process.

(*b*) *Nature of co-ligands*: As such there is no perceptible co-ligand effect observed in these complexes. They merely tend to bind to the site left free by the tridentate ligands, may be due to domination of O_P bridging. Accordingly, since the Zn_2O_2 unit is centrosymmetric in **1** and **3**, two co-ligands would be expected to lies *trans* to each other and indeed the torsional angle between them is 180°. The Zn_2O_2 unit in **1′** is non-centrosymmetric in nature where co-ligand need not have to occupy *trans* position, as a result the torsional angle between two cyanate ligands is 28.1(3)°.

(*c*) *Effect of weak interaction*: In the crystal engineering point of view, weak interactions (< 4 Å) play a crucial role in the arrangement of molecules in the lattice [339]. Here in these six compounds, weak interactions also play a role in the self-assembly of chelated racemic Schiff bases. Among them, C–H···O and C–H···π interactions are involved in assembling the dimers of **3** in head-to-tail fashion to a 1D structure. An enantioselective H–bonding N–H···O interaction that occur between the secondary amine hydrogen and cyanato oxygen atoms selectively links adjacent enantiomeric dimers of **1′** to one-dimensional *RR* or *SS* hydrogen-bonded polymers. The

adjacent *RR* and *SS* H–bonded polymers are interlinked by H–bonding interaction N2–H2···N3, 3.435(6) Å and other weak interaction such as: C3–H3···O3, 3.470(8); C10–H10···O3, 3.392(8); and C10–H10···π, 3.554(9) Å, to a 2D sheet structure along *a*-axis. The oxygen atoms of DMF molecule play an important role in assembling *RR* and *SS* bis-chelates, by hydrogen-bonding with the N_A atoms of **2′**.

6.4 Thermal analyses

The thermogravimetric analyses of **2′·2DMF** and **3′·DMF** were carried out in the temperature range 25 – 600 °C in a static atmosphere of nitrogen. Freshly prepared samples were kept in desiccators overnight prior to TG analysis and the profiles are displayed in Fig. 12. In compound **2′**, the weight loss of 9.19% (Calcd. 8.96%) was observed in the temperature range of 105 – 143 °C, corresponding to the loss of one DMF molecule. Loss of second DMF molecule is along with one azide ion occur for weight loss of 19.41% (Calcd. 19.24%) in the temperature range 256 – 375 °C. From the X-ray structure data (*vide supra*), it has been observed that one of the DMF molecules exhibits a shorter H–bonding distance of 2.804(1) Å than the other (2.966(5) Å) with N_A atoms in compound **2′**. It is consistent with the TG profile that the DMF molecule having a shorter H–bonding distance could be lost at the higher temperature range. In compound **3′**, the weight loss of 7.95% (Calcd. 8.4%) was observed in the temperature range of 117 – 245 °C, that corresponds to the loss of one DMF molecule. Since the monodentate co-ligands can be expected to lose prior to tridentate chelating ligands, the weight loss of 19.31% (Calcd. 11.2%) for cyanate ion can be expected to occur in the temperature range 254 – 376 °C. Overall in both compounds the Zn_2O_2 units are quite stable upto a calculated temperature of ~375 °C.

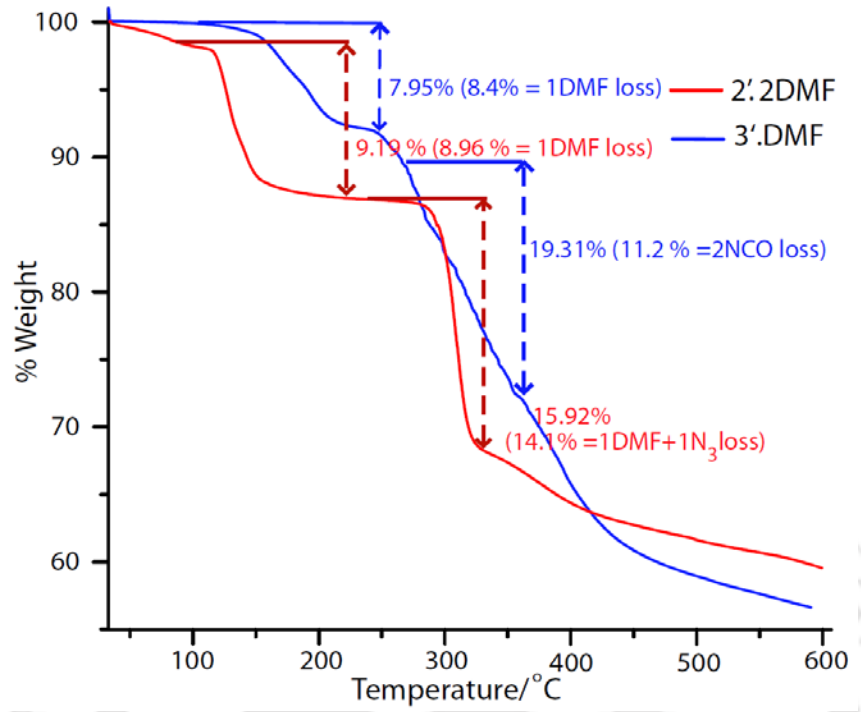

Fig. 12. TG profiles of **2′·2DMF** and **3′·DMF**.

6.5 Conclusion

Six zinc(II) complexes were synthesized using a racemic mixture of tridentate imine and their reduced amine ligands. Determination of their molecular structures revealed the presence of a Zn_2O_2 unit in all complexes. The tridentate imine and amine ligands respectively span *meridional* and *facial* positions due to sp^2 and sp^3 hybridization on N-atom. Compound **1**–**3** have center of symmetry in the Zn_2O_2 unit and has a *RS* combination of racemic Schiff bases around zinc centers. Where as in **1′**, the Zn_2O_2 unit do not have center of symmetry in it and has a *RR*(*SS*) combination of amine ligand. In **2′** and **3′**, *hexa*-coordinated zinc(II) bis-chelates of amine are formed having *RR*(*SS*) combination of ligand. These two complexes have a *cis*-$(O_P)_2$ disposition which coordinate to another *tetra*-coordinated zinc(II) center. The Zn–N_Y bonds in imine compounds are longer than Zn–N_I bonds, but are shorter than Zn–N_A bonds in the amine complex. In these complexes no perceptible co-ligand effect has been observed and they merely tend to bind to the site left free by tridentate ligands, which may be due to the domination of O_P bridging. In **1′**, 1D polymeric chain exists that are formed by

enantioselective H–bonding interaction between adjacent enantiomeric dimers. In **2′** and **3′**, solvent DMF molecules are involved in assembling *RR* and *SS* bis-chelates. Also the *RR* and *SS* bis-chelates respectively have Δ and Λ configurations. Although we were not able to isolate pure homochiral dimers, the diastereoselective self-assembly observed here will add to the understanding of self-sorting of *meridionally* and *facially* coordinating chiral tridentate ligands around the dimetallic core.

Conclusion and Future Perspectives

In conclusion, the effect of anions, bridging ligands, co-ligands and ligand geometry on the self-assembly of tridentate imines and amines around the dimetallic core are described in this thesis. Anions such as Cl^- and NO_3^- offers heterochiral combination of imines around M_2O_2 core in self-discrimination manner whereas OAc^- and SO_4^{2-} leads to homochiral combination of imines in self-recognition manner. Co-ligands such as N_3^-, NCO^-, and NCS^- ions bind in μ–1 and μ–1,1 (azide ion only) bridging modes whereas and $N(CN)_2^-$ ion binds in μ–1 and μ–1,5 coordination modes, assembling homo- and heterochiral dimerization of imines and amines around the M_2X_2 core (X = O, N, Cl). In some cases the μ–1,5 dca ion bridge results in formation of 1D and 2D coordination polymer. The chiral tridentate imine and amine ligands respectively span the *meridional* and *facial* positions resulting in homo- and hetero-chirality, around M_2X_2 core. The role of enantioselective and diastereoselective H–bonding interactions as well as C–H···N, C–H···O, C–H···π and π···π interactions on the self-assembly are also observed.

In future, I believe that, the self-assembly observed in this thesis will add to the understanding of self-sorting process of chiral tridentate imine and amine ligands around the dimetallic core.

References

[1] H. Schiff, Ann. Chem. (Paris) 131 (1864) 118–119.

[2] "The Chemistry of the Carbon-Nitrogen Double Bond", Ed. S. Patai, Interscience, London, 1970.

[3] M. M. Sprung, Chem. Rev. 26 (1940) 297–338.

[4] R. W. Layer, Chem. Rev. 63 (1963) 489–510.

[5] P. A. Vigato, S. Tamburini, Coord. Chem. Rev. 248 (2004) 1717–2128.

[6] A. Von Zelewsky, O. Mamula, J. Chem. Soc. Dalton Trans. (2000) 219–231.

[7] U. Knof, A. Von Zelewsky, Angew. Chem. Int. Ed. 38 (1999) 303–322.

[8] C. Provent, A. F. Williams, Transition Metals in Supramolecular Chemistry; J. P. Sauvage, Ed.; John Wiley and Sons: New York, (1999) 135–191.

[9] S. G. Telfer, G. Bernardinelli, A. F. Williams, Chem. Commun. (2001) 1498–1499.

[10] S. G. Telfer, R. Kuroda, T. Sato, Chem. Commun. (2003) 1064–1065.

[11] I. Ojima, Catalytic Asymmetric Synthesis, VCH, Weinheim 1993.

[12] L. Canali, D. C. Sherrington, Chem. Soc. Rev. 28 (1999) 85–93.

[13] R. Lde, K. Noda, Y. Ito, T. Kalsuki, Tetrahedron Lett. 32 (1991) 1055–1058.

[14] N. H. Lee, E. N, Jacobsen, Tetrahedron Lett. 32 (1991) 6533–6536.

[15] E. N. Jacobsen, W. Zhang, A. R. Muci, J. R. Ecker, L. Deng, J. Am. Chem. Soc. 113 (1991) 7063–7064.

[16] Absolute Stereochemistry of Fungal Metabolites: Icterinoidins A1 and B1, and Atrovirins B1 and B2 Melvyn Gill and Peter M. Morgan Arkivoc (RI-1154C) 2004.

[17] J. C. Ruble, H. A. Latham, G. C. Fu, J. Am. Chem. Soc. 119 (1997) 1492–1493.

[18] A. C. Dalla, L. Mandolini, C. Pasquini, L. Schiaffino, New J. Chem. 28 (2004) 1198–1199.

[19] A. Szumna, Chem. Soc. Rev. 39 (2010) 4274–4285.

[20] A. Von Zelewsky, "Stereochemistry of Coordination Compounds" John Wiley: Chichester, 1995. ISBN 047195599.

[21] G. P. Moss, Pure Appl. Chem. 68 (1996) 2193–2222.

[22] P. Cintas, Angew. Chem. Int. Ed. 46 (2007) 4016–4024.

[23] E. L. Eliel, S. H. Wilen, "The Stereochemistry of Organic Compounds" John Wiley & Sons; 300–322 (1994) 159.

[24] J. Jacques, A. Collet, S. Wilen, Enantiomers, Racemates, and Resolutions. New York: John Wiley & Sons; (1981) 3–5.

[25] K. A. Wheeler, R. C. Grove, R. E. Davis, W. Scott Kassel, Angew. Chem. Int. Ed. 47 (2008) 78–81.

[26] C. J. Welch, Chirality 13(2001) 425–427.

[27] G. B. Kauffman, I. Bernal, H. -W. Schütt, Enantiomer 4 (1999) 33–45.

[28] H. Brunner, M. Weber, M. Zabel, Coord. Chem. Rev. 242 (2003) 3–13.

[29] Q. -H. Xia, H. -Q. Ge, C. -P. Ye, Z. -M. Liu, K. -X. Su, Chem. Rev. 105 (2005) 1603–1662.

[30] G. Koeckelberghs, C. Samyn, A. Miura, S. De Feyter, F. C. De Schryver, S. Sioncke, T. Verbiest, G. De Schaetzen, A. Persoons, Adv. Mater. 17 (2005) 708–712.

[31] R. P. Lemieux, Acc. Chem. Res. 34 (2001) 845–853.

[32] W. Eerenstein, N. D. Mathur, J. F. Scott, Nature 442 (2006) 759–765.

[33] A. Van Dorsselaer, B. Kniesel, D. Fenske, J. Am. Chem. Soc. 119 (1997) 10956–10962.

[34] M. C. Calama, P. Timmerman, D. N. Reinhoudt, Angew. Chem. Int. Ed. 39 (2000) 755–758.

[35] F. Hof, C. Nuckolls, J. Jr. Rebek, J. Am. Chem. Soc. 122 (2000) 4251–4252.

[36] J. -M. Lehn, Chem. Eur. J. 5 (1999) 2455–2463.

[37] G. R. L. Cousins, S. A. Poulsen, J. K. M. Sanders, Curr. Opin. Chem. Biol. 4 (2000) 270–279.

[38] T. Kondo, K. Oyama, K. Yoshida, Angew. Chem. Int. Ed. 40 (2001) 894–897.

[39] L. J. Prins, J. Huskens, F. de Jong, P. Timmerman, D. N. Reinhoudt, Nature 398 (1999) 498–502.

[40] L. J. Prins, F. de Jong, P. Timmerman, D. Reinhoudt, Nature 408 (2000) 181–184.

[41] S. F. Mason, Molecular Optical Activity and the Chiral Discriminations; Cambridge University Press: Cambridge, 1982.

[42] W. A. Bonner, Origins Life Evol. Biospheres 24 (1994) 63–78.

[43] J. Zhang, S. Chen, A. Zingiryan, X. J. Bu, J. Am. Chem. Soc. 130 (2008) 17246–17247.

[44] A. J. MacDermott, D. B. Cline, Eds. American Institute of Physics: Woodbury, NY, 1996.

[45] M. Avalos, R. Babiano, P. Cintas, J. L. Jimenez, J. C. Palacios, Chem. Commun. (2000) 887–892.

[46] J. Zhang, X. Bu. Chem. Commun. (2009) 206–208.

[47] A. N. Collins, G. N. Sheldrake, J. Crosby, Eds. Chiral in Industry II; Wiley: New York, 1998.

[48] Y. Okamoto, T. Nakano, Chem. Rev. 94 (1994) 349–372.

[49] R. J. M. Nolte, Chem. Soc. Rev. 23 (1994) 11–19.

[50] W. Lin, MRS Bull. 32 (2007) 544–548.

[51] B. Kesanli, W. B. Lin, Coord. Chem. Rev. 246 (2003) 305–326.

[52] G. Fërey, Chem. Soc. Rev. 37 (2008) 191–214.

[53] M. A. Mateos-Timoneda, M. Crego-Calama, D. N. Reinhoudt, Chem. Soc. Rev. 33 (2004) 363–372.

[54] O. Mamula, A. Von Zelewsky, Coord. Chem. Rev. 242 (2003) 87–95.

[55] R. Kramer, J. M. Lehn, A. Marquis-Rigault, Proc. Natl. Acad. Sci. USA 90 (1993) 5394–5398.

[56] J. -M. Vincent, C. Philouze, I. Pianet, J. -B. Verlhac, Chem. Eur. J. 6 (2000) 3595–3599.

[57] L. Isaacs, D. Witt, Angew. Chem. Int. Ed. 41 (2002) 1905–1907.

[58] T. W. Kim, J. -I. Hong, M. S. Lah, Chem. Commun. (2001) 743–744.

[59] H. -J. Kim, D. Moon, M. S. Lah, J. -I. Hong, Angew. Chem. Int. Ed. 41 (2002) 3174–3177.

[60] S. G. Telfer, R. Kuroda, Coord. Chem. Rev. 242 (2003) 33–46.

[61] C. -D. Wu, H. L. Ngo, W. Lin, Chem. Commun. (2004) 1588–1589.

[62] Y. Cui, H. L. Ngo, P. S. White, W. Lin, Chem. Commun. (2002) 1666–1667.

[63] W. Cui, O. R. Evans, H. L. Ngo, P. S. White, W. Lin, Angew. Chem. Int. Ed. 41 (2002) 1159–1162.

[64] O. R. Evans, D. R. Manke, W. Lin, Chem. Mater. 14 (2002) 3866–3874.

[65] Y. Cui, S. J. Lee, W. Lin, J. Am. Chem. Soc. 125 (2003) 6014–6015.

[66] H. L. Ngo, W. L. Lin, J. Am. Chem. Soc. 124 (2002) 14298–14299.

[67] H. L. Ngo, W. Lin, W. Chem. Commun. (2003) 1388–1389.

[68] B. Kesanli, Y. Cui, M. R. Smith, E. W. Bittner, B. C. Brockrath, W. Lin, Angew. Chem. Int. Ed. 44 (2005) 72–75.

[69] S. J. Lee, J. S. Kim, W. Lin, Inorg. Chem. 43 (2004) 6579–6588.

[70] H. Jiang, W. Lin, J. Am. Chem. Soc. 126 (2004) 7426–7427.

[71] S. J. Lee, C. R. Luman, F. N. Castellano, W. Lin, Chem. Commun. 17 (2003) 2124–2125.

[72] H. Jiang, W. Lin, J. Am. Chem. Soc. 125 (2003) 8084–8085.

[73] Y. Cui, H. L. Ngo, P. S. White, W. Lin, Chem. Commun. 8 (2003) 994–995.

[74] Y. Cui, H. L. Ngo, P. S. White, W. Lin, Inorg. Chem. 42 (2003) 652–654.

[75] Y. Cui, H. L. Ngo, W. Lin, Inorg. Chem. 41 (2002) 5940–5942.

[76] T. J. Burchell, D. L. Eisler, M. C. Jennings, R. J. Puddephatt, Chem. Commun. (2003) 2228–2229.

[77] T. J. Burchell, D. J. Eisler, R. J. Puddephatt, Chem. Commun. (2004) 944–945.

[78] T. J. Burchell, D. J. Eisler, R. J. Puddephatt, Inorg. Chem. 43 (2004) 5550–5557.

[79] G. L. J. A. Rikken, E. Raupach, Nature 390 (1997) 493–494.

[80] C. Train, R. Gheorghe, V. Krstic, L. -M. Chamoreau, N. S. Ovanesyan, G. L. J. A. Rikken, M. Gruselle, M. Verdaguer, Nat. Mater. 7 (2008) 729–734.

[81] K. Inoue, K. Kikuchi, M. Ohba, H. Ökawa, Angew. Chem. Int. Ed. 42 (2003) 4810–4812.

[82] H. Imai, K. Inoue, K. Kikuchi, Y. Yoshida, M. Ito, T. Sunahara, S. Onaka, Angew. Chem. Int. Ed. 43 (2004) 5618–5621.

[83] E. Coronado, C. J. Gómez-García, A. Nuez, F. M. Romero, J. C. Waerenborgh, Chem. Mater. 18 (2006) 2670–2681.

[84] W. Kaneko, S. Kitagawa, M. Ohba, J. Am. Chem. Soc. 129 (2007) 248–249.

[85] E. Coronado, J. R. Galán-Mascarós, C. J. Gómez-García, J. M. Martínez-Agudo, Inorg. Chem. 40 (2001) 113–120.

[86] Y. -L. Bai, J. Tao, W. Wernsdorfer, O. Sato, R. -B. Huang, L. -S. Zheng, J. Am. Chem. Soc. 128 (2006) 16428–16429.

[87] L. Cavigli, R. Sessoli, M. Gurioli, L. Bogani, Phys. Status Solidi A 203 (2006) 1402–1408.

[88] G. Christou, D. Gatteschi, D. N. Hendrickson, R. Sessoli, MRS Bull. 25 (2000) 66–71.

[89] D. Gatteschi, R. Sessoli, Angew. Chem. Int. Ed. 42 (2003) 268–297.

[90] H. Oshio, M. Nakano, Chem. Eur. J. 11 (2005) 5178–5185.

[91] C. Coulon, H. Miyasaka, R. Clérac, Struct. Bonding 122 (2006) 163–206.

[92] J. W. Steed, J. L. Atwood, Supramolecular Chemistry; VCH: New York 2000.

[93] B. J. Holliday, C. A. Mirkin, Angew. Chem. Int. Ed. 40 (2001) 2022–2043.

[94] Y. Sunatsuki, Y. Motoda, N. Matsumoto, Coord. Chem. Rev. 226 (2002) 199–209.

[95] V. Balamurugan, W. Jacob, J. Mukherjee, R. Mukherjee, CrystEngComm. (2004) 396–400.

[96] K. Biradha, CrystEngComm. (2003) 374–384.

[97] A. M. Beatty, Coord. Chem. Rev. 246 (2003) 131–143.

[98] H. W. Roesky, M. Andruh, Coord. Chem. Rev. 236 (2003) 91–119.

[99] S. Kitagawa, S. Kawata, Coord. Chem. Rev. 224 (2002) 11–34.

[100] M. Tadokoro, K. Nakasuji, Coord. Chem. Rev. 198 (2000) 205–218.

[101] B. Conerney, P. Jensen, P. E. Kruger, B. Moubaraki, K. S. Murray, CrystEngComm. (2003) 454–458.

[102] M. Albrecht, Chem. Rev. 101 (2001) 3457–3497.

[103] R. C. Scarrow, D. L. White, K. N. Raymond, J. Am. Chem. Soc. 107 (1985) 6540–6546.

[104] J. -M. Lehn, A. Rigault, J. Siegel, J. Harrowfield, B. Chevrier, D. Moras, Proc. Natl. Acad. Sci. USA 84 (1987) 2565–2569.

[105] W. Zarges, J. Hall, J. -M. Lehn, C. Bolm, Helv. Chim. Acta 74 (1991) 1843–1852.

[106] R. Krämer, J. -M. Lehn, A. De Cian, J. Fischer, Angew. Chem. Int. Ed. Engl. 32 (1993) 703–706.

[107] E. J. Enemark, T. D. P. Stack, Angew. Chem. Int. Ed. Engl. 34 (1995) 996–998.

[108] M. Albrecht, S. Kotila, Angew. Chem. Int. Ed. Engl. 34 (1995) 2134–2136.

[109] E. J. Enemark, T. D. P. Stack, Inorg. Chem. 35 (1996) 2719–2720.

[110] G. S. Hanan, C. R. Arana, J. -M. Lehn, D. Fenske, Angew. Chem. Int. Ed. Engl. 34 (1995) 1122–1124.

[111] C. O. Dietrich-Buchecker, J. -P. Sauvage, J. Am. Chem. Soc. 106 (1984) 3043–3046.

[112] C. O. Dietrich-Buchecker, J. -P. Sauvage, N. Armaroli, P. Ceroni, V. Balzani, Angew. Chem. Int. Ed. Engl. 35 (1996) 1119–1121.

[113] P. Baxter, J. -M. Lehn, A. De Cian, J. Fischer, Angew. Chem. Int. Ed. Engl. 32 (1993) 69–72.

[114] R. W. Saalfrank, R. Burak, A. Breit, D. Stalke, R. Herbst-Irmer, J. Daub, M. Porsch, E. Bill, M. Müther, A. X. Trautwein, Angew. Chem. Int. Ed. Engl. 33 (1994) 1621–1623.

[115] T. Beissel, R. E. Powers, K. N. Raymond, Angew. Chem. Int. Ed. Engl. 35 (1996) 1084–1086.

[116] B. Hasenknopf, J. -M. Lehn, B. O. Kneisel, G. Baum, D. Fenske, Angew. Chem. Int. Ed. Engl. 35 (1996) 1838–1840.

[117] D. S. Lawrence, T. Jiang, M. Levett, Chem. Rev. 95 (1995) 2229–2260.

[118] J. P. Schneider, J. W. Kelly, Chem. Rev. 95 (1995) 2169–2187.

[119] R. Ziessel, M. -T. Youinou, Angew Chem. Int. Ed. Engl. 32 (1993) 877–880.

[120] E. C. Constable, A. M. W. C. Thompson, P. Harveson, L. Macko, M. Zehnder, Chem. Eur. J. 1 (1995) 360–367.

[121] M. A. Masood, E. J. Enemark, T. D. P. Stack, Angew Chem. Int. Ed. 37 (1998) 928–932.

[122] Y. Wang, J. L. Du Bois, B. Hedman, K. O. Hodgson, T. D. P. Stack, Science 279 (1998) 537–538.

[123] J. Hamblin, L. J. Childs, N. W. Alcock, M. J. Hannon, J. Chem. Soc. Dalton Trans. (2002) 164–169.

[124] S. G. Telfer, T. Sato, T. Harada, R. Kuroda, J. Lefebvre, D. B. Leznoff, Inorg. Chem. 43 (2004) 6168–6176.

[125] E. N. Jacobsen, In Catalytic Asymmetric Synthesis; I. Ojima, Ed.; VCH: Weinheim, 1993.

[126] E. N. Jacobsen, In Comprehensive Organometallic Chemistry II; G. Wilkinson, F. G. A. Stone, E. W. Abel, L. S. Hegedus, Eds.; Pergamon Press, New York, 1995; Vol. 12.

[127] T. Katsuki, Coord. Chem. Rev. 140 (1995) 189–214.

[128] C. T. Dalton, K. M. Ryan, V. M. Wall, C. Bousquet, D. G. Gilheany, Top. Catal. 5 (1998) 75–91.

[129] T. Katsuki, Adv. Synth. Catal. 344 (2002) 131–147.

[130] T. Katsuki, Curr. Chem. Org. (2001) 663–678.

[131] M. Palucki, N. S. Finney, P. J. Pospisil, M. L. Guler, T. Ishida, E. N. Jacobsen, J. Am. Chem. Soc. 120 (1998) 948–954.

[132] M. Tokunaga, J. F. Larrow, F. Kakiuchi, E. N. Jacobsen, Science 277 (1997) 936–938.

[133] E. N. Jacobsen, Acc. Chem. Res. 33 (2000) 421–431.

[134] D. M. Murphy, I. Caretti, E. Carter, I. A. Fallis, M. C. Göbel, J. Landon, S. V. Doorslaer, D. J. Willock, Inorg. Chem. 50 (2011) 6944–6955.

[135] W. Tam, D. F. Eaton, J. C. Calabrese, I. D. Williams, Y. Wang, A. G. Anderson, Chem. Mater. 1 (1989) 128–140.

[136] O. König, H. -B. Bürgi, T. Armbruster, J. Hullinger, T. Weber, J. Am. Chem. Soc. 119 (1997) 10632–10640.

[137] A. Quintel, J. Hullinger, M. Wübbenhorst, J. Phys. Chem. B 102 (1998) 4277–4283.

[138] K. T. Holman, A. M. Pivovar, M. D. Ward, Science 294 (2001) 1907–1911.

[139] X. X. Zhang, J. S. Bradshaw, R. M. Izatt, Chem. Rev. 97 (1997) 3313–3361.

[140] E. Brunet, Chirality 14 (2002) 135–143.

[141] L. Pérez-García, D. B. Amabilino, Chem. Soc. Rev. 31 (2002) 342–356.

[142] L. -X. Dai, Angew Chem. Int. Ed. 43 (2004) 5726–5729.

[143] V. K. Muppidi, P. S. Zacharias, S. Pal, Chem. Commun. (2005) 2515–2517.

[144] V. K. Muppidi, P. S. Zacharias, S. Pal, J. Solid State Chem. 180 (2007) 132–137.

[145] P. Pallavicini, V. Amendola, Y. D. Fernandez, M. Ghisalberti, L. Linati, C. Mangano, A. M. Lanfredi, C. Massera, Dalton Trans. (2003) 575–580.

[146] T. H. Benson, M. S. Bilton, N. S. Gill, M. J. Sterns, J. Chem. Soc. Chem. Commun. (1976) 936–937.

[147] L. Flores-Lopéz, M. Parra-Hake, R. Somanathan, P. J. Walsh, Organometallics 19 (2000) 2153–2160.

[148] M. L. Glówka, A. Olczak, J. Karolak-Wojciechowska, E. Ciechanowska-Urbanska, Acta. Crystallogr. B 54 (1998) 250–256.

[149] J. W. Canary, Chem. Soc. Rev. 38 (2009) 747–756.

[150] J. W. Canary, C. S. Allen, J. M. Castagnetto, Y. H. Wang, J. Am. Chem. Soc. 117 (1995) 8484–8485.

[151] J. W. Canary, S. Mortezaei, J. Liang, Chem. Commun. 46 (2010) 5850–5860.

[152] J. W. Canary, C. S. Allen, J. M. Castagnetto, Y. H. Chiu, P. J. Toscano, Y. H. Wang, Inorg. Chem. 37 (1998) 6255–6262.

[153] S. Nieto, V. M. Lynch, E. V. Anslyn, H. Kim, J. Chin. Org. Lett. 10 (2008) 5167–5170.

[154] J. M. Castagnetto, J. W. Canary, Chem. Commun. (1998) 203–204.

[155] J. M. Rowland, M. M. Olmstead, P. K. Mascharak, Inorg. Chem. 41 (2002) 1545–1549.

[156] T. J. Burchell, D. L. Eisler, R. J. Puddephatt, J. Chem. Soc. Dalton Trans. (2005) 268–272.

[157] S. Muthu, J. H. K. Yip, J. J. Vittal, J. Chem. Soc. Dalton Trans. (2002) 4561–4568.

[158] S. Muthu, J. H. K. Yip, J. J. Vittal, J. Chem. Soc. Dalton Trans. (2001) 3577–3584.

[159] C. L. Schauer, E. Matwey, F. W. Fowler, J. W. Lauher, J. Am. Chem. Soc. 119 (1997) 10245–10246.

[160] C. B. Aakeröy, A. M. Beatty, Chem. Commun. (1998) 1067–1068.

[161] C. B. Aakeröy, A. M. Beatty, J. Desper, M. OShea, J. Valdés-Martínez, J. Chem. Soc. Dalton Trans. (2003) 3956–3962.

[162] Z. Qin, M. C. Jennings, R. J. Puddephatt, Chem. Eur. J. 8 (2002) 735–738.

[163] Z. Qin, M. C. Jennings, R. J. Puddephatt, Inorg. Chem. 40 (2001) 6220–6228.

[164] Z. Qin, M. C. Jennings, R. J. Puddephatt, Chem. Commun. (2001) 2676–2677.

[165] X. Xu, S. L. James, M. P. Mingos, A. J. P. White, D. J. Williams, J. Chem. Soc. Dalton Trans. (2000) 3783–3790.

[166] C. J. Kuehl, F. M. Tabellion, A. M. Arif, P. J. Stang, Organometallics 20 (2001) 1956–1962.

[167] G. Li, Y. Song, H. Hou, L. Li, Y. Fan, Y. Zhu, X. Meng, L. Mi, Inorg. Chem. 42 (2003) 913–920.

[168] T. J. Burchell, R. J. Puddephatt, Inorg. Chem. 44(2005) 3718–3730.

[169] T. J. Burchell, R. J. Puddephatt, Inorg. Chem. 45 (2006) 650–659.

[170] C. Janiak, Dalton Trans. (2003) 2781–2804.

[171] S. L. James, Chem. Soc. Rev. 32 (2003) 276–288.

[172] S. Kitagawa, R. Kitaura, S. I. Noro, Angew. Chem. Int. Ed. 43 (2004) 2334–2375.

[173] T. Nakano, Y. Okamoto, Chem. Rev. 101 (2001) 4013–4038.

[174] E. Yashima, K. Maeda, T. Nishimura, Chem. Eur. J. 10 (2004) 42–51.

[175] L. Han, M. C. Hong, Inorg. Chem. Commun. 8 (2005) 406–419.

[176] N. F. Curtis, J. Chem. Soc. (1960) 4409–4413.

[177] N. F. Curtis, J. Chem. Soc. (1965) 924–931.

[178] N. F. Curtis, J. Chem. Soc. (1967) 2644–2646.

[179] N. F. Curtis, Y. M. Curtis, H. J. K. Powell, J. Chem. Soc. A (1966) 1015–1018.

[180] L. G. Warner, N. J. Rose, D. H. Busch, J. Am. Chem. Soc. 89 (1967) 703–704.

[181] L. G. Warner, N. J. Rose, D. H. Busch, J. Am. Chem. Soc. 90 (1968) 6938–6946.

[182] N. F. Curtis, Y. M. Curtis, J. Chem. Soc. A (1966) 1653–1669.

[183] X. -D. Zheng, L. Jiang, X. -L. Feng, T. -B. Lu, Dalton Trans. (2009) 6802–6808.

[184] G. -C. Ou, X. -L. Feng, T. -B. Lu, Cryst. Growth Des. 11 (2011) 851–856.

[185] H. -Y. Li, L. Jiang, H. Xiang, T. A. Makal, H -C. Zhou, T. -B. Lu, Inorg. Chem. 50 (2011) 3177–3179.

[186] M. Yoshizawa, Y. Takeyama, T. Kusukawa, M. Fujita, Angew. Chem. Int. Ed. 41 (2002) 1347–1349.

[187] V. F. Slagt, P. W. N. M. Van Leeuwen, J. N. H. Reek, Chem. Commun. (2003) 2474–2475.

[188] N. C. Gianneschi, P. A. Bertin, S. T. Nguyen, C. A. Mirkin, L. N. Zakharov, A. L. Rheingold, J. Am. Chem. Soc. 125 (2003) 10508–10509.

[189] P. Braunstein, G. Clerc, X. Morise, New J. Chem. 27 (2003) 68–72.

[190] G. F. Swiegers, T. J. Malefetse, Chem. Rev. 100 (2000) 3483–3537.

[191] J. Hausmann, S. Brooker, Chem. Commun. (2004) 1530–1531.

[192] M. Barboiu, E. Petit, G. Vaughan, Chem. Eur. J. 10 (2004) 2263–3370.

[193] J. K. Bera, J. Bacsa, B. W. Smucker, K. R. Dunbar, Eur. J. Inorg. Chem. (2004) 368–375.

[194] S. B. Cortright, J. C. Huffman, R. A. Yoder, J. N. Coalter, J. N. Johnston, Organometallics 23 (2004) 2238–2250.

[195] M. Takacs, D. S. Reddy, S. A. Moteki, D. Wu, H. Palencia, J. Am. Chem. Soc. 126 (2004) 4494–4495.

[196] J. M. Takacs, P. M. Hrvatin, J. M. Atkins, D. S. Reddy, J. L. Clark, New J. Chem. 29 (2005) 263–265.

[197] J. T. Goodwin, D. G. Lynn, J. Am. Chem. Soc. 114 (1992) 9197–9198.

[198] T. Nishinaga, A. Tanatani, K. Oh, J. S. Moore, J. Am. Chem. Soc. 124 (2002) 5934–5935.

[199] M. C. Etter, Acc. Chem. Res. 23 (1990) 120–126.

[200] E. A. Archer, H. Gong, M. J. Krische, Tetrahedron 57 (2001) 1139–1159.

[201] N. N. L. Madhavi, C. Bilton, J. A. K. Howard, F. H. Allen, A. Nangia, G. R. Desiraju, New J. Chem. 24 (2000) 1–4.

[202] G. R. Desiraju, Nature 412 (2001) 397–400.

[203] V. R. Vangala, B. R. Bhogala, A. Dey, G. R. Desiraju, C. K. Broder, P. S. Smith, R. Mondal, J. A. K. Howard, C. C. Wilson, J. Am. Chem. Soc. 125 (2003) 14495–14509.

[204] M. -J. Brienne, J. Gabard, M. Leclercq, J. -M. Lehn, M. Cesario, C. Pascard, M. Chevé, G. Dutruc-Rosset, Tetrahedron Lett. 35 (1994) 8157–8160.

[205] X. D. Shi, J. C. Fettinger, M. Cai, J. T. Davis, Angew. Chem. Int. Ed. 39 (2000) 3124–3127.

[206] B. L. Feringa, R. A. Van Delden, Angew. Chem. Int. Ed. 38 (1999) 3418–3438.

[207] X. Shi, J. C. Fettinger, J. T. Davis, J. Am. Chem. Soc. 123 (2001) 6738–6739.

[208] R. H. Holm, M. J. Ö Connor, Prog. Inorg. Chem. 14 (1971) 241–401.

[209] G. V. Panova, N. K. Vikulova, V. M. Potapov, Russ. Chem. Rev. 49 (1980) 655–667.

[210] A. D. Garnovskii, A. P. Sadimenko, M. I. Sadimenko, D. A. Garnovskii, Coord. Chem. Rev. 173 (1998) 31–77.

[211] S. Yamada, Coord. Chem. Rev. 190–192 (1999) 537–555.

[212] R. M. Wang, C. J. Hao, Y. F. He, Y. P. Wang, S. B. Li, J. Mol. Catal. A. 147 (1999) 173–178.

[213] R. M. Wang, C. J. Hao, Y. F. He, C. G. Xia, J. R Wang, Y. P. Wang, J. Appl. Polym. Sci. 75 (2003) 1138–1150.

[214] R. M. Wang, C. J. Hao, Y. F. He, Y. P. Wang, C. G. Xia, Polym. Adv. Technol. 13 (2002) 6–12.

[215] J. Huang, B. Lian, Y. Qian, W. Zhou, Macromolecules 35 (2002) 4871–4874.

[216] M. Mitani, J. Mohri, Y. Yoshida, J. Saito, S. Ishii, K. Tsuru, S. Matsui, R. Furuyama, T. Nakano, H. Tanaka, S. Cojoh, T. Matsugi, N. Kashiwa, T. Fujita, J. Am. Chem. Soc. 124 (2002) 3327–3336.

[217] V. G. Gibson, S. K. Spitzmesser, Chem. Rev. 103 (2003) 283–315.

[218] A. Berkessel, M. Frauenkron, T. Schwenkreis, A. Steinmetz, J. Mol. Catal. 117 (1997) 339–346.

[219] L. Canali, D. C. Sherrington, H. Deleuze, React. Funct. Polym. 40 (1999) 155–168.

[220] R. I. Kureshy, N. H. Khan, S. H. R. Abdi, S. T. Patel, R. V. Jasra, Tetrahedron: Asymmetry 12 (2001) 433–437.

[221] X. G. Zhou, J. S. Huang, P. H. Ko, K. K. Cheung, C. M. Che, J. Chem. Soc. Dalton Trans. (1999) 3303–3309.

[222] Z. Li, M. Fernández, E. N. Jacobsen, Org. Lett. 1 (1999) 1611–1613.

[223] A. G. Dossetter, T. F. Jamison, E. N. Jacobsen, Angew. Chem. Int. Ed. Engl. 38 (1999) 2398–2400.

[224] H. Nozaki, H. Takaya, S. Moriuti, R. Noyori, Tetrahedron 24 (1968) 3655–3669.

[225] T. Aratani, Pure Appl. Chem. 57 (1985) 1839–1844.

[226] Z. Li, Z. Zheng, H. Cheng, Tetrahedron: Asymmetry 11 (2000) 1157–1165.

[227] S. Wang, M. Ferbinteanu, M. Yamashita, Inorg. Chem. 46 (2007) 610–612.

[228] S. W. Choi, H. Y. Kwak, J. H. Yoon, H. C. Kim, E. K. Koh, C. S. Hong, Inorg. Chem. 47 (2008) 10214–10216.

[229] T. D. Harris, C. Coulon, R. Clérac, J. R. Long, J. Am. Chem. Soc. 133 (2011) 123–130.

[230] R. Lescouezec, J. Vaissermann, C. Ruiz-Pérez, F. Lloret, R. Carrasco, M. Julve, M. Verdaguer, Y. Dromzee, D. Gatteschi, W. Wernsdorfer, Angew. Chem. Int. Ed. 42 (2003) 1483–1486.

[231] E. J. Schelter, A. V. Prosvirin, K. R. Dunbar, J. Am. Chem. Soc. 126 (2004) 15004–15005.

[232] Y. Zhang, D. Li, R. Clérac, M. Kalisz, C. Mathoniére, S. M. Holmes, Angew. Chem. Int. Ed. 49 (2010) 3752–3756.

[233] D. F. Weng, Z. M. Wang, S. Gao, Chem. Soc. Rev. 40 (2011) 3157–3181.

[234] X. Y. Wang, C. Avendanoa, K. R. Dunbar, Chem. Soc. Rev. 40 (2011) 3213–3238.

[235] L. M. Toma, R. Lescouezec, F. Lloret, M. Julve, J. Vaissermann, M. Verdaguer, Chem. Commun. (2003) 1850–1851.

[236] T. S. Venkatakrishnan, S. Sahoo, N. Bréfuel, C. Duhayon, C. Paulsen, A. L. Barra, S. Ramasesha, J. P. Sutter, J. Am. Chem. Soc. 132 (2010) 6047–6056.

[237] M. Shatruk, C. Avendano, K. R. Dunbar, Prog. Inorg. Chem. 56 (2009) 155–334.

[238] P. Jiang, Z. Guo, Coord. Chem. Rev. 248 (2004) 205–229.

[239] G. Berggren, A. Thapper, P. Huang, P. Kurz, L. Eriksson, S. Styringa, M. F. Anderlund, Dalton Trans. (2009) 10044–10054.

[240] H. M. El-Kaderi, J. R. Hunt, J. L. Mendoza-Cortes, A. P. Cote, R. E. Taylor, M. O Keeffe, O. M. Yaghi, Science 316 (2007) 268–272.

[241] K. E. Jelfs, X. Wu, M. Schmidtmann, J. T. A. Jones, J. E. Warren, D. J. Adams, A. I. Cooper, Angew. Chem. Int. Ed. 50 (2011) 1–5.

[242] J. Chen, S. Korner, S. L. Craig, D. M. Rudkevich, J. Rebek, Jr., Nature 415 (2002) 385–386.

[243] T. Hasell, X. Wu, J. T. A. Jones, J. Bacsa, A. Steiner, T. Mitra, A. Trewin, D. J. Adams, A. I. Cooper, Nat. Chem. 2 (2010) 750–755.

[244] T. Tozawa, Nat. Mater. 8 (2009) 973–978.

[245] J. R. Holst, A. Trewin, A. I. Cooper, Nat. Chem. 2 (2010) 915–920.

[246] E. Yashima, K. Maeda, Y. Okamoto, Nature 399 (1999) 449–451.

[247] K. Maeda, K. Morino, Y. Okamoto, T. Sato, E. Yashima, J. Am. Chem. Soc. 126 (2004) 4329–4342

[248] W. O. Foye, Cancer Chemotherapeutic Agents, American Chemical Society, Washington, DC, 1995.

[249] K. Hellmann, S. K. Caryer, Fundamentals of Cancer Chemotherapy, McGraw-Hill, New York, 1987.

[250] J. Kapuscinski, Z. Darzynkiewicz, Methods Cell Biol. 33 (1990) 655–669.

[251] M. A. Fuertes, C. Alonso, M. J. Perez, Chem. Rev. 103 (2003) 645–662.

[252] M. J. Clarke, F. C. Zhu, D. R. Frasca, Chem. Rev. 99 (1999) 2511–2533.

[253] M. Magnarin, A. Bergamo, M. E. Carotenuto, S. Zorzet, G. Sava, Anticancer Res. 20 (2000) 2939–2944.

[254] J. M. Rademaker-Lakhai, D. Van den Bongard, D. Pluim, J. H. Beijnen, J. H. Schellens, Clin. Cancer Res.10 (2004) 3717–3727.

[255] G. Sava, K. Clerici, I. Capozzi, M. Cocchietto, R. Gagliardi, E. Alessio, G. Mestroni, Anti-Cancer Drugs 10 (1999) 129–138.

[256] G. Sava, R. Gagliardi, A. Bergamo, E. Alessio, G. Mestroni, Anticancer Res. 19 (1999) 969–972.

[257] S. K. Mandal, A. R. Chakravarty, Inorg. Chem. 32 (1993) 3851–3854.

[258] K. Ghosh, S. Kumar, R. Kumar, U. P. Singh, N. Goel, Inorg. Chem. 49 (2010) 7235–7237.

[259] G. M. Sheldrick, SADABS, 1996, based on the method described in: R. H. Blessing, Acta Crystallogr. A51 (1995) 33–38.

[260] SMART and SAINT, Siemens Analytical X-ray Instruments Inc., Madison, WI, 1996.

[261] G. M. Sheldrick, Acta Crystallogr. A64 (2008) 112–122.

[262] J. W. Canary, Y. Wang, R. Jr. Roy, L. Jr. Que, H. Miyake, Inorg. Synth. 32 (1998) 70–73.

[263] L. K. Frevel, J. Am. Chem. Soc. 58 (1936) 779–782.

[264] S. Koner, S. Saha, K. -I. Okamoto, J. -P. Tuchagues, Inorg. Chem. 42 (2003) 4668–4672.

[265] Y. -B. Jiang, H. -Z. Kou, R. -J. Wang, A. -L. Cui, Eur. J. Inorg. Chem. (2004) 4608–4615.

[266] S. Mandal, G. Rosair, J. Ribas, D. Bandyopadhyay, Inorg. Chim. Acta 362 (2009) 2200–2204.

[267] S. K. Padhi, D. Saha, R. Sahu, J. Subramanian, V. Manivannan, Polyhedron 27 (2008) 1714–1720.

[268] T. V. Brinzari, C. Tian, G. J. Halder, J. L. Musfeldt, M. -H. Whangbo, J. A. Schlueter, Inorg. Chem. 48 (2009) 7650–7658.

[269] A. W. Addison, T. N. Rao, J. Reedijk, J. Van Rijn, G. C. Verschor, J. Chem. Soc. Dalton Trans. (1984) 1349–1356.

[270] J. Cano, G. D. Munno, F. Lloret, M. Julve, Inorg. Chem. 39 (2000) 1611–1614.

[271] X. -H. Bu, M. Du, L. Zhang, D. -Z. Liao, J. -K. Tang, R. -H. Zhang, M. Shionoya, J. Chem. Soc. Dalton Trans. (2001) 593–598.

[272] S. Sarkar, A. Mondal, M. S. Fallah, J. Ribas, D. Chopra, H. S. Evans, K. K. Rajak, Polyhedron 25 (2006) 25–30.

[273] S. K. Dey, N. Mondal, M. S. Fallah, R. Vicente, A. Escuer, X. Solans, M. Font-Bardía, T. Matsushita, V. Gramlich, S. Mitra, Inorg. Chem. 43 (2004) 2427–2434.

[274] A. S. Rao, A. Pal, R. Ghosh, S. K. Das, Inorg. Chem. 48 (2009) 1802–1804.

[275] T. R. Holman, C. Juarez-Garcia, M. P. Hendrich, L. Que, Jr. E. Münck, J. Am. Chem. Soc. 112 (1990) 7611–7618.

[276] K. Yamaguchi, S. Koshino, F. Akagi, M. Suzuki, A. Uehara, S. Suzuki, J. Am. Chem. Soc. 119 (1997) 5752–5753.

[277] R. Bocă, M. Bocă, M. Gembickyá, L. Jäger, C. Wagner, H. Fuess, Polyhedron 23 (2004) 2337–2348.

[278] B. Sarkar, S. Konar, C. J. Gómez-García, A. Ghosh, Inorg. Chem. 47 (2008) 11611–11619.

[279] M. Fondo, N. Ocampo, A. M. Garícıa-Deibe, J. Cano, J. Sanmartín, Dalton Trans. 39 (2010) 10888–10899.

[280] J. B. Fontecha, S. Goetz, V. McKee, Angew. Chem. Int. Ed. 41 (2002) 4553–4556.

[281] S. Majumder, S. Sarkar, S. Sasmal, E. C. Sañudo, S. Mohanta, Inorg. Chem. 50 (2011) 7540–7554.

[282] W. E. Estes, J. R. Wasson, J. W. Hall, W. E. Hatfield, Inorg. Chem. 17 (1978) 3657–3664.

[283] C. R. Lucas, S. Liu, Inorg. Chem. 36 (1997) 4336–4340.

[284] A. Rodríguez-Fortea, P. Alemany, S. Alvarez, E. Ruiz, Inorg. Chem. 41 (2002) 3769–3778.

[285] M. E. Bluhm, M. Ciesielski, H. Görls, O. Walter, M. Döring, Inorg. Chem. 42 (2003) 8878–8885.

[286] A. Biswas, M. G. B. Drew, C. J. Gómez-García, A. Ghosh, Inorg. Chem. 49 (2010) 8155–8163.

[287] L. K. Thompson, Z. Xu, A. E. Goeta, J. A. K. Howard, H. J. Clase, D. O. Miller, Inorg. Chem. 37 (1998) 3217–3229.

[288] D. Hagrman, R. P. Hammond, R. Haushalter, J. Zubieta, Chem. Mater. 10 (1998) 2091–2100.

[289] B. Greener, S. P. Foxon, P. H. Walton, New J. Chem. 24 (2000) 269–273.

[290] H. Ohtsu, I. Shinobu, S. Nagatomo, T. Kitagawa, S. Ogo, Y. Watanabe, S. Fukuzumi, Chem. Commun. (2000) 1051–1052.

[291] T. D. Hamilton, G. S. Papaefstathiou, L. R. MacGillivray, CrystEngComm. 4 (2002) 223–226.

[292] N. Lah, I. K. Cigic, I. Leban, Inorg. Chem. Commun. 6 (2003) 1441–1444.

[293] S. G. Telfer, T. Sato, T. Harada, R. Kuroda, J. Lefebvre, D. L. Leznoff, Inorg. Chem. 43 (2004) 421–429.

[294] H. Araki, K. Tsuge, Y. Sasaki, S. Ishizaka, N. Kitamura, Inorg. Chem. 44 (2005) 9667–9615.

[295] C. H. Springsteen, R. D. Sweeder, R. L. LaDuca, Cryst. Growth Des. 6 (2006) 2308–2314.

[296] Y. -K. He, Z. -B. Han, Acta Crystallogr. Sect. E 62 (2006) m2676–m2677.

[297] W. Ouellette, A. V. Prosvirin, V. Chieffo, K. R. Dunbar, B. Hudson, J. Zubieta, Inorg. Chem. 45 (2006) 9346–9366.

[298] W. -J. Shi, L. Hou, D. Li, Y. -G. Yin, Inorg. Chim. Acta 360 (2007) 588–598.

[299] K. K. Sarker, D. Sardar, K. Suwa, J. Otsuki, C. Sinha, Inorg. Chem. 46 (2007) 8291–8301.

[300] C. Basu, S. Biswas, A. P. Chattopadhyay, H. Stoeckli-Evans, S. Mukherjee, Eur. J. Inorg. Chem. (2008) 4927–4935

[301] L. E. Cheruzel, M. S. Pometun, M. R. Cecil, M. S. Mashuta, R. J. Wittebort, R. M. Buchanan, Angew. Chem. Int. Ed. 42 (2003) 5452–5455.

[302] A. Mukherjee, M. K. Saha, M. Nethaji, A. R. Chakravarty, Chem. Commun. (2004) 716–717.

[303] B. Sreenivasulu, J. J. Vittal, Angew. Chem. Int. Ed. 43 (2004) 5769–5772.

[304] Z. Fei, D. Zhao, T. J. Geldbach, R. Scopelliti, P. J. Dyson, S. Antonijevic, G. Bodenhausen, Angew. Chem. Int. Ed. 44 (2005) 5720–5725.

[305] B. Lou, F. Jiang, D. Yuan, B. Wu, M. Hong, Eur. J. Inorg. Chem. (2005) 3214–3216.

[306] J. -F. Song, J. Lu, Y. Chen, Y. -B. Liu, R. -S. Zhou, X. -Y. Xu, J. -Q. Xu, Inorg. Chem. Commun. 9 (2006) 1079–1082.

[307] L. Li, M. L. Zhu, L. P. Lu, Acta Crystallogr. Sect. C: Cryst. Struct. Commun. 62 (2006) m227–m228.

[308] C. Biswas, M. G. B. Drew, A. Ghosh, Inorg. Chem. 47 (2008) 4513–4519.

[309] I. Bernal, CrystEngComm. 10 (2008) 1265–1265.

[310] R. J. Butcher, J. W. Overman, E. Sinn, J. Am. Chem. Soc. 102 (1980) 3276–3278.

[311] H. Adams, S. Clunas, D. E. Fenton, T. J. Gregson, P. E. McHugh, S. E. Spey, Inorg. Chem. Commun. 5 (2002) 211–214.

[312] D. A. Brown, W. K. Glass, N. J. Fitzpatrick, T. J. Kemp, W. Errington, G. J. Clarkson, W. Haas, F. Karsten, A. H. Mahdy, Inorg. Chim. Acta 357 (2004) 1411–1436.

[313] A. K. Sharma, F. Lloret, R. Mukherjee, Inorg. Chem. 46 (2007) 5128–5130.

[314] P. Mukherjee, M. G. B. Drew, C. J. Gómez-García, A. Ghosh, Inorg. Chem. 48 (2009) 4817–4827.

[315] K. Nakamoto, Infrared and Raman Spectra of Inorganic and Coordination Compounds, Part B, fifth ed., John Wiley & Sons, New Jersey, 2009.

[316] S. R. Batten, K. S. Murray, Coord. Chem. Rev. 246 (2003) 103–130.

[317] B. Vangdal, J. Carranza, F. Lloret, M. Julve, J. Sletten, J. Chem. Soc. Dalton Trans. (2002) 566–574.

[318] F. A. Mautner, C. N. Landry, A. A. Gallo, S. S. Massoud, J. Mol. Struct. 837 (2007) 72–78.

[319] S. Das, K. Bhar, S. Chattopadhyay, S. Chantrapromma, H. -K. Fun, J. Ribas, B. K. Ghosh, Inorg. Chim. Acta 363 (2010) 1513–1522.

[320] M. Biswas, G. B. Drew, J. Ribas, C. Diaz, A. Ghosh, Eur. J. Inorg. Chem. (2011) 2405–2412.

[321] M. D. Allendorf, C. A. Bauer, R. K. Bhakta, R. J. T. Houk, Chem. Soc. Rev. 38 (2009) 1330–1352.

[322] S. Wang, Coord. Chem. Rev. 21 (2001) 79–98.

[323] G. Marinescu, A. M. Madalan, C. Tiseanu, M. Andruh, Polyhedron 30 (2011) 1070–1075.

[324] X. X. Zhou, H. C. Fang, Y. Y. Ge, Z. Y. Zhou, Z.G. Gu, X. Gong, G. Zhao, Q. G. Zhan, R. H. Zeng, Y. P. Cai, Cryst. Growth Des. 10 (2010) 4014–4022.

[325] J. Carranza, C. Brennan, J. Sletten, F. Lloret, M. Julve, J. Chem. Soc. Dalton Trans. (2002) 3164–3170.

[326] G. A. van Albada, I. Mutikainen, U. Turpeinen, J. Reedijk, Acta Cryst. E57 (2001) m421–m423.

[327] M. Du, X. -J. Zhao, S. R. Batten, J. Ribas, Cryst. Growth Des. 5 (2005) 901–909.

[328] M. Munakata, M. Maekawa, S. Kitagawa, Matsuyama, H. Masudat, Inorg. Chem. 28 (1989) 4300–4302.

[329] Y. Ishida, T. Aida, J. Am. Chem. Soc. 124 (2002) 14017–14019.

[330] A. Tessa ten Cate, P. Y. W. Dankers, H. Kooijman, A. L. Spek, R. P. Sijbesma, E. W. Meijer, J. Am. Chem. Soc. 125 (2003) 6860–6861.

[331] J. Carranza, J. Sletten, F. Lloret, M. Julve, Inorg. Chim. Acta 357 (2004) 3304–3316.

[332] J. L. Manson, J. Gu, J. A. Schlueter, H. -H. Wang, Inorg. Chem. 42 (2003) 3950–3955.

[333] E. Colacio, F. Lloret, I. Ben Maimoun, R. Kivekäs, R. Sillanpää, J. S. Varela, Inorg. Chem. 42 (2003) 2720–2724.

[334] Y. -J. Zhao, M. -C. Hong, D. -F. Sun, R. Cao, Inorg. Chem. Commun. 5 (2002) 565–568.

[335] E. J. Enemark, T. D. P. Stack, Angew. Chem. Int. Ed. 37 (1998) 932–935.

[336] C. Imbert, H. P. Hratchian, M. Lanznaster, M. J. Heeg, L. M. Hryhorczuk, B. R. McGarvey, H. B. Schlegel, C. N. Verani, Inorg. Chem. 44 (2005) 7414–7422.

[337] V. K. Muppidi, S. Das, P. Raghavaiah, S. Pal, Inorg. Chem. Commun. 10 (2007) 234–238.

[338] F. D. Lesh, S. S. Hindo, M. J. Heeg, M. M. Allard, P. Jain, B. Peng, L. Hryhorczuk, C. N. Verani, Eur. J. Inorg. Chem. (2009) 345–356.

[339] G. R. Desiraju, Angew. Chem. Int. Ed. 34 (1995) 2311–2327.

Publications

Journals:

1. Diastereoselectivity in Dinuclear Complexes of Chiral Tridentate Ligands.

   H. S. Jena, V. Manivannan, Inorg. Chim. Acta 2012 (doi:10.1016/j.ica.2012.04.017).

2. Molecular Structures of Nickel(II) Monochelates of a Racemic Tridentate Ligand and Co-ligand Induced Structural Variations.

   H. S. Jena, J. Subramanian, V. Manivannan, Inorg. Chim. Acta 365 (2011) 177–185.

3. Molecular Structures of Dinuclear Zinc(II) Complexes of Chiral Tridentate Imine and Amine Ligands: Effect of Ligand Geometry on Diastereoselectivity.

   H. S. Jena, V. Manivannan, Communicated.

4. Copper(II) Acetate Mediated Conversion of Ortho Aminomethyl Substituted Isoquinolines to Bis(Isoquinolylcarbonyl)Amides.

   R. Sahu, V. K. Fulwa, H. S. Jena, V. Manivannan, Polyhedron 33 (2012) 9–12.

5. Structural and Magnetic Properties of Nanocrystalline $Sn_{0.98}co_{0.02}o_2$ Under Different Annealing Conditions.

   S. Mohanty, S. Ravi, H. S. Jena, V. Manivannan, Int. J. Nanoscience 10 (2011) 1–5.

6. Conversion of 2–(Aminomethyl) Substituted Pyridine and Quinoline to Their Dicarbonyldiimides Using Copper(II) Acetate.

   R. Sahu, S. K. Padhi, H. S. Jena, V. Manivannan, Inorg. Chim. Acta 363 (2010) 1448–1454.

7. Novel Synthesis of 2,4–Bis(2–pyridyl)–5–(pyridyl)imidazoles and Formation of N–(3–(Pyridyl)imidazo[1,5–*a*]pyridine)picolinamidines: Nitrogen–Rich Ligands.

   V. K. Fulwa, R. Sahu, H. S. Jena, V. Manivannan, Tetrahedron Lett. 50 (2009) 6264–6267.

Conferences:

1. Nickel(II) Complexes of (((2-Pyridyl)Ethylamine)Methyl)Phenolate Ion and Co-Ligand Induced Structural Variation.

   IRIS–12, August 16–21, **2009**, Goa.

2. Synthesis and Structural Studies on Ni(II) and Cu(II) Racemic Complexes.

   MTIC–XIII, December 07–10, **2010**, Inorganic Chemistry Unit, IISc Bangalore.

3. **ICCOSS–XX**, June 25–30, **2011**. Solid State and Structural Chemistry Unit, IISc Bangalore.

4. Coligand Dependent Chirality Selective Dimetallic Core Formation By a Monochelated Racemic Tridentate Ligand.

   ACCC–3, October 17–20, **2011**, Indian Habitat Center, New Delhi.

5. Conversion of *Ortho*-Aminomethyl Substituted Pyridine, Quinoline and Isoquinolines to Their Bis(carbonyl)amides and Iron(III) Chloride Mediated Reduction of Bis(1-isoquinolylcarbonyl)amide to an Asymmetric Amide.

   MTIC–XIV, December 10–13, **2011**, School of Chemistry, University of Hyderabad, Hyderabad.